Evaluation of Methane and Water Structure at a Hematite Surface

A Hydrate Prevention Perspective

Marthe Haaland Austrheim

A Master of Science thesis in process technology

Department of Physics and Technology

UNIVERSITY OF BERGEN

August 2017

Abstracts

In Norway oil and gas is found in reservoirs below the North Sea and the Barents Sea. When this is transported through pipelines it is exposed to temperatures and pressures in the hydrate stability zone. If sufficient amounts of water are present in the fluid steam, hydrates may form and plug the pipelines. Mineral surfaces may structure the water present in the fluid stream, as well as function as adsorption sites for water, and enhance the possibility for hydrate formation. Different routes to hydrate formation are investigated by a thermodynamic approach and it is concluded that the formation route involving hematite is the one which allows the lowest amount of water present to form hydrates. Based on this a system consisting of hematite, water and methane with conditions in the hydrate stability zone is further studied by molecular dynamics simulations. A second system with the addition of a PVP inhibitor is then studied. Two models for water (modified TIP3P and TIP4P/2005) were evaluated but a correct density could not be provided. Methane was hypothesized to be located in the low-density layers of water near the surface but instead the results indicate that they prefer to be located in the high-density layers. The PVP inhibitor does not seem to have any significant effect on structuring water in the systems. None of the system showed any clear signs of hydrate structures starting to form.

Acknowledgements

First I would like to thank my supervisor Professor Bjørn Kvamme for helping me with this thesis. I am also grateful for the advices from Professor Tatiana Kuznetsova. I would also like to thank Bjørnar Jensen for guidance through setting up the simulations and for discussing the results with me. I really appreciate your time and all your good advices.

My fellow student Anette Knarvik should also be thanked, for both professional and not so professional discussions at the office.

Finally I would like to thank my friends and family for supporting me throughout the years of my education and for keeping me in company when needed.

Table of Contents

List of Tables

Symbols

A	Helmholtz energy
a	Acceleration
E	Total energy
E	Electrostatic field
F	Force
g	Number of degrees of freedom
K	Kelvin
k_B	Boltzmann's constant
k	Force constant
m	Mass
N	Number of particles
n	Number density
p	Pressure
q_i	Electric charge of a particle i
p	Momentum of a particle
q	Generalized coordinate
Q	Effective mass associated to the time scaling coordinate s
Q (N,V,T)	Canonical partition function
r	Position vector
r	Radius (bond length in chapter 5.6)
S	Entropy
S(z)	Structure factor
T	Temperature
t	Time
U	Potential energy
V	Volume
v	Velocity
ε	Well depth
ε_0	Permittivity of free space
ξ	Thermodynamic friction coefficient

ϕ	Electrostatic potential
$\mathcal{H}$	Hamiltonian
θ	Angle
σ	Collision diameter
μ	Chemical potential
ρ	Density

1 Introduction

In Norway oil and gas is found in reservoirs below the North Sea and the Barents Sea. When this it produced it needs to be transported through pipelines lying on the seabed to processing plants for further treatment before it can be sold. Hydrates are ice-like structures composed by cages in which gas can be trapped inside. Pressure and temperature conditions on the seabed are often in the zone which favors hydrate formation, and if the stream contains a sufficient amount of water natural gas hydrates may form and plug the pipeline. It is both dangerous and costly to remove natural gas hydrate plugs [1].

The inner surface of the pipelines is usually initially covered by a layer of hematite (rust). Hematite is hydrophilic and if liquid water condenses out from the gas stream it will most likely be adsorbed on the hematite surface. Water tends to be structured by the hematite surface where layers of water with higher density than normal are formed. Between these layers a low density area exits and methane may fill this space which makes it easy for water to form natural gas hydrates.

In an article done in conjunction with this Master thesis, three different hydrate formation routes were investigated with different types and composition of guest molecules by a thermodynamic approach. The conclusion obtained was that the formation route including hematite (rust) is the route that allows the lowest amount of water in the gas to make hydrates. This article is enclosed in Appendix 2.

Based on the mentioned article this thesis further investigates a system consisting of water, methane and hematite with pressure and temperature conditions in the hydrate stability zone, checks if there are signs of hydrate structures and how water is structured by the hematite surface. A second system with addition of the kinetic inhibitor PVP investigates how this may affect the structuring of water.

2 Goals and Motivation

In this thesis the aim is to investigate a system of water, methane and hematite, and one with the addition of PVP by using molecular dynamics. From this the main goals are as follows:

1: Investigate how water interacts with the hematite surface.

2: Determine if methane molecules are placed in between layers of water near the surface.

3: Check if there are any signs of hydrate structure forming.

4: See how PVP as an inhibitor influences the water phase.

3 Scientific Methods and Environment

Molecular dynamics and Monte Carlo are the two methods that usually are considered when a microscale system is investigated. Monte Carlo is based on a random movement/rotation/insertion/deletion of molecules in each step, where a random number decides if a molecule is to move or not. Molecular dynamics works by calculating the force acting on each particle and uses this information to study the physical movements in the system like position and velocity. This makes molecular dynamics able to study a system develop through time. The aim is to study the systems through time and that is the reason for choosing a molecular dynamics simulation method for this thesis. Few other techniques can yield as detailed results at atomistic level. Another reason for choosing molecular dynamics is that this is the most well-known and used method in the group for thermodynamic modeling at the Institute for Physics and Technology where this thesis is written. In-house tools, knowledge of the method and resources are available and previous experiments are done with similar systems.

4 Hydrates

Gas hydrates are ice-like structures made up of water molecules and guest molecules. The water molecules make cavities (cages) and the guest molecule is trapped inside of them. Hydrates form under high pressures and low temperatures if water and guest molecules are present. Gas hydrates can be viewed in two aspects, both as an energy source (natural gas hydrates) and as a problem in the industry.

4.1 Hydrate Types and Guest Molecules

There exist three well known types of hydrate structures. They are usually named as structure I, II and H. Structure I and II are the most common types in the petroleum industry [1]. Gas hydrates are made up of five types of cavities (cages), one small, three large and one intermediate. Each structure has its own combination of these cavities. Inside the cavities different guest molecules, also called hydrate formers, can occupy the available space. What types of guest molecules each structure will contain depends on the size of the cavities it is built up of. Small guest molecules prefer to occupy the small cavity and vice versa for large guest molecules. Thus, the type of cages and guest molecules are what distinguishes the structures from each other. The different types of cavities (cages), hydrate structures and typical guest molecules are shown in Figure 4.1.

The cavities consist of either square faces, pentagonal faces, hexagonal faces or a combination of these. To describe which faces and how many of each a cavity is built up of, they are named in a specific way. The faces are written in terms of the number of edges, (i. e. pentagonal face is written as 5) and the amount of them in the cavity as a power of it. The cavity called $5^{12}6^2$ will then consist of 12 pentagonal faces and two hexagonal faces.

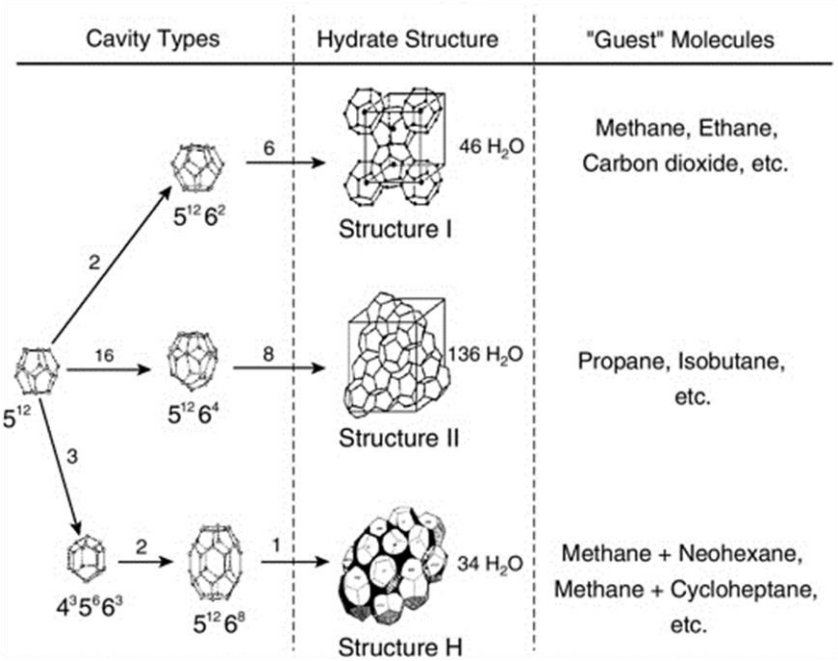

Figure 4.1: This figure shows the different types of cavities, the composition of each of the hydrate structures and what types of guest molecules which are typical for each structure [2].

4.1.1 Structure I

Structure I is built up of two types of cavities, two small and six large cavities. The small cavity (5^{12}) is called dodecahedron and is a polyhedron with twelve pentagonal faces. Tetrakaidecahedron is the name of the large cavity ($5^{12}6^2$) and has twelve pentagonal faces and two hexagonal faces. In total there are 46 water molecules in one unit cell of structure I.

Methane (CH_4), ethane (C_2H_6), carbon dioxide (CO_2) and hydrogen sulfide (H_2S) are the most common types of guest molecules in structure I. Ethane is too large to fit into the small cavities, so it will only occupy the large ones. On the other hand CH_4, CO_2 and H_2S are small enough to occupy both the small and the large cavities.

4.1.2 Structure II

As for structure I structure II is also built up two types of cavities, sixteen small and eight large. The small cavity is exactly the same as the small one in structure I, the dodecahedron. The large cavity ($5^{12}6^4$) is called hexakaidecahedron and is built up of twelve pentagonal faces and four hexagonal faces. This structure has a total of 136 molecules of water.

The typical guest molecules are methane, propane (C_3H_8), iso-butane and nitrogen. Methane only fills the small cavities because there will be too much left-over space in the large cavities. Propane and iso-butane only fills the large cages. Both the small and large cavities

can be occupied by nitrogen. A common case for structure II is that only the large cavities are occupied by guest molecules [1].

4.1.3 Structure H

Structure H is the only structure made up of three types of cavities, three small cavities, two intermediate cavities ($4^3 5^6 6^3$) and one large cavity makes up one unit cell of structure H. Like structure I and II, the small cavity (5^{12}) is a dodecahedron. The intermediate cavity ($4^3 5^6 6^3$) is an irregular dodecahedron consisting of three square faces, six pentagonal faces and three hexagonal faces. Finally the third and largest cavity type ($5^{12} 6^8$) is an irregular icosahedral and is built up of twelve pentagonal faces and eight hexagonal faces.

This type of hydrate structure does not occur as often as structure I and II. One reason to this can be that it needs two types of guest molecules to form, one small type of molecule and a larger type [1]. The small molecule is typically a methane molecule, while the large molecules can be cycloheptane or cyclohexane.

4.2 Hydrate Formation, Routes and Stability

For hydrates to form there are three requirements that need to be fulfilled [1]. The first is to have a combination of pressure and temperature that favors hydrate formation, the hydrate stability zone, a high pressure and a low temperature. Figure 4.2 shows the hydrate stability zone. The next is the presence of guest molecules like methane or carbon dioxide. Finally, the last requirement is that water is present in a sufficient amount. Nucleation is the first stage of hydrate formation where clusters form. If these clusters reach a critical size further growth is continued and hydrates forms.

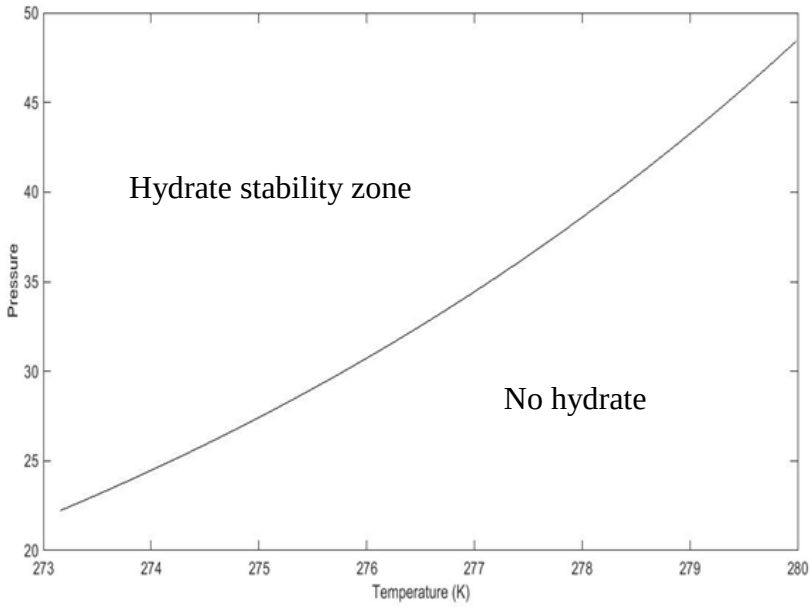

Figure 4.2: The hydrate stability zone. If guest molecule and a sufficient amount of water is present hydrates may form in the hydrate stability zone.

There are several routes to hydrate formation [3]. The one which is studied in this thesis is the route where water is adsorbed onto hematite. Mineral surfaces (e. g hematite) will most often be water wetting and adsorbs water well onto the surface. If a mineral surface is present during hydrate formation it can structure the water in a way where it gets zones with lower and higher density than in bulk near the surface, and the guest molecules can be adsorbed into the low-density areas. This situation favors hydrate formation.

4.3 Problems in the Industry

If hydrates form during transport of natural gas in pipelines they can form a plug and block the pipeline and it is both costly dangerous to remove these [1]. On a processing plant equipment can be damaged if hydrates form inside. To prevent the formation of hydrates, it is important to keep the conditions outside of the temperature and pressure region which favors hydrate formation, the hydrate stability zone. There are several ways to obtain this state. The main methods are to raise the temperature, lower the pressure or change the chemical potential of the system by adding a sufficient amount of inhibitor to the fluid stream. An inhibitor inhibits hydrates from forming and several types of inhibitors exist like thermodynamic and kinetic inhibitors. Thermodynamic inhibitors can change the hydrate stability zone so that a higher pressure or a lower temperature is needed to form hydrate.

Common types of thermodynamic inhibitors are alcohols and glycols [1]. Kinetic inhibitors prevent the hydrates form crystalizing and PVP (Polyvinylpyrrolidone) is an example of this type.

4.4 Gas Hydrates in Nature

Gas hydrates exist in nature, and is especially located in the seabed. Here methane is the most common type of guest molecule and it arises from either degradation of organic material located in the upper layers of the seabed (biogenic) or from old organic material buried deep down under the seabed which has been degraded for over millions of years (thermogenic). Natural gas hydrate reservoirs can be found in cold areas of the world, such as the arctic parts of Canada, Russia and Alaska [1]. As these hydrates contain methane, they could be used as an energy source [4]. These resources of methane can be produced by dissociating the hydrate structure in the reservoir. This can be done by depressurization, by increasing the temperature in the reservoir or by adding inhibitors like methanol. Another interesting method that could produce the methane is to inject CO_2 into the hydrate reservoir and replace methane with CO_2 [5].

5 Molecular Dynamics

A molecular dynamics simulation is a concept which can be used instead of physical experiments [6]. If an experiment is too difficult to carry out in reality due to for example high pressures or low temperatures, it is useful to use the concept of molecular dynamics. This way a vast amount of different systems can be observed.

In molecular dynamics the force acting on each particle in the system is calculated and this information is used to study the physical movements in the system through time like position and velocity.

There are a lot of concepts used in molecular dynamics simulations like boundary conditions, ensembles, phase space, algorithms to include the equations of motion and methods to keep specific variables constant. All of these are discussed in the following subchapters.

Another important aspect is that a force field has to be generated. It is made up of two different interactions, bonded interactions and non-bonded interactions, as shown in equation (5.1)

$$U_{total} = U_{bonded} + U_{non-bonded} \tag{5.1}$$

These interactions are discussed later in chapters 5.6 and 5.7.

5.1 Boundary Conditions

In a box with atoms, the ones near the edges will experience a different pressure than those in the center of the box. If an atom is placed outside of the box, it will result in a slight change of the density, because the box now is left with one less atom than before. An example of a box like this is shown in Figure 5.1.

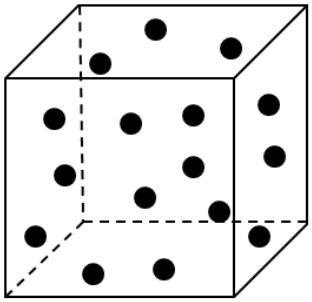

Figure 5.1: Box of atoms.

To account for these problems, the concept of periodic boundary conditions is used. A large number of identical copies are placed around the system, and all the boxes are identical on an atomic level. This is illustrated in Figure 5.2, where the original box has black atoms, and the copies have grey atoms. Each atom in the copied boxes will undergo the same change in movement as the corresponding atom in the original box. If an atom moves from one box to a neighbor box, the corresponding atom in all boxes will have the same movement, and the density is kept constant. This movement is shown by the black arrows in Figure 5.2. The atoms near the edges will now experience the same pressure because they are influenced by all the atoms in the copied boxes.

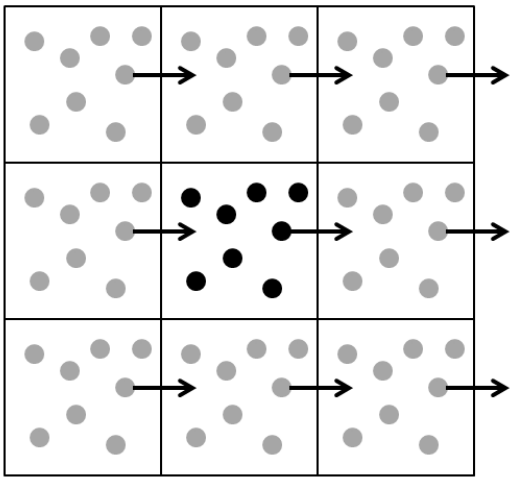

Figure 5.2: A two-dimensional section of a system with periodic boundary conditions. The black box is the original, while the grey boxes are identical copies.

5.2 The Ensemble

An ensemble is a collection of microstates that all share some given thermodynamic properties. Particle properties may vary between each microstate, but all the microstates are equal on a macroscopic level. The classical thermodynamics do not usually consider particles.

This implies that the cells in the ensemble do not necessarily have to be equal on a microscopic level. On the other hand, equality on a macroscopic level is a requirement when dealing with ensembles. There are different types of ensembles:

- Canonical ensemble
- Microcanonical ensemble
- Isothermal – isobaric ensemble
- Grand canonical ensemble

Canonical ensemble (NVT): In the canonical ensemble the number of particles, N, the volume, V, and the temperature, T is kept constant. This ensemble is shown in Figure 5.3.

Microcanonical ensemble (NVE): N, V and the total energy, E, are the constant variables in the Microcanonical ensemble.

Isothermal – isobaric ensemble (NPT): This ensemble has constant values for N, T, and the pressure, p.

Grand canonical ensemble (VTμ): The grand canonical ensemble has constant values for V, T and the chemical potential, μ. What distinguishes this from the other ensembles is that the number of particles is a variable.

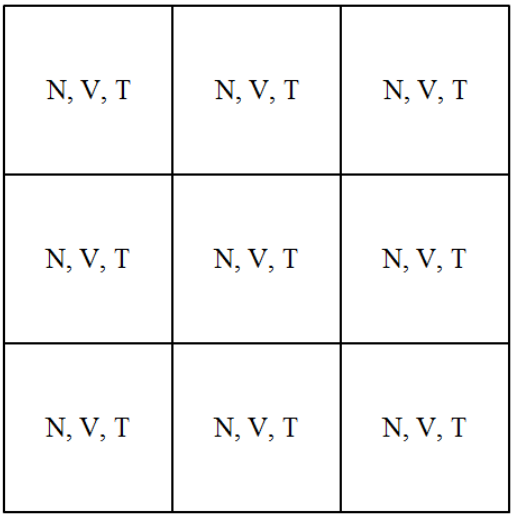

Figure 5.3: A section of a canonical ensemble, where the number of particles N, volume V and temperature T is the variables to be kept constant.

The canonical ensemble is further considered. It has a total of N^* microstates. The total energy in the ensemble is constant, but the energy is allowed to vary between the microstates. E_1^* is the possible total energy that the N particles placed in microstates N_1^* can have. The possible total energy E^* and the microstates N^* are related to each other by equation (5.2), suggested by Boltzmann [7].

$$\frac{N_i^*}{N^*} = \frac{e^{\left(-\frac{E_i^*}{k_B T}\right)}}{\sum_i e^{\left(-\frac{E_i^*}{k_B T}\right)}} \tag{5.2}$$

An important aspect with this equation is the denominator. It has its own symbol Q (N, V, T), and it is called the canonical partition function, shown in equation (5.3).

$$Q(N,V,T) = \sum_i e^{\left(-\frac{E_i^*}{k_B T}\right)} \tag{5.3}$$

The canonical partition function is used to calculate the thermodynamic internal energy, U_{th}, the Helmholtz energy, A, the entropy, S, and equations of state and pressure.

5.2.1 The ergodicity theorem

The ergodicity theorem states that if a system is said to be ergodic then the time average will be exactly the same as the ensemble average [8].

5.3 Phase Space

The phase space contains all the possible states of the system, and is a 6N-dimensional space with N particles in molecular dynamics. If a single particle is considered, its place in phase space is a function of three coordinates **q**, and three momentums **p**. For a general system with N particles, the 6N-dimensional phase space will be determined by the 3N coordinates **q** and the 3N momentums **p**, which together makes up the space. A point in phase space is usually denoted Γ.

In the case of problems in particle dynamics, it is possible to treat this systematic with the help of the Hamiltonian and Lagrangian formulations of classical mechanics. When using Hamilton's method, the total energy is written as the Hamiltonian $\mathcal{H}$, which is the sum of the

kinetic energy and the potential energy. If the potentials are time independent, the $\mathcal{H}$ will be a constant. Generalized coordinates ($\mathbf{q}_1$, $\mathbf{q}_2$, $\mathbf{q}_3$, …, $\mathbf{q}_n$) and generalized momenta ($\mathbf{p}_1$, $\mathbf{p}_2$, $\mathbf{p}_3$, …, p_n) are applied, and $\mathcal{H}$ is written in terms of these q's and p's. Hamilton's equations of motion are shown in equation (5.4) and (5.5).

$$\frac{d\boldsymbol{q}_i}{dt} = \frac{\partial \mathcal{H}}{\partial \boldsymbol{p}_i} \tag{5.4}$$

$$\frac{d\boldsymbol{p}_i}{dt} = -\frac{\partial \mathcal{H}}{\partial \boldsymbol{q}_i} \tag{5.5}$$

5.4 Leapfrog and Verlet Algorithm

Equations of motion have to be numerically solved by integrating Newton's second law, in molecular dynamics. Leapfrog and Verlet algorithms are both common methods to integrate Newton's equation of motion:

$$\mathbf{F}_A = m_A \boldsymbol{a}_A = m_A \frac{d^2 \boldsymbol{r}_A}{dt^2} \tag{5.6}$$

where $\mathbf{F}_A$ is the force acting on a particle A, m_A is the mass, $\boldsymbol{a}_A$ is the acceleration and $\boldsymbol{r}_A$ is the position vector. Because this is a second-order differential equation, it is appropriate to write it as two first-order differential equations:

$$\mathbf{F}_A = m_A \left(\frac{d\boldsymbol{v}_A}{dt}\right) \tag{5.7}$$

$$\boldsymbol{v}_A = \left(\frac{d\boldsymbol{r}_A}{dt}\right) \tag{5.8}$$

where $\boldsymbol{v}_A$ is the velocity of particle A. Equation (5.7) and (5.8) is then integrated numerically in small time steps, Δt, by using Taylor expansion for either $\mathbf{v}(t)$ or $\mathbf{r}_A(t)$.

5.4.1 Verlet

This method starts by considering the Taylor expansion for $\mathbf{r}_A(t)$, as shown in equation (5.9).

$$\boldsymbol{r}_A(t+\Delta t) = \boldsymbol{r}_A(t) + \left(\frac{d\boldsymbol{r}_A}{dt}\right)_t \Delta t + \frac{1}{2!}\left(\frac{d^2\boldsymbol{r}_A}{dt^2}\right)_t (\Delta t)^2 + \frac{1}{3!}\left(\frac{d^3\boldsymbol{r}_A}{dt^3}\right)_t (\Delta t)^3 + \cdots$$

$$\boldsymbol{r}_A(t-\Delta t) = \boldsymbol{r}_A(t) - \left(\frac{d\boldsymbol{r}_A}{dt}\right)_t \Delta t + \frac{1}{2}\left(\frac{d^2\boldsymbol{r}_A}{dt^2}\right)_t (\Delta t)^2 - \frac{1}{3!}\left(\frac{d^3\boldsymbol{r}_A}{dt^3}\right)_t (\Delta t)^3 + \cdots \quad (5.9)$$

By adding the two equations under the assumption that fourth-order and higher terms are negligible, the following equation, known as the Verlet equation, is obtained:

$$\boldsymbol{r}_A(t+\Delta t) = 2\boldsymbol{r}_A(t) - \boldsymbol{r}_A(t-\Delta t) + \left(\frac{d^2\boldsymbol{r}_A}{dt^2}\right)_t (\Delta t)^2 \quad (5.10)$$

Due to the fact that the third order terms are included but cancelled out, this method gives a high preciseness.

The acceleration can be found from the force atom A experiences at time *t*. Equation (5.10) does not include the velocity term. By using the finite difference formula, it is possible to find the following expression for the velocity:

$$\boldsymbol{v}_A(t) = \frac{\boldsymbol{r}_A(t+\Delta t) - \boldsymbol{r}_A(t-\Delta t)}{2\Delta t} \quad (5.11)$$

To calculate a new position at time $t+\Delta t$, the positions and accelerations at time t and the position at time $t-\Delta t$ are needed when the Verlet algorithm is used. This information is stored at every iteration step. An appropriate time increment, Δt, when using molecular dynamics is a femtosecond (10^{-15} s).

Another variant of the Verlet algorithm exist, called the velocity Verlet. This version only requires storage of the information that corresponds to the same time step, to find the next time step. It also includes a term for all the required variables; position, velocity and acceleration. The position and velocity equation for the velocity Verlet is shown in equation (5.12) and (5.13) respectively.

$$\boldsymbol{r}_A(t+\Delta t) = \boldsymbol{r}_A(t) + \left(\frac{d\boldsymbol{r}_A}{dt}\right)_t \Delta t + \frac{1}{2}\left(\frac{d^2\boldsymbol{r}_A}{dt^2}\right)_t (\Delta t)^2 \quad (5.12)$$

$$\boldsymbol{v}_A(t+\Delta t) = \left(\frac{d\boldsymbol{r}_A}{dt}\right)_t + \frac{1}{2}\left(\left(\frac{d^2\boldsymbol{r}_A}{dt^2}\right)_t + \left(\frac{d^2\boldsymbol{r}_A}{dt^2}\right)_{t+\Delta t}\right)\Delta t \tag{5.13}$$

5.4.2 Leapfrog

In contrast to the Verlet algorithm, the Leapfrog algorithm considers the Taylor expansion for **v**(*t*) as a starting reference. Equation (5.14) shows the Taylor expansion for **v**(*t*).

$$\begin{aligned}\boldsymbol{v}_A\left(t+\frac{\Delta t}{2}\right) &= \boldsymbol{v}_A(t) + \left(\frac{d\boldsymbol{v}_A}{dt}\right)_t \frac{\Delta t}{2} + \frac{1}{2}\left(\frac{d^2\boldsymbol{v}_A}{dt^2}\right)_t \left(\frac{\Delta t}{2}\right)^2 + \cdots \\ \boldsymbol{v}_A\left(t-\frac{\Delta t}{2}\right) &= \boldsymbol{v}_A(t) - \left(\frac{d\boldsymbol{v}_A}{dt}\right)_t \frac{\Delta t}{2} + \frac{1}{2}\left(\frac{d^2\boldsymbol{v}_A}{dt^2}\right)_t \left(\frac{\Delta t}{2}\right)^2 + \cdots\end{aligned} \tag{5.14}$$

After subtracting and rearranging, the following equation is obtained:

$$\boldsymbol{v}_A\left(t+\frac{\Delta t}{2}\right) = \boldsymbol{v}_A\left(t-\frac{\Delta t}{2}\right) + \boldsymbol{a}_A(t)\Delta t + \cdots \tag{5.15}$$

As for the Verlet algorithm, the acceleration is obtained from the force, when using the Leapfrog algorithm.

The Taylor expansion is used once more with the same procedure, but now for $\mathbf{r}_A(t+(\Delta t/2))$, and results in the following equation:

$$\boldsymbol{r}_A(t+\Delta t) = \boldsymbol{r}_A(t) + \boldsymbol{v}_A\left(t+\frac{\Delta t}{2}\right)\Delta t + \cdots \tag{5.16}$$

Combined, equation (5.15) and (5.16) forms the Leapfrog algorithm. In molecular dynamics, the Leapfrog algorithm is said to be one of the most stable and accurate integration method [7], due to the use of half time steps.

5.5 Control of system variables

Depending on the type of ensemble being used, it is necessary to include a thermostat if the temperature (T) is to be kept constant. Likewise, if the pressure (P) is a constant variable, a barostat has to be used.

5.5.1 Thermostat

For molecular dynamic simulations with constant temperature, such as the canonical ensemble (NVT), it is common to use a method to maintain a constant temperature. Amongst several molecular dynamic schemes for temperature control that exist, the Anderson thermostat [9] and the Nosé-Hoover thermostat [10] are the most widely used for the canonical ensemble [6].

Simple velocity scaling is one of the simplest methods to obtain constant temperature [7]. Temperature is related to the average kinetic energy by the following equation:

$$\langle \frac{1}{2} m v^2 \rangle = \frac{3}{2} k_b T \tag{5.17}$$

Here, m is the particle mass, v is the particle velocity, k_b is the Boltzmann constant and T is the temperature. If the particle velocity increases or decreases, the average kinetic energy will increase or decrease respectively. This relation can be used to keep the temperature constant by scaling the particle velocity to fit the desired temperature. The velocities are scaled either at specific time steps, for example every 500 time step, or when the temperature reaches a given deviation from the intended temperature. Though this is a simple method to use, it has some negative aspects; it is discontinuous, it is not ergodic and is considered as unphysical.

Another method for keeping the temperature constant is the Nosé-Hoover thermostat [10]. Nosé first suggested a set of equations [11], and then Hoover improved and simplified these equations which then became the Nosé-Hoover thermostat. This version does not contain fluctuating time intervals, and is therefore formulated by real variables instead of virtual variables.

The Nosé-Hoover equations of motion are shown in equation (5.18), (5.19) and (5.20).

$$\frac{d\mathbf{q}_i}{dt} = \frac{\mathbf{p}_i}{\mathrm{m}_i} \tag{5.18}$$

$\mathbf{q}_i$ is the position of particle i, t is the time, $\mathbf{p}_i$ is the momentum of particle i and m_i is the mass of particle i.

$$\frac{d\mathbf{p}_i}{dt} = -\frac{\partial U(\mathbf{q})}{\partial \mathbf{q}_i} - \xi \mathbf{p}_i \tag{5.19}$$

U(**q**) is the potential energy at position **q**, ξ is a called the thermodynamic friction coefficient and is defined as $\xi = \dot{s}\dot{p}_s/Q$; where s is a time scaling coordinate that Nosé added to the Lagrangian, p is the momenta conjugate to s and Q is associated to s as an effective mass.

$$\frac{d\xi}{dt} = \frac{\left(\sum_i \frac{\mathbf{p}_i{}^2}{\mathrm{m}_i} - gTk_b\right)}{\mathrm{Q}} \tag{5.20}$$

Here, g = 3N because real-variable formulation is used, where N is the number of particles. The velocity distribution and the diffusion coefficient are independent of the choice of Q, but this does not apply to the kinetic temperature [6]. If Q is too low it results in rapid temperature fluctuations and if Q is too high the temperature deviation will get a slow corrective response.

$$\mathcal{H}_{Nose-Hoover} = \sum_{i=1}^{N} \frac{\mathbf{p}_i{}^2}{2\mathrm{m}_i} + U(\mathbf{q}) + \frac{\xi^2}{2} + gTk_b \ln(s) \tag{5.21}$$

Equation (5.21) is the Hamiltonian used in the Nosé-Hoover Thermostat. The Nosé-Hoover equations of motion cannot be derived from a Hamiltonian [6], so equation (5.21) is not really a true Hamiltonian equation.

5.5.2 Barostat

Equivalent to a situation where a thermostat is used to maintain a constant temperature, a barostat has to be used in the isothermal – isobaric ensemble (NPT) to achieve a constant pressure in the system. To maintain a constant pressure, the system volume is regulated to match the desired pressure. For homogeneous systems, it is enough to change the volume of the simulation box. However, if the system is inhomogeneous, there can be a need to change the shape of the simulation box as well [6].

5.6 Bonded interactions

Bonded interactions are the forces that keep the atoms together within a molecule, called intramolecular forces. The bonded term consist of a bond stretching interaction, an angle bending interaction and a dihedral angle interaction:

$$U_{bonded} = U_{bond\ stretching} + U_{angle\ bending} + U_{dihedral\ angles} \quad (5.22)$$

5.6.1 Bond stretching

Molecules are often described by the ball and spring model, where atoms and bonds are treated as balls held together by springs. In a molecule the length of the bonds will vary because of vibrations, and it can be necessary to consider the bond stretching. Hooke's law can be used to describe this bond stretching, because it satisfies the ball and spring model [7]. Each bond stretch between two atoms in a molecule will contribute to the total interaction U, with

$$U_{bond\ stretching} = \frac{1}{2} k_{bond}(r - r_e)^2 \quad (5.23)$$

where k_{bond} is the force constant, r is the instantaneous bond length and r_e is the equilibrium bond length, as shown in Figure 5.4.

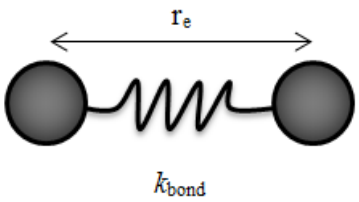

Figure 5.4: The ball and spring model. Two atoms are held together, where r_e is the equilibrium bond length and k_{bond} is the force constant.

The total interaction can also be expressed by the Morse potential:

$$U_{bond\ stretching} = D\left(1 - e^{-\alpha(r - r_e)}\right)^2 \quad (5.24)$$

or by using the simple harmonic expression with an extra term added

$$U_{bond\ stretching} = k_1(r - r_e)^2 + k_2(r - r_e)^2 \quad (5.25)$$

5.6.2 Angle bending

When three atoms are connected, the angle bending vibration has to be considered. The contribution to the total interaction U, is usually written as a harmonic potential[7]:

$$U_{angle\ bending} = \frac{1}{2} k_{angle}(\theta - \theta_e)^2 \tag{5.26}$$

where k_{angle} is the force constant, θ is the instantaneous angle and θ_{e} is the equilibrium angle, as shown in Figure 5.5.

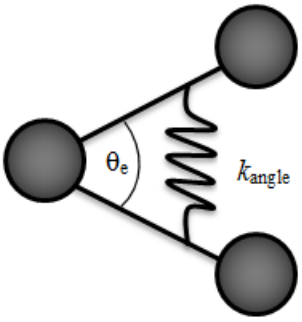

Figure 5.5: Harmonic angle bending. Three atoms makes up an angle, where k_{angle} is the force constant and θ_{e} is the equilibrium angle.

5.6.3 Dihedral angles

A dihedral angle can be defined as the angle between the two planes ABC-BCD, when four atoms ABCD are connected by three bonds in a sequence. Dihedrals have full rotation about the B-C bond. The dihedral contributes to the total interaction U, by equation (5.27) which is a Fourier series.

$$U_{dihedral} = \frac{V_1}{2}(1 + cos\theta) + \frac{V_2}{2}(1 - cos2\theta) + \frac{V_3}{2}(1 + cos3\theta) \tag{5.27}$$

V_1, V_2 and V_3 are force constants and θ is the dihedral angle. This angle is illustrated in Figure 5.6.

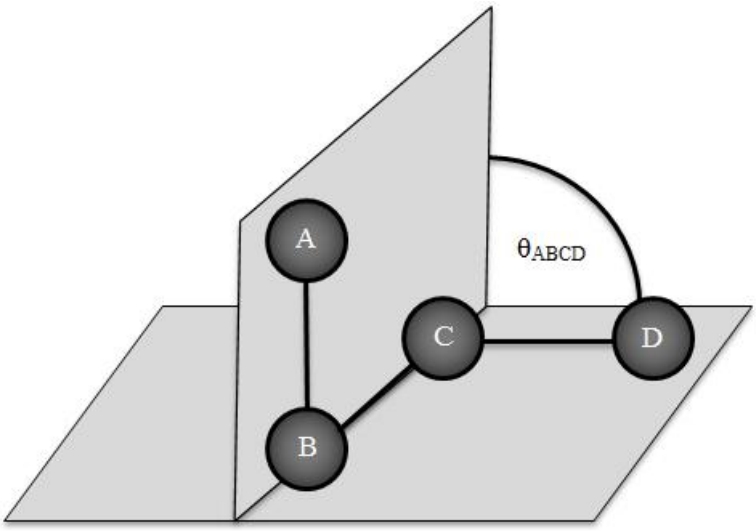

Figure 5.6: Dihedral angle.

5.7 Non-bonded interactions

If two molecules, atoms or a combination of both gets close enough to influence each other, it is necessary to consider the repulsion and attraction forces. These interactions are non-bonded, and can be both intermolecular and intramolecular. The non-bonded term consist of electrostatic interactions and van der Waals interactions:

$$U_{non-bonded} = U_{electrostatic} + U_{van\ der\ Waals} \tag{5.28}$$

Electrostatic interactions are long-range forces, while the van der Waals interactions are short-range forces.

5.7.1 Electrostatic interactions

There are two types of electrical charges in nature, positive charges and negative charges. Between these electrical charges there is an electrostatic force. Two positive charges will always have repulsive force acting between them, and the same applies for two negative charges. On the other hand, one negative and one positive charge will always attract each other. The fundamental building blocks in atoms and molecules are protons, electrons and neutrons. Protons are positively charged, while the electrons are negatively charged. Neutrons do not have any charge, and are neutral. The electron charge is equal and opposite of the proton charge. Usually atoms and molecules contain the same amount of electrons and protons, and as a result they have a net charge of zero. In reality electrons and protons have a

finite size, but in a study of charges, they are normally at rest, and the force between two point charges is considered [7].

Point charges are a mathematical abstraction, and their dimension is small compared to the distance between them. In Figure 5.7, two point charges, q_A and q_B, and their position vector, R_A and R_B, is shown. The vector $R_{AB} = R_B - R_A$ points from q_A to q_B and joins them together.

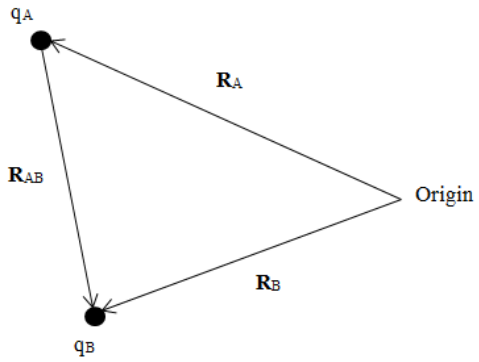

Figure 5.7: Point charges.

To describe the force between the two point charges mathematically, Coulombs law is used:

$$\mathbf{F}_{AB} = \frac{1}{4\pi\varepsilon_0}\frac{q_A q_B}{R_{\mathrm{AB}}^3}\mathbf{R}_{\mathrm{AB}} \tag{5.29}$$

$\mathbf{F}_{AB}$ is the force that q_A exerts on q_B, ε_0 is the permittivity of free space and has a value of ε_0=8.854 x 10^{-12} C^2 N^{-1} m^{-2}, q_A and q_B is the point charges and $\mathbf{R}_{AB}$ is the vector between q_A and q_B.

If a third point charge, q_C, with position vector $\mathbf{R}_C$ is added as shown in Figure 5.8, the total force on q_B is given by Coulomb's law as follows [7]:

$$\mathbf{F}_B = \frac{q_B}{4\pi\varepsilon_0}\left(q_A\frac{\mathbf{R}_{\mathrm{AB}}}{R_{\mathrm{AB}}^3} + q_C\frac{\mathbf{R}_{\mathrm{CB}}}{R_{\mathrm{AB}}^3}\right) \tag{5.30}$$

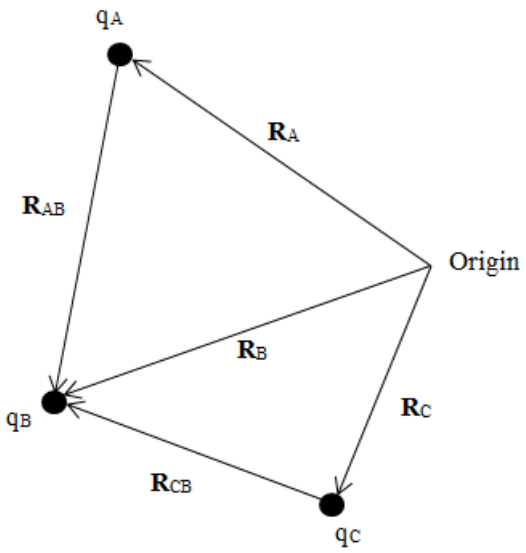

Figure 5.8: A third point charge is added.

Forces that add as in equation (5.30) are described by pair wise additivity, and this is valid for point charges.

Since the electrostatic forces are vectors, it is more usual to consider the mutual potential energy, U, rather than the force **F**, because U is a scalar quantity. **F** is related to U by the following equation:

$$\mathbf{F} = -\nabla U \tag{5.31}$$

The same applies for the electrostatic field **E**, which is related to the electrostatic potential ϕ scalar field as follows:

$$\mathbf{E} = -\nabla \phi \tag{5.32}$$

Electrostatic potential as a function of the field point **r** due to a point charge Q at the coordinate origin is given by:

$$\phi(\mathbf{r}) = \frac{q}{4\pi\varepsilon_0}\frac{1}{r} \tag{5.33}$$

The electrostatic potential from a small dipole $\mathbf{p}_e$, on a field point **r,** falls off as $1/r^2$ and has the equation:

$$\phi(\mathbf{r}) = \frac{q}{4\pi\varepsilon_0}\frac{\mathbf{p}_e\mathbf{r}}{r^3} \tag{5.34}$$

If two atoms are considered and they can be treated as point charges, the mutual potential energy is calculated by using Coulomb's law, equation (5.29).

5.7.2 Van der Waals interactions

Van der Waals interactions are mainly made up of Keesom forces, Debye forces and London dispersion forces as shown in equation (5.35).

$$U_{\text{van der Waal}} = U_{\text{Keesom}} + U_{\text{Debye}} + U_{\text{London}} \tag{5.35}$$

These forces are weak and only acts on a short range.

The Keesom force acts between two polar molecules because of the electrostatic interaction between them. It is mostly made up of the interaction between two permanent dipoles. Other combinations of polar molecules contribute to the Keesom force as well. These are permanent quadrupole interactions and permanent multipole interactions. Sometimes, the Keesom interaction is just called dipole-dipole interaction.

Debye forces come from the interaction between a permanent dipole and an induced dipole. When a molecule with a permanent dipole is in presence of a nonpolar molecule, it can repel its electrons and thus make it into an induced dipole.

The last contributing force is the London dispersion force. It occurs between two nonpolar molecules or atoms. The electron cloud on the molecules/atoms has the ability to induce each other slightly, because of the movement of electrons in the cloud. The electrons are not evenly distributed around the nucleus at all times. If most of the electrons are on one side of the nucleus, the atom/molecule becomes a temporary dipole. This gives rise to polarization of the neighbor atoms, and makes them temporary dipoles as well.

All of the contributions discussed above are attractive forces. The total short-range interaction between two atoms is $U_{\text{short-range}} = U_{\text{repulsion}} + U_{\text{attraction}}$, so a repulsive term is added. Together

the Keesom force, Debye force and the London dispersion force make the attractive contribution, and it is given by:

$$\mathrm{U}_{attraction} = \mathrm{U}_{Keesom} + \mathrm{U}_{Debye} + \mathrm{U}_{London\ dispersion} = \frac{C}{R^6} \tag{5.36}$$

Repulsion between two atoms is caused by their electron clouds. The nuclei, which are positively charged, will get less well shielded when the clouds overlap, and this results in repulsion, which can be written as:

$$\mathrm{U}_{repulsion} = Ae^{(-Br)} \tag{5.37}$$

Both A and B have to be determined from experiments or approximated from quantum mechanical calculations, and are specific to the particular pair of atoms. The total short-range interaction can be expressed as:

$$\mathrm{U} = Ae^{(-Br)} - \frac{C}{R^6} \tag{5.38}$$

This is the equation for the Buckingham potential.

Another way to express these forces is through the Lennard-Jones potential. This potential is also composed by a repulsive and an attractive term. The repulsive term is set to be proportional to $1/r^{12}$ in the Lennard-Jones 12-6 potential which is written as:

$$\mathrm{U}_{L-J} = \frac{C_{12}}{R^{12}} - \frac{C_6}{R^6} = 4\varepsilon\left(\left(\frac{\sigma}{r}\right)^{12} - \left(\frac{\sigma}{r}\right)^{6}\right) \tag{5.39}$$

The value for *C* has to be determined by experiments. Usually the Lennard-Jones potential is written in terms of the collision diameter, σ, and the well depth, ε, where the repulsive term falls off as 1/12 and the attractive term falls off as 1/6. The most common form of this potential is the Lennard-Jones 12-6 potential, but other versions with different exponents exists. One of them is the Lennard-Jones 12-8 potential, and is shown in equation (5.40).

$$\mathrm{U}_{L-J} = 4\varepsilon\left(\left(\frac{\sigma}{r}\right)^{12} - \left(\frac{\sigma}{r}\right)^{8}\right) \tag{5.40}$$

For two similar atoms, the general form of their mutual potential energy is shown in Figure 5.9. U(r) is called pair potential, and r is the distance between the two atoms. The distance that equals U(r)=0 is called the collision diameter σ, and the value of U(r) at the minimum r is referred to as the well depth, ε, and is defined as a positive quantity.

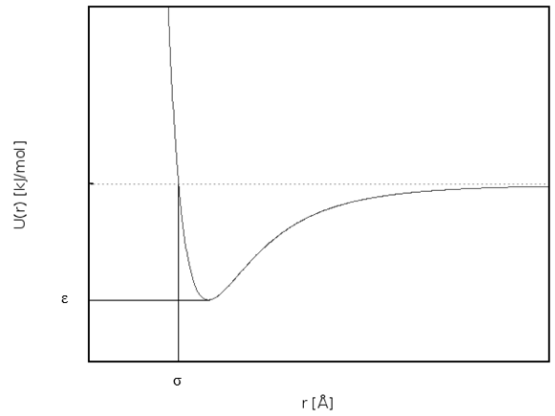

Figure 5.9: General form of the interaction between two similar atoms. U is the potential energy, r is the distance between two substances, σ is the collision diameter and ε is the well depth.

The Lennard-Jones 12-6 potential has two parameters that have to be determined, but the Buckingham potential has tree parameters, and allows for a bit more flexibility. More recent research presents potentials with many more parameters that have to be determined and the more parameters the better the result [7], but it adds a computational expense.

5.7.3 Combination Rules

Values for the collision diameter σ and the well depth ε are needed when the Lennard-Jones potential is to be calculated. For pure substances, these values are usually available in literature, but that is not the case for interaction between two different substances. To find the total interaction when dealing with a pair of different atoms or molecules, *i* and *j*, combination rules have to be used. The Lorentz-Berthelot combination rule [12] is the most well-known rule and states that:

$$\varepsilon_{ij} = \sqrt{\varepsilon_{ii}\varepsilon_{jj}} \tag{5.41}$$

and

$$\sigma_{ij} = \frac{(\sigma_{ii} + \sigma_{jj})}{2} \tag{5.42}$$

The well depth is calculated by using a geometric mean as shown in equation (5.41) (the Berthelot rule). Equation (5.42) shows that the value for the collision diameter is calculated by the use of arithmetic mean (the Lorentz rule).

Another common rule is the geometric mixing rule. For this rule, both the collision diameter and the well depth are calculated by using a geometric mean as shown in equation (5.43) and (5.44).

$$\varepsilon_{ij} = \sqrt{\varepsilon_{ii}\varepsilon_{jj}} \tag{5.43}$$

$$\sigma_{ij} = \sqrt{\sigma_{ii}\sigma_{jj}} \tag{5.44}$$

It is also possible to find the total interaction between two diatomic molecules with the atoms A, B and C, D, called a site-site potential. The L-J potential is calculated for the interactions (A-C), (A-D), (B-C) and (B-D). These interactions are summed together to find the total interaction:

$$\mathrm{U_{L-J}} = \mathrm{U_{L-J}}(A - C) + \mathrm{U_{L-J}}(A - D) + \mathrm{U_{L-J}}(B - C) + \mathrm{U_{L-J}}(B - D) \tag{5.45}$$

5.8 Cut-Offs

When dealing with a molecular dynamics system, all interactions contributing to the total molecular potential energy U, have to be calculated. The number of interactions can be enormous, depending on the size of the system. A large computational effort is required, and it demands a lot of computational time. The use of cut-offs is a tricks that saves both computational time and money.

Consider a large molecule, where the number of non-bonded interactions exceeds the number of bonded interactions. At some limited distance it is favorable to cut the non-bonded forces off to zero. So, if two atoms are separated by a distance greater than the cut-off distance, the interaction between them is not taken into account. This type of cut-off reduces the computer

processing time significantly. Figure 5.10 shows a plot of a Lennard-Jones 12-6 interaction, with a cut-off at a distance r.

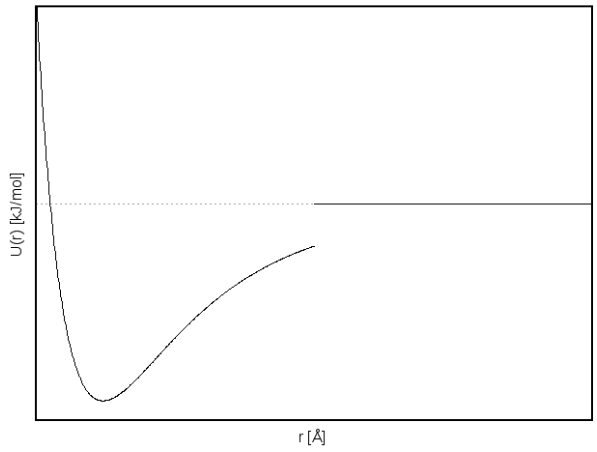

Figure 5.10 A Lennard-Jones 12-6 interaction with cut-off at a distance r.

Even though this seems like a good solution, the method offers a chance of mathematical difficulties due to the discontinuity [7], so care has to be taken when using the concept of cut-offs. As long as the cut-off distance is reasonably large (8-12 Å) it is usually not a problem using it on the short-range van der Waals interactions [13]. On the other hand, if it is used on long-range electrostatic interactions, it could leave out an important interaction in the system.

5.9 Ewald sums

In a system with periodic boundary conditions, Ewald sums are used to compute the long range contribution to the total potential energy. It is assumed that each particle i in the system has a charge q_i [6]. The particle is surrounded by a diffuse charge distribution, which in total has a charge that equals - q_i. This charge will then cancel out the charge q_i belonging to particle i. Because of this screening charge distribution, the interaction is made short-ranged. A compensating charge distribution q_i is added to correct for the previously added screening charge cloud to all particles. So in total, there are three contributions to the electrostatic potential; the particle charge q_i, the screening charge distribution - q_i and the compensating charge distribution q_i. It is also necessary to account for the Coulomb self-interaction, due to periodic boundary conditions and the fact that the charge sees itself in the other copied boxes. The reason for using the compensating charge distribution is that it is a smoothly varying function and it is periodic. A Fourier series can be used to represent this type of function.

The total electrostatic energy which contributes to the total potential energy has three contributions; the long-range Fourier (reciprocal) contribution, $U_{Fourier}$, a correction for self-interaction, U_{self}, and then the short-range real-space contribution from the screened charges, $U_{short\text{-}range}$ as shown in equation (5.46).

$$U_{coulomb} = U_{Fourier} - U_{self} + U_{short-range} \tag{5.46}$$

Below, the equations for $U_{Fourier}$, U_{self} and $U_{short\text{-}range}$ are shown in equation (5.47), (5.49) and (5.50) respectively.

$$U_{Fourier} = \frac{1}{2V}\sum_{k\neq 0}\frac{4\pi}{k^2}|\rho(\mathbf{k})|^2 e^{\frac{-k^2}{4\alpha}} \tag{5.47}$$

V is the volume, $\mathbf{k} = (2\pi/L)\mathbf{l}$ where $\mathbf{l} = (l_x, l_y, l_z)$ are the lattice vectors inside the Fourier space, $\rho(\mathbf{k})$ is the charge distribution and is shown in equation (5.48) and α is a parameter included in the expression for the width of a Gaussian which is used to calculate the compensating charge distribution [6].

$$\rho(\mathbf{k}) = \sum_{i=1}^{N} q_i e^{i\mathbf{k}\cdot r_i} \tag{5.48}$$

Here, N is the number of particles, q_i is the charge of particle i and r_i is the position to particle i.

$$U_{self} = \left(\frac{\alpha}{\pi}\right)^2 \sum_{i=1}^{N} q_i^2 \tag{5.49}$$

In the equation for U_{self} (5.49), all parameters are already described above.

$$U_{short-range} = \frac{1}{2}\sum_{i\neq j}^{N}\frac{q_i q_j erfc\left(\sqrt{\alpha r_{ij}}\right)}{r_{ij}} \tag{5.50}$$

Here erfc is an error function which has to be included in the short-range real-space contribution term.

6 Analysis theory

When a molecular dynamics simulation is complete, further analyses of the systems are often done. In this thesis the number density of the components are measured, the orientation of the water molecules are found and radial distribution functions (RDF) are made. In this chapter the general theory of these analyses methods are presented. The scripts used to do these analyses can be found in appendix 1.

6.1 Density

Density is defined as mass per volume and is shown in equation (6.1).

$$\rho = \frac{m}{V} \tag{6.1}$$

Where ρ is density, m is mass and V is volume. It can also be measured in terms of number density, which is what is done in this work. Number density is defined as the number of atoms per volume and is shown in equation (6.2).

$$n = \frac{N}{V} \tag{6.2}$$

Here n is number density, N is number of particles and V is volume. The number density is found in each frame by dividing the length in z-direction on the resolution 0.5 and this result in a number of bins. The total amount of molecules per bin is counted and then divided on the volume of the bin. When this is done for all the frames an average value per bin is calculated, and the average value for each bin can be used to plot the result. The script for this analysis was written on the Tcl language and was run in VMD[14]. The results were written to a file that could be used for plotting the results afterwards.

6.2 Orientation order

Near a mineral surface the water molecules tends to be structured and get a specific orientation towards the surface. In a large volume of water without any extern influences the molecules get a random orientation. Equation (6.3) [15] can be used to calculate the structure parameter S(z) for the water molecules in the simulations.

$$S(z) = \langle \frac{1}{N_z} \sum_{i=1}^{N_z} \frac{1}{2} [3cos^2(\theta_i) - 1] \rangle \tag{6.3}$$

Here N_z is the number of molecules at a distance z + Δz from the surface and θ is the angle between the dipole moment in water and the surface normal. Figure 6.1 shows a how the value for the structure factor as a function of the z-axis is related to the orientation of a water molecule. If the structure factor is 1 then the dipole moment in the water molecule has an orientation of 0° or 180°. The corresponding value of cos(θ) can be used to determine if it is 0° or 180° because cos(0°)=1 and cos(180°)=-1. A value of 0.25 for the structure parameter indicates that the water molecule has an orientation of 45°, 135°, 225° or 315°. If the orientation is 45° or 315° cos(θ)=0.7 and if it is 225° or 315° cos(θ)=-0.7. An orientation of 90° or 270° corresponds to a structure factor of -0.5 and cos(θ)=0.

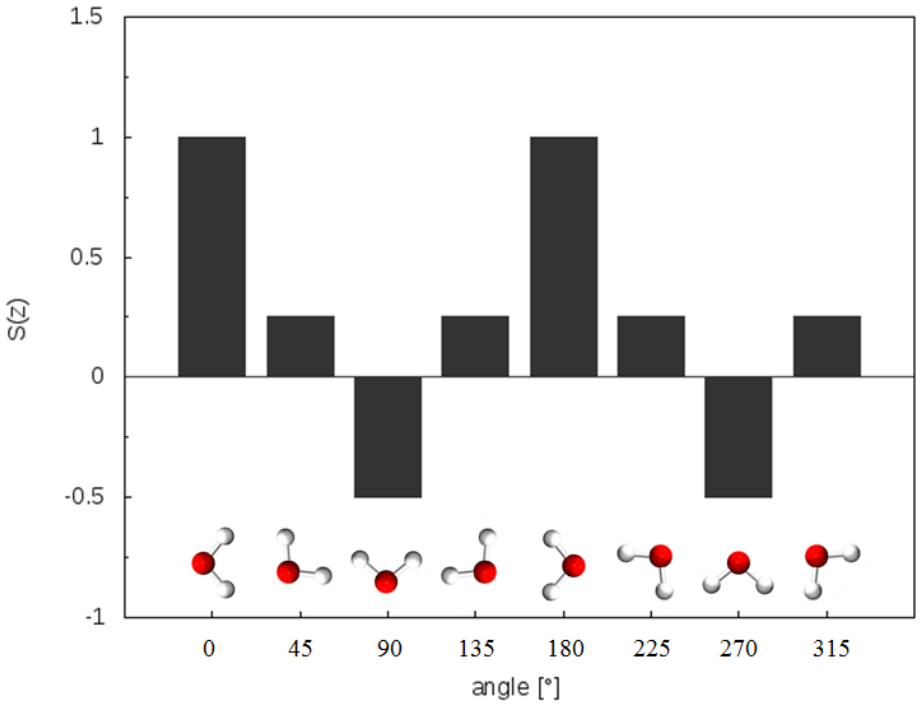

Figure 6.1: The value of S(z) related to the orientation of the water molecule.

6.3 RDF – Radial Distribution Function

In a system consisting of particles a radial distribution function can be used to show how the probability for finding these particles near a given particle varies as a function of distance from the given particle. The number of particles within a radius r from the given particle is measured and divided on the corresponding volume. The radius from the particle is then increased by dr, the total number of particles is divided on the volume and this is again repeated for increasing radiuses until the desired radius is reached. Figure 6.2 shows a picture describing this. Equation (6.4) shows the equation [7] for calculating the radial distribution functions.

$$g(r)dr = \frac{1}{N}\sum_{i=1}^{N} g_i\,(r)dr \tag{6.4}$$

Here N is the number of particles, $g_i(r)$ is the result for particle *i* and r is the radius.

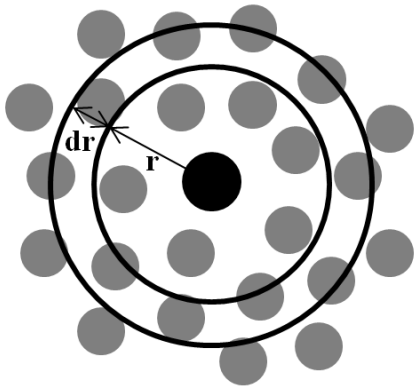

Figure 6.2: The number for particles (grey) within a radius from a given particle (black) is measured and divided on the volume. This is repeated for the increased radius r + dr.

7 Models

In molecular dynamics a model for each of the chemical compounds is needed. The models are supposed to give all the information needed to make sure that the compound acts as it would do in a physical experiment. Parameters for interactions, charges, bond lengths, angles and dihedrals are examples of the information which could be necessary to know. This section contains a description of the different molecules and crystal structures used in this thesis; the hematite crystal, methane, water and PVP. It also contains information about the different mixing rules that are used.

7.1 Hematite

Hematite has the chemical formula Fe_2O_3, and is one of the most common types of rust, iron oxide. It is made when iron comes in contact with water. Water tends to be very hydrophilic towards the hematite surface. The mineral structure is found from Maslen et al. 1994 [16]. The hematite model has the (001) surface, which is one of the most common faces in natural occurring hematite [17]. Though some crystal surfaces sometimes have to be hydroxylated, the (001) surface has no contiguous singly coordinated OH groups [17], so the hydroxylation is not done in this study. A picture of one unit cell of the hematite crystal is shown in Figure 7.1.

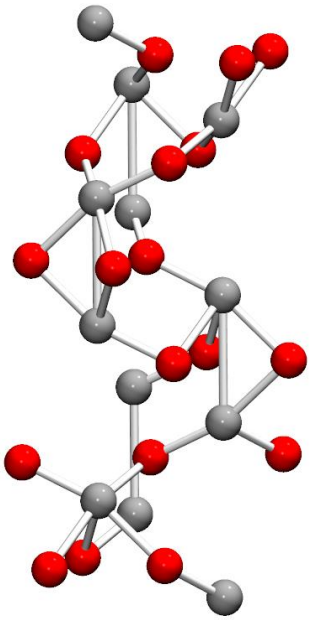

Figure 7.1: A unit cell of the hematite crystal. It contains 18 atoms of oxygen and 12 atoms of iron.

Lennard-Jones parameters for the hematite crystal are obtained from Kerisit, 2011 [18], while the values for the partial atomic charges are obtained from Olsen et al. 2014 [19].

Table 7.1: Lennard-Jones parameters [18] and partial atomic charges [19] for oxygen and iron in the hematite crystal

Lennard-Jones Parameters			Partial Atomic Charge	
Atom	ε [kJ/mol]	σ [Å]	Atom	q [e]
O	0.6502	3.1655	O	-0.8733
Fe	0.000037767	4.0722	Fe	1.31

7.1.1 Pair-interactions Between Hematite and Water

Interactions between hematite and water use special pair-interactions [18] to recreate the way they influence each other, instead of mixing rules like Lennard-Jones and geometric. These pair-interactions are shown in Table 7.2. This exception is made based on the modified TIP3P water model. The same pair-interaction was used for the TIP4P/2005 water model which has different values for the Lennard-Jones parameters. This implies that the two different water models get exactly the same interaction with the hematite crystal, which would not have happened if either the geometric or Lorentz-Berthelot mixing rule was used for both of them.

Hydrogen in water does not have Lennard-Jones parameters, so the interaction between the hematite crystal and hydrogen atoms in water does not have any short-range potential. They do however interact on a long range and they have a coulomb potential.

Table 7.2: The special interactions between hematite and water [18].

Atom type 1	Atom type 2	Type	Parameters
Fe in hematite	O in water	Lennard-Jones 12-8	ε=105.658, σ=0.9988
Fe in hematite	O in water	Buckingham	A=152358, B=3.7286, C=695.659
O in hematite	O in water	Lennard-Jones 12-6	ε=0.6502, σ=4.0722
Fe in hematite	H in water	Coulomb	-
O in hematite	H in water	Coulomb	-

For the interaction between iron in hematite and oxygen in water, both a Lennard-Jones 12-8 interaction and a Buckingham interaction are used to describe the short-range interaction.

Lennard-Jones 12-8 is a special form of the Lennard-Jones potential, and a comparison between the more common Lennard-Jones 12-6 potential is shown in Figure 7.2. The black curve corresponds to the 12-8 interaction while the gray corresponds to the 12-6 interaction. The Lennard-Jones 12-6 interaction gets a smaller well-depth and a steeper curve than the Lennard-Jones 12-6 interaction.

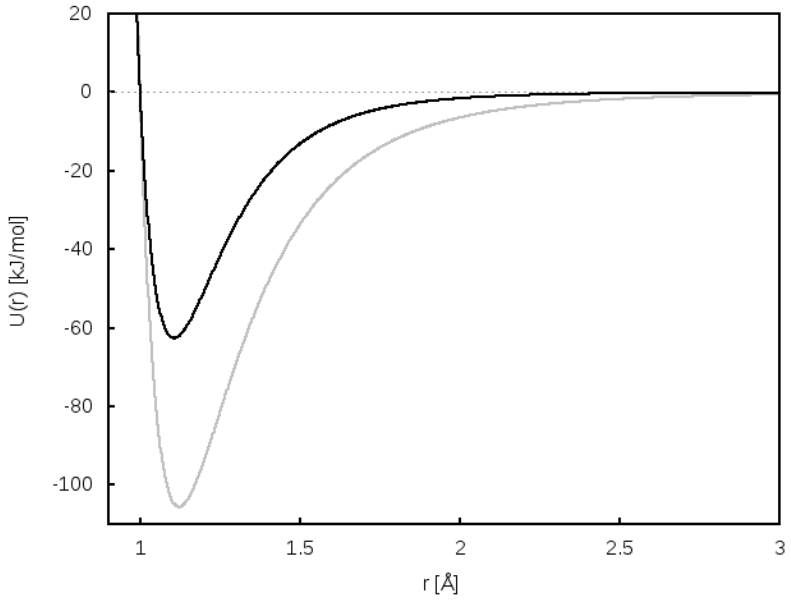

Figure 7.2: A plot of the Lennard-Jones 12-8 interaction (black) and the Lennard-Jones 12-6 interaction for iron in hematite and oxygen in water.

Figure 7.3 shows a plot of the different interactions contributing to the interaction between iron in hematite and oxygen in water. The green line is the Buckingham interaction, the red line is the Lennard-Jones 12-8 interaction, the blue line is the Coulomb interaction and the black line is the sum of the mentioned interactions. The Buckingham- and the Coulomb interaction have a large contribution to the total, while the Lennard-Jones 12-8 has a minor contribution to the total interaction.

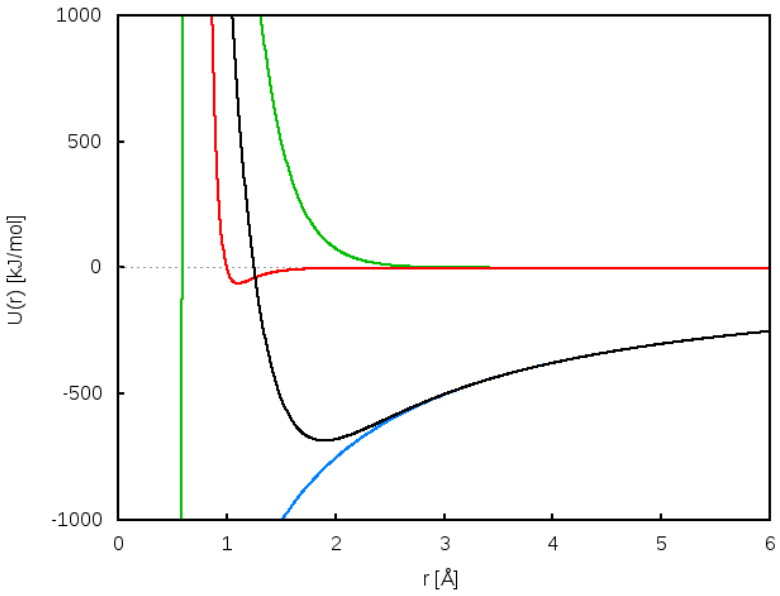

Figure 7.3: A plot of the Buckingham interaction (green), Lennard-Jones 12-8 interaction (red), Coulomb interaction (blue) and the total interaction (black) for iron in hematite and oxygen in water.

7.2 Methane

Methane is the simplest type of hydrocarbons. It consists of one carbon atom and four hydrogens atoms and has the chemical formula CH_4. At room temperature and atmospheric pressure methane is a gas. Methane is the main component in natural gas and is flammable. It is also one of the greenhouse gases.

A one site model is used for methane in this thesis. In this model the molecule is treated as a single atom with one Lennard-Jones center. The hydrogen atoms are incorporated in the carbon atom and they are not treated. This model is used to reduce the computational time. Lennard-Jones parameter and charge are obtained from Jorgensen et al. 1984 [20], and are shown in Table 7.3.

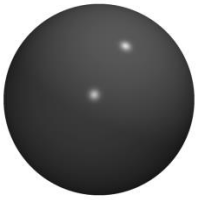

Figure 7.4: The one-site methane molecule.

Table 7.3: Lennard-Jones parameters and charge distributions for the one site methane model [20].

Lennard-Jones Parameters			Charge Distribution	
Atom	ε [kJ/mol]	σ [Å]	Atom	q [e]
Cm	1.2301	3.73	Cm	0.0

7.3 Water

Water consists of two hydrogen atoms and one atom of oxygen, has the chemical formula H_2O and is a polar compound. It is one of the most common and used chemical compounds on earth [21]. An interesting property of water is the temperature density maximum; the maximum density for water is at 4°C and it gets less dense when the temperature drops, so the solid state has a lower density than the liquid state, ice. Several models are proposed to recreate its properties in MD simulations. In this thesis the water models used are the modified TIP3P model [22] and the TIP4P/2005 model [23].

7.3.1 Modified TIP3P

The modified TIP3P model [22] is the first water model considered in this study. A picture of the molecule is shown in Figure 7.5. TIP3P is a three point model, where the point charges are centered on each of the three atoms in the water molecule. The original TIP3P model uses relatively short non-bonded truncation schemes for molecular dynamics simulation. To improve this model in order to use Ewald summation, the charges and Lennard-Jones parameters are modified. It is assumed that the hydrogen atoms in this model are in absence of Lennard-Jones parameters. This assumption makes this modified version of TIP3P only require a limited number of Lennard-Jones calculations, because it becomes independent of combination rules which are used when non-bonded heteroatomic interaction energies are calculated. At 1 atmosphere and 25°C this model gives a correct value of density, but when it comes to the characteristic temperature density maximum it is not able to reproduce this.

The water molecule is chosen to be flexible where bonds and angles are allowed to vibrate, so parameters for bonds and angles are included. Values for Lennard-Jones parameters and charge distribution are obtained from Price et al. 2004 [22] and are shown in Table 7.4, while the values for bond and angle parameters are obtained from Field et al. 1990 [24] and are shown in Table 7.5.

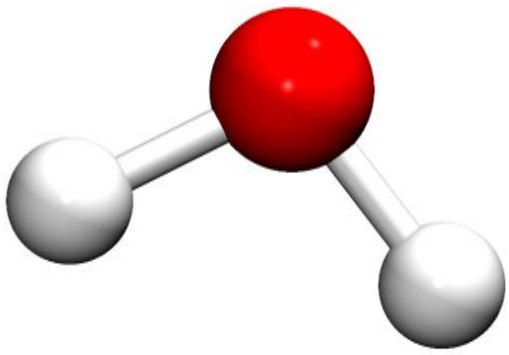

Figure 7.5 A TIP3P water molecule. The white atoms are hydrogen, while the red atom is oxygen.

Table 7.4: Lennard-Jones parameters and charge distribution for the modified TIP3P model [22]. The parameters correspond to model B in the reference.

Lennard-Jones 12-6 Parameters			Charge Distribution	
Atom	ε [kJ mol^{-1}]	σ [Å]	Atom	q [e]
Ow	0.4268	3.188	Ow	-0.83
Hw	0	0	Hw	0.415

Table 7.5: Bond and angle parameters for the TIP3P model [24].

Bond Parameters			Angle Parameters		
Bond	K_r [kJ mol^{-1}]	r [Å]	Angle	K_θ [kJ mol^{-1}]	θ [°]
Ow–Hw	1882.8	0.9572	Hw–Ow–Hw	230.12	104.52

7.3.2 TIP4P/2005

TIP4P/2005 [23] is the second water model considered. Figure 7.6 shows a picture of the TIP4P/2005 molecule. It is a rigid four-point model with three point charges and one Lennard-Jones center. Two of the three point charges are localized on each of the hydrogen atoms, the third point charge is localized in a massless atom beneath the oxygen atom. The Lennard-Jones center is localized in the oxygen atom. As for the TIP3P model, the hydrogen atoms do not have Lennard-Jones parameters.

The temperature of the maximum density and the stability of different ice polymers are the main target quantities the parametrization has been made to fit. At 1 bar the model provides a good prediction for the density and shows the maximum density at 4°C (295 K).

Values for Lennard-Jones parameters and charge distribution are obtained from Abascal and Vega, 2005 [23], and are shown in Table 7.6.

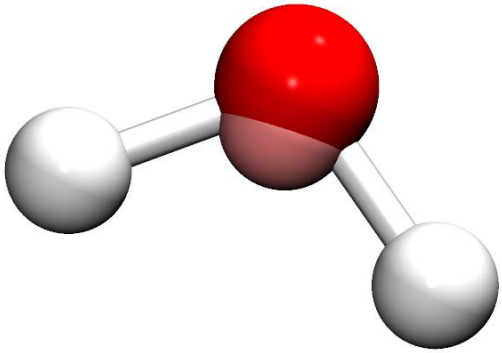

Figure 7.6 A TIP4P/2005 water molecule. The white atoms are hydrogen, the red are oxygen and the pink particle partly inside the oxygen atom is the massless point charge.

Table 7.6 Lennard Jones parameters and charge distribution for the TIP4P/2005 model [23].

Lennard-Jones 12-6 Parameters			Charge Distribution	
Atom	ε [kJ mol^{-1}]	σ [Å]	Atom	q [e]
Ow	0.7749	3.1589	pc	-1.1128
Hw	0	0	Hw	0.5564

7.4 PVP

Polyvinylpyrrolidone, usually referred to as PVP, is a common kinetic inhibitor used to prevent hydrate formation. The polymer consists of a carbon backbone with five-member lactam rings attached to it [25]. In this study, the polymer chain includes five sequences of the ring structure. In reality the PVP has a significantly larger number of sequences when used as an inhibitor in the petroleum industry. Because of the small simulation system, it is not possible to use the original size and that is why it is reduced to five sequences. The PVP polymer is shown in Figure 7.7.

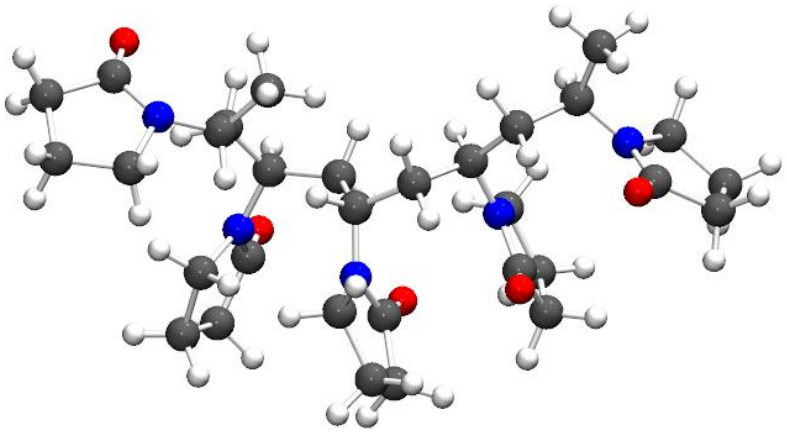

Figure 7.7: A PVP polymer with five sequences.

Avogadro [26, 27] was used to build the PVP polymer. The values for atom, bond, angle and dihedral parameters are obtained from the OPLS All-Atom Force Field [28-36]. Lennard – Jones parameters and charges are listed in Table 7.7, bond parameters are listed in Table 7.8, angle parameters are listed in Table 7.9 and the dihedral parameters are listed in Table 7.10.

Figure 7.8 shows a single PVP monomer. The carbon atoms are numbered to distinguish the different carbon-types in the PVP to relate them to the different carbon OPLS-parameters. C1 are the carbon atom attached to both ends of the polymer and it is connected to three hydrogen atoms. C2 are the backbone carbon connected to the lactam ring and it is connected to one hydrogen atom. C3, C4, C5 and C7 are carbons in a chain and they are connected to two hydrogen atoms. C6 is the carbon in the lactam ring which has a double bond to the oxygen atom. O is oxygen, N is nitrogen and H is hydrogen.

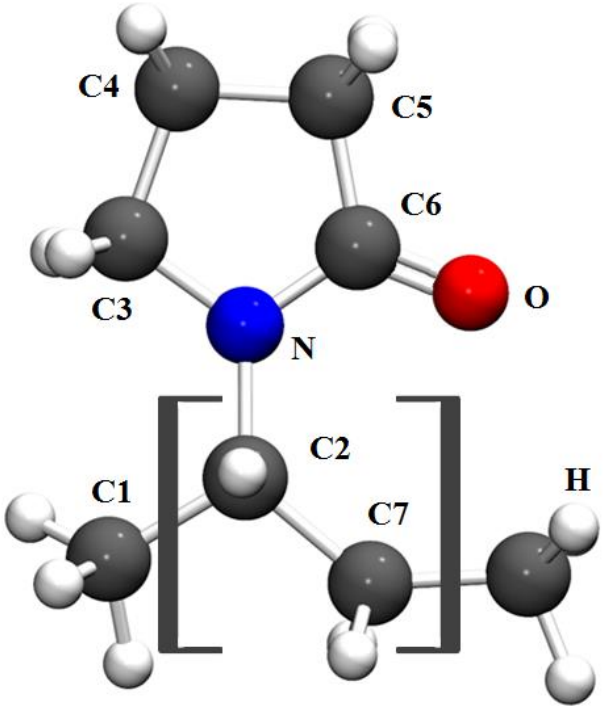

Figure 7.8: A PVP monomer. Grey atoms are carbon (C), white atoms are hydrogen (H), blue is nitrogen (N) and red is oxygen (O). Carbon atoms are numbered to distinguish the different types of carbons in the PVP from each other when OPLS parameters are found.

Table 7.7: Lennard-Jones parameters and charges for the PVP polymer [28-36].

OPLS-type	Description (See Figure 7.8)	Lennard – Jones parameters		Charge
		ε [kJ/mol]	σ [Å]	q [e]
C	C6	0.439	3.750	0.600
O	O	0.879	2.960	-0.600
NM	N	0.711	3.250	-0.360
CT	C3, C4, C5, C7	0.276	3.500	-0.120
CT	C2	0.276	3.500	0.120
CT	C1	0.276	3.500	-0.180
HC	H	0.063	2.420	0.060

Table 7.8: Bond parameters for the PVP polymer [28-36].

Bond Parameters		
Bond	r [Å]	K_r [kJ mol^{-1}]
C – O	1.229	2384.880
C – NM	1.335	2050.160
C – CT	1.522	1326.328
CT – NM	1.449	1410.008
CT – CT	1.529	1121.312
CT – HC	1.090	1422.560

Table 7.9: Angle parameters for the PVP polymer [28-36].

Angle Parameters		
Angle Type	θ [°]	K_θ [kJ mol^{-1}]
CT – CT – CT	112.7	244.14
HC – CT – HC	107.8	138.07
CT – CT – HC	110.7	156.90
CT – CT – NM	109.7	334.72
HC – CT – NM	109.5	146.44
NM – C – O	122.9	334.72
CT – C – NM	116.6	292.88
CT – C – O	120.4	334.72
C – CT – HC	109.5	146.44
C – CT – CT	111.1	263.59
C – NM – CT	121.9	209.20
CT – NM – CT	118.0	209.20

Table 7.10: Dihedral parameters for the PVP polymer [28-36].

Dihedral Parameters			
Dihedral Type	V_1 [kJ mol^{-1}]	V_2 [kJ mol^{-1}]	V_3 [kJ mol^{-1}]
HC – CT – CT – HC	0	0	1.2552
NM – CT – CT – HC	0	0	1.9414
C – NM – CT – HC	0	0	-0.5816
C – NM – CT – CT	-5.8090	-1.7866	0
NM – CT – CT – CT	8.2174	0	2.7573
CT – CT – CT – CT	5.4392	-0.2092	0.8368
CT – NM – CT – HC	0	0	0
CT – NM – CT – CT	19.8866	-3.0710	0
HC – CT – CT – CT	0	0	1.2552
CT – C – NM – CT	0	20.5016	0
HC – CT – C – O	0	0	0
CT – NM – C – O	0	20.5016	0
CT – CT – C – O	0	0	0
C – CT – CT – HC	0	0	0.3096
CT – CT – C – NM	0	4.6024	0
HC – CT – C – NM	0	0	0
CT – NM – CT – O	0	0	0

7.5 Mixing Rules

The mixing rules used for the different compounds used are listed in Table 7.11. Most of the interactions use the geometric mixing rule, but there are some exceptions. Hematite self-interaction uses the Lorentz-Berthelot mixing rule. The interaction between hematite and water uses special pair-interactions which remains the same regardless of which water model used. These pair-interactions are discussed in more detail in chapter **Error! Reference source not found.**.

Table 7.11: Mixing rules for the different components.

Type 1	Type 2	Mixing rule
Hematite	Hematite	Lorentz-Berthelot
Hematite	Methane	Geometric
Hematite	Water	Pair-interaction
Hematite	PVP	Geometric
Methane	Methane	Geometric
Methane	Water	Geometric
Methane	PVP	Geometric
Water	Water	Geometric
Water	PVP	Geometric

8 Simulation setup details

Three different systems are investigated in this thesis called system 1, system 2 and system 3. A total of six simulations are carried out because each system is run twice, once with a NVT ensemble and once with a NPT ensemble. In all of the simulation systems the temperature (T) is set to 278.15 K (5°C) and the pressure (P) is set to 78 bar because this corresponds to typical temperatures and pressure on the seabed[37]. One time step is 1 fs and the systems are run for a total of 15.005 ns (15.005 x 10^6 fs), where the warm-up time is 0.005 ns of the total run time and one time step in the warm-up is 0.1 fs. The dump frequency is set to be 500, so the information is saved to a dcd-file every 500 time step. This implies that each system will have a total of 30100 frames. Another variable which applies for all of the system is the cut-off distance and it is set to be 12 Å. Both systems have the initial size 60.4269 x 52.3305 x 184 Å but the NPT system is allowed to regulate the z-length in order to regulate the pressure. All of the common parameters for all of the systems are shown in Table 8.1.

Table 8.1: Simulation variables all of the systems have in common.

Variable	Value
Temperature (T)	278.15 K
Pressure (P)	80 bar
Warm-up time step	0.1 fs
Warm-up steps	50 x 10^3
Main run time step	1 fs
Main run steps	15.0 x 10^6
Dump frequency	500
Cut off distance	12.0 Å
System size (x, y, z)	60.4269 x 52.3305 x 184 Å

What separates the different systems from each other is which type of components they consist of, and what type of ensemble being used, NVT or NPT. Specifications for each constituent and each system assembly are discussed later in this chapter.

8.1 Constituents

Three different constituents contribute to the system assemblies. These constituents are presented in this chapter.

8.1.1 Hematite Crystal

The hematite crystal consists of 5184 atoms of oxygen and 3456 atoms of iron. Figure 8.1 a) shows a picture of the thickness of the hematite crystal where the left and right surfaces are the interacting surface in the system. In Figure 8.1 one of the equal interaction surfaces of the hematite crystal is shown. The size of the hematite crystal is 60.4260 Å x 52.3305 Å x 27.5 Å.

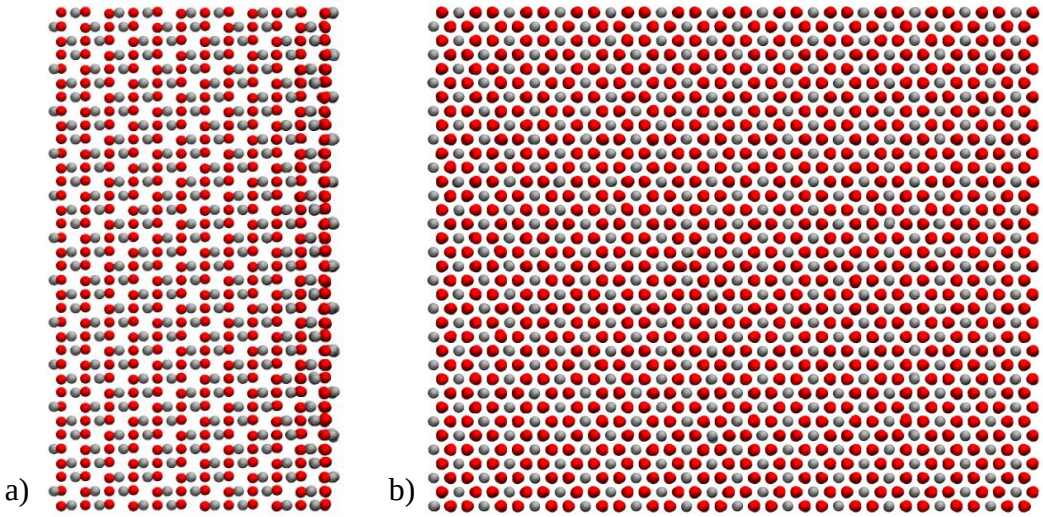

Figure 8.1: a) The hematite crystal seen from the side, where each of the sides is interaction surfaces and the middle is the bulk. b) One of the interaction surfaces on the hematite surface.

8.1.2 Methane box

The methane section was chosen to have three layers of methane, so the length of the box in z-direction was set to be 13 Å and 60 x 52 x 13 Å is the total box size. To find out how many methane molecules that would fill this space under the temperature and pressure in this system, a density versus pressure plot for the given temperature from NIST [38] was used. From this it was found that the density for methane under the given conditions is 66.632 kg/m^3. This density was used to calculate that 103 molecules of methane would occupy the available space. The box was made by making an input file with information about box size, type of molecules and number of molecules and then Packmol [39] used the input file to pack the molecules inside the box.

8.1.3 Water box

Water fills the rest of the system and has a box size of 60 x 52 x 141 Å. To find the density of water and the number of water molecules that would occupy the available space at these conditions a density versus pressure plot for the given temperature from NIST [38] was used. It was found that water density under these conditions is 1003.8 kg/m^3. The number of water molecules was calculated to be 14962. As for the methane box an input file was made containing information about the box size, the type of molecules and the number of molecules. For systems containing PVP molecules, the PVP molecules are added in the input file for water.

8.2 System Assemblies

Each of the components recently discussed are combined together to form the simulation systems. An input file containing information about the types of components and where they were placed relative to each other was made, and Packmol [39] was used to pack the system. The different systems are presented in this chapter.

8.2.1 System 1 – Hematite, Water (TIP3P) and Methane

System 1 consists of a hematite crystal, a box containing 103 molecules of methane and a box containing 14 962 molecules of water from the TIP3P model.

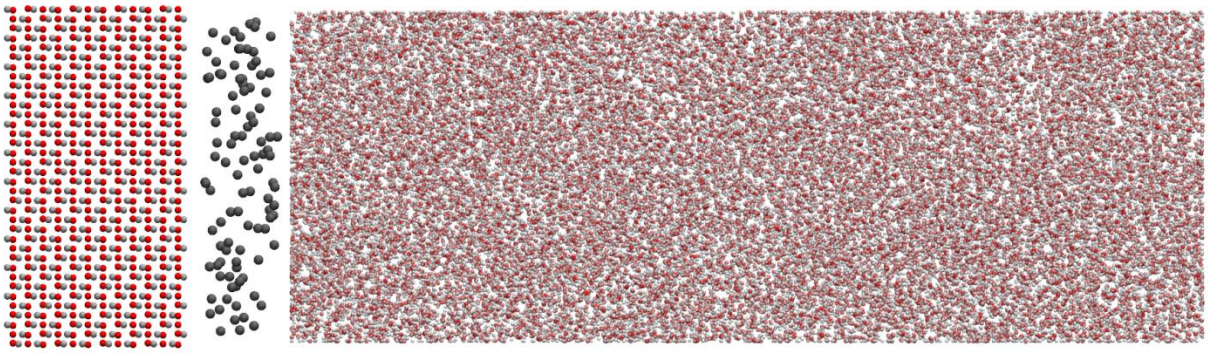

Figure 8.2: A picture of the initial system 1. From the left side; the hematite crystal, the methane box and the water (TIP3P) box.

8.2.2 System 2 – Hematite, Water (TIP3P), Methane and PVP

System 2 is composed by the hematite crystal, a box containing 103 molecules of methane and a box containing 14 962 molecules of water from the TIP3P model and 5 PVP molecules.

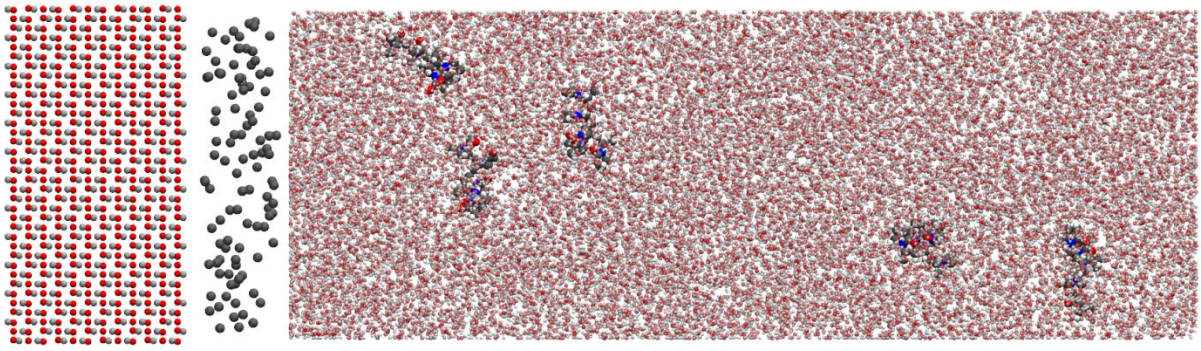

Figure 8.3: A picture of the initial system 2. From the left side; the hematite crystal, the methane box and the water (TIP3P) box containing 5 PVP molecules.

8.2.3 System 3 – Hematite, Water (TIP4P), Methane and PVP

System 3 is composed by the hematite crystal, a box containing 103 methane molecules and a box containing 14 962 TIP4P water molecules and 5 PVP-molecules.

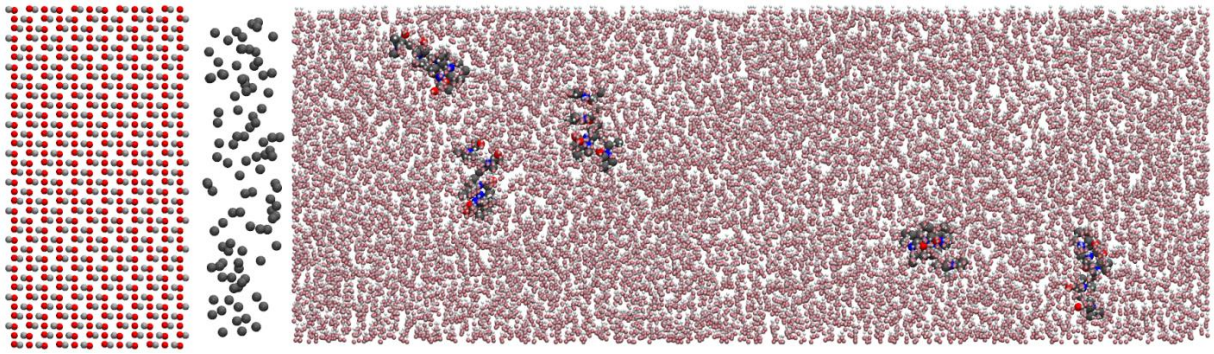

Figure 8.4 A picture of the initial system 3. From the left side; the hematite box, the methane box and the water (TIP4P) box containing 5 PVP molecules.

9 Results and Discussion

In this chapter the results are presented and discussed. Some results are based on visual observations while some are obtained by further analysis methods of the simulations.

9.1 Visual observations of each system

Each system is viewed in VMD (Visual Molecular Dynamics) [14] and the visual observations are described in the following section.

9.1.1 System 1 – NVT

System 1 consists of a hematite crystal, methane molecules and water molecules from the TIP3P model. Figure 9.1 (a) shows a picture of the initial system before simulation start, where the hematite crystal is on the left side, the water box is on the right side and the methane box is in the middle. Quickly after start water moves towards the hematite surface and makes a bridge through the methane because the water is strongly attracted by the hematite crystal. This bridge is shown in Figure 9.1 (b). After a short time, the whole hematite surface is covered by water, and the bridge vanishes. Water is structured by the hematite surface and two different density layers near the surface can be observed. The methane molecules are gathered together in a sphere without any water molecules inside, which are shown in Figure 9.1 (c). Only a limited amount of the methane molecules are dissolved into the water phase, and for a limited time, before they are moving back to the sphere. Some of them are dissolved in the water bulk, while some appears to lie in the first low-density layer of water near the hematite surface.

Water interacts with the hematite crystal on both sides of the crystal. The right side of the system where no methane is present can be used as a reference to see how water interacts with hematite without being disturbed by the methane molecules.

The density of water was measured by selecting a sequence of the water phase in VMD[14] where the number of water molecules is given and used to calculate the mass density which became ~1037 kg/m^3. This deviates from the desired density of water of 1003.8 kg/m^3 and the density in the simulation system is ~33 kg/m^3 higher than the desired density.

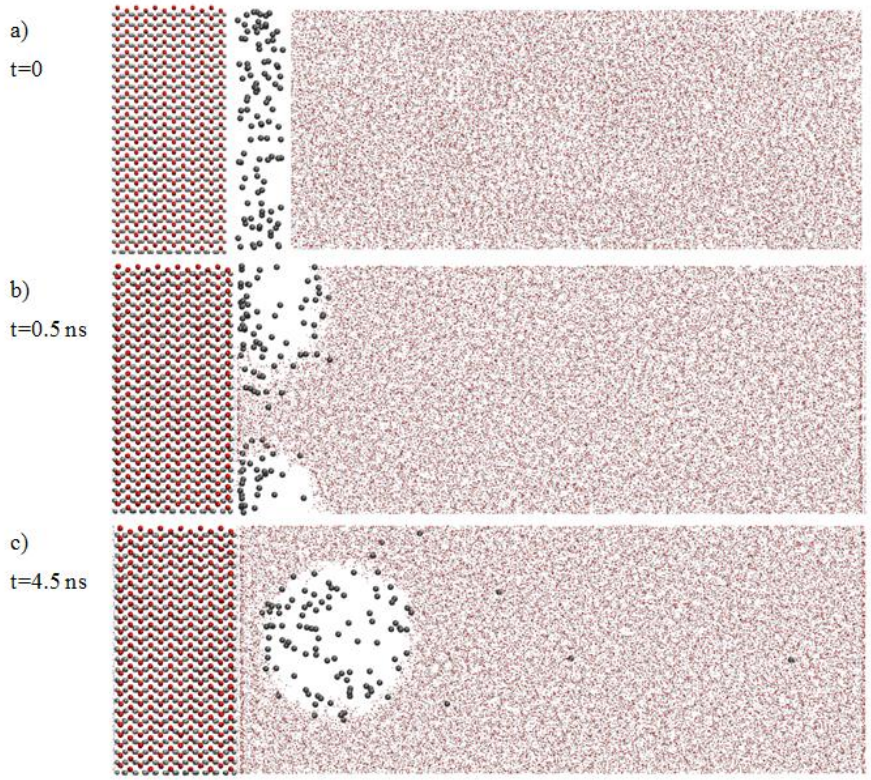

Figure 9.1: a) System 1-NVT before simulation start. b) Water is attracted to the hematite surface and starts moving towards it through a bridge. c) The methane molecules are gathered together in a sphere and water has fully covered the hematite surface. Some methane molecules are dissolved into the water bulk. This picture is from frame 7013, 3.5 ns after simulation start.

9.1.2 System 1 – NPT

System 1 – NPT has the same contents as System 1 – NVT; a hematite crystal, a methane section and a water section with TIP3P water molecules. The only difference between these two systems is that this simulation is run with a NPT ensemble rather than NVT. Therefore the picture of the initial system before simulation start is equal to the same picture in the previous section and is shown in Figure 9.1 (a).

When the simulation is started a large vibration in the z-direction can be observed. This is due to the fact that in a NPT simulation the volume is regulated to obtain the given pressure. At frame 160, 0.08 ns after start, the system has stabilized and the total length of the system is 164.5 Å and is shorter than in the NVT simulation where the length was 184 Å. Figure 9.2 (a) shows the system after stabilization, where water has been adsorbed on the surface. In this system the water molecules starts moving toward the surface quickly after start, but in

contrast to the NVT simulation it do not form a bridge, they move directly through the methane molecules and onto the surface. The methane molecules do not gather together into a sphere as in the NVT simulation. Here they make a sphere-like shape in the start, but they are surrounded by water molecules so they are not acting as a single phase. Figure 9.2 (b) shows a picture of this sphere. This shape disappears further into the simulation and the methane molecules seem to be more or less dissolved into the water phase. In Figure 9.2 (c) this can be observed.

As in the NVT simulation water seems to be structured near the hematite surface. Hydrogen atoms lay closest to the surface and the oxygen atoms lies behind it. An area behind this has some free space until the next structured layer comes, a low density area, and after this the water seems like it stops being structured. This can be viewed in Figure 9.2 (c) where hydrogen atoms (a white line) lie closest to the surface and oxygen (a red line) lies next to the hydrogens. Occasionally some of the methane molecules seem to be placed in the low density area in the structured layer. As in the NVT simulation the density was measured to ~1058 kg/m^3 in VMD[14] which is even higher and has a larger deviation of ~54 kg/m^3 from desired density.

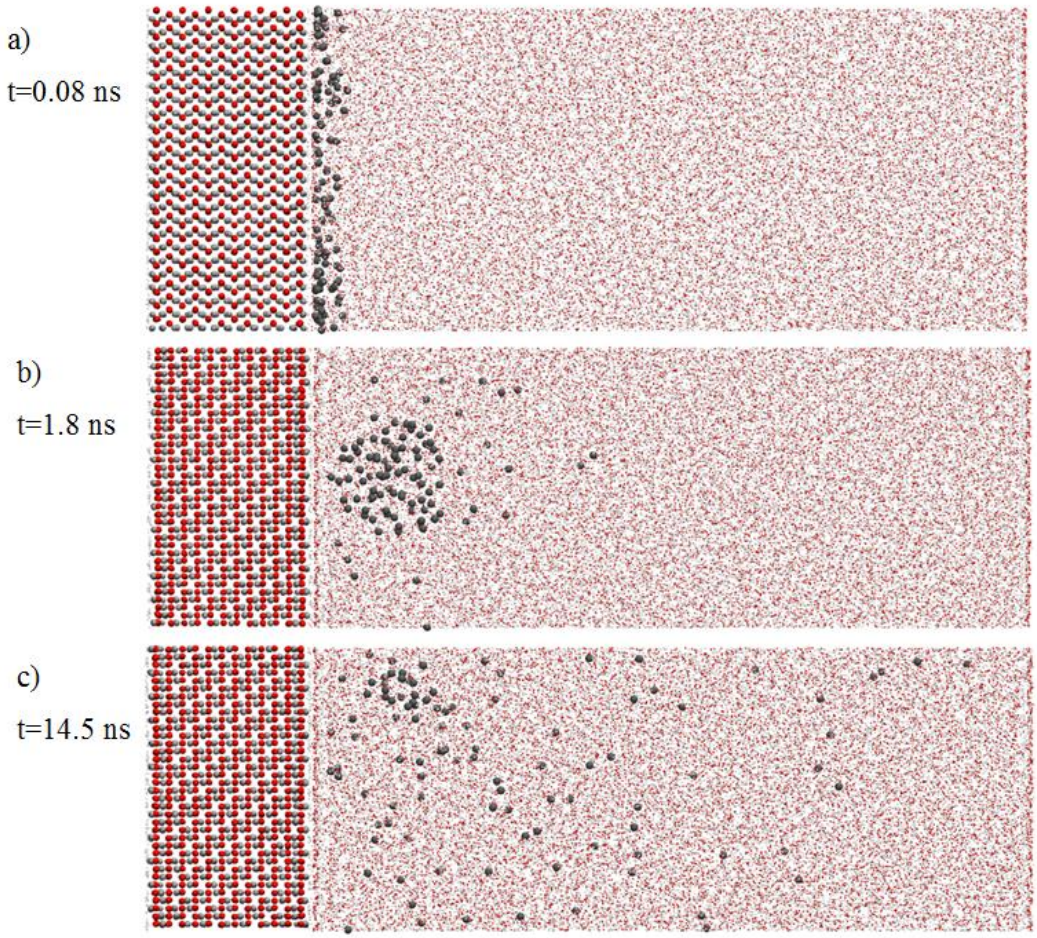

Figure 9.2: a) System 1 – NPT after 0.8 ns when the vibration in z-direction is done and the volume corresponding to the given pressure is obtained. b) The system after 1.8 ns where the methane molecules are gathered together in a sphere-like shape, but each molecule is surrounded by water molecules. This picture is rotated 90 degrees compared to the precious pictures, so the hematite crystal looks a bit different from that side. c) At 14.5 ns the methane molecules are more or less dissolved into the water phase.

9.1.3 System 2 – NVT

System 2 – NVT is composed of a hematite crystal, a section of methane and a section of water and 5 PVP molecules. The system before simulation start is shown in Figure 9.3 (a). Three of the PVP molecules are placed near the surface with the methane layer, while the two other are placed in water bulk and closer to the other side of the hematite surface. A short time after simulation start water moves towards the surface and forms a bridge through the methane layer. The situation after 0.7 ns is shown in Figure 9.3 (b).

The structured water near the hematite surface can be observed is this system as well. As in system 1 – NVT the bridge vanishes and the methane molecules gather together in a sphere. A few methane molecules are dissolved in the water at certain times, some placed in the water bulk and some appears to be placed in the low-density zone in the structured water close to the hematite surface. Figure 9.3 (c) shows a picture of the methane sphere where two of the methane molecules that seem to be placed in the low-density zone at that time and some are dissolved in the water phase. It can also be observed that one of the PVP molecules interacts with the methane phase. The carbon backbone is placed towards the methane phase while the lactam rings are placed in the water phase. After 14 ns two PVP molecules are placed in the interface between methane and water, where one of them lies close to the hematite surface, which is shown in Figure 9.3 (d). The measured density in this system was ~1044 kg/m^3.

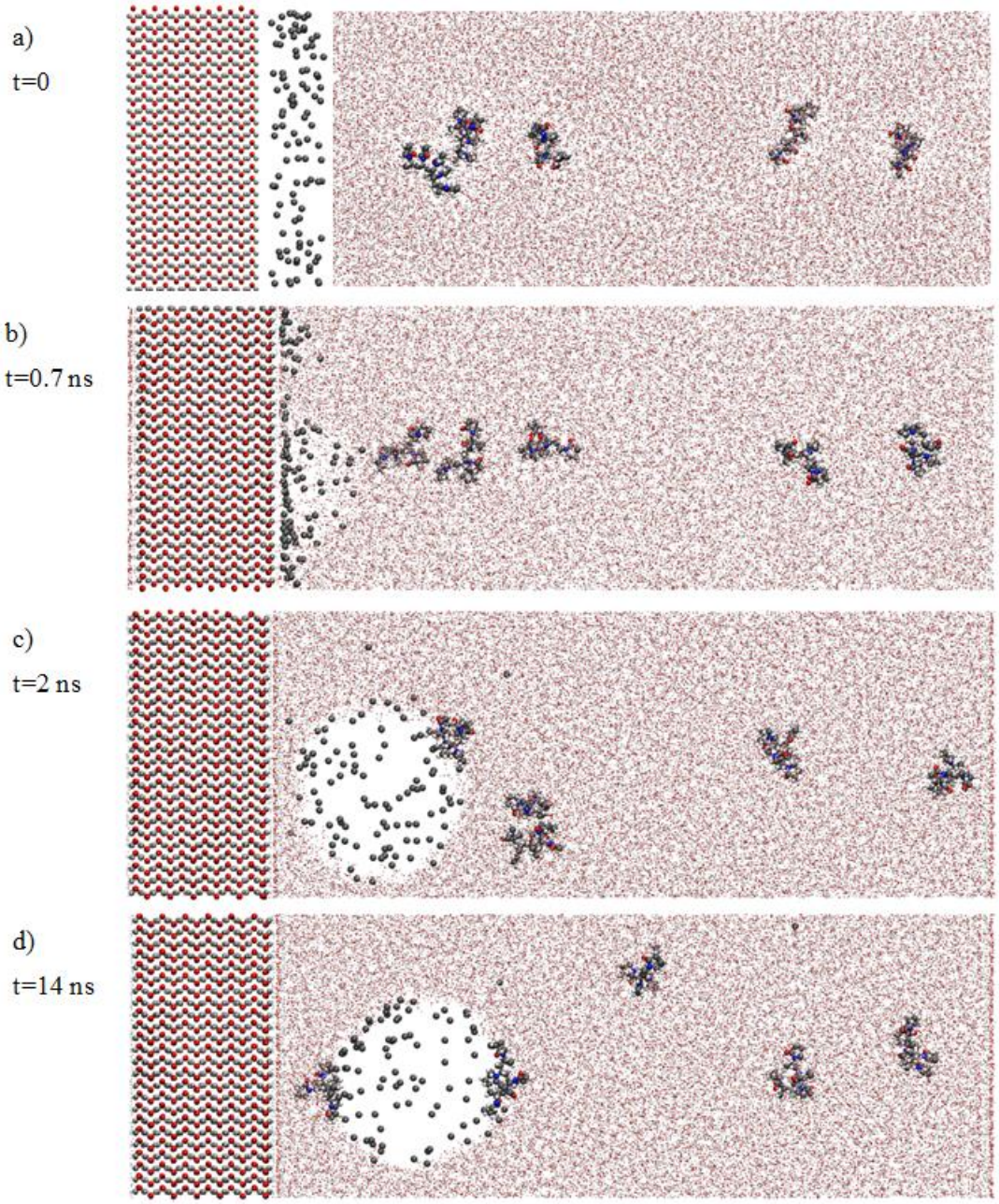

Figure 9.3: a) System 2 – NVT before simulation start. b) The system after 0.7 ns where water forms a bridge of water that goes towards the surface and gets adsorbed on it. c) a methane sphere is formed, some methane molecules seem to lie in the low-density layer and some in the water bulk. One of the PVP molecules interacts with the methane sphere. d) The system after 14 ns. Two PVP molecules are now interacting with methane and one of them is placed close to the hematite surface.

9.1.4 System 2 – NPT

System 2 – NPT is composed by the same components as system 2 – NVP, but in this simulation the NPT ensemble is used. The system before simulation start is equal to the NVT version and is shown in Figure 9.3 (a). Because of the NPT ensemble the volume is regulated until the desired temperature is obtained. 1.2 ns after simulation start the vibration in z-direction has stabilized and a shorter system length of 166.2 Å is obtained. This could again imply that the density of water is too low in the NVT simulation. Figure 9.4 (a) shows the system at this point and water has moved through the methane molecules and covers the hematite surface. Methane is more or less dissolved in the water phase together with the PVP molecules, but some molecules keep together and form a sphere-like shape. Throughout the simulation the methane molecules get a bit more spread out in the water and the PVP molecules move around. Figure 9.4 (b) shows this where the simulation has run for 12 ns. For this system the density was measured to be ~1049 kg/m^3.

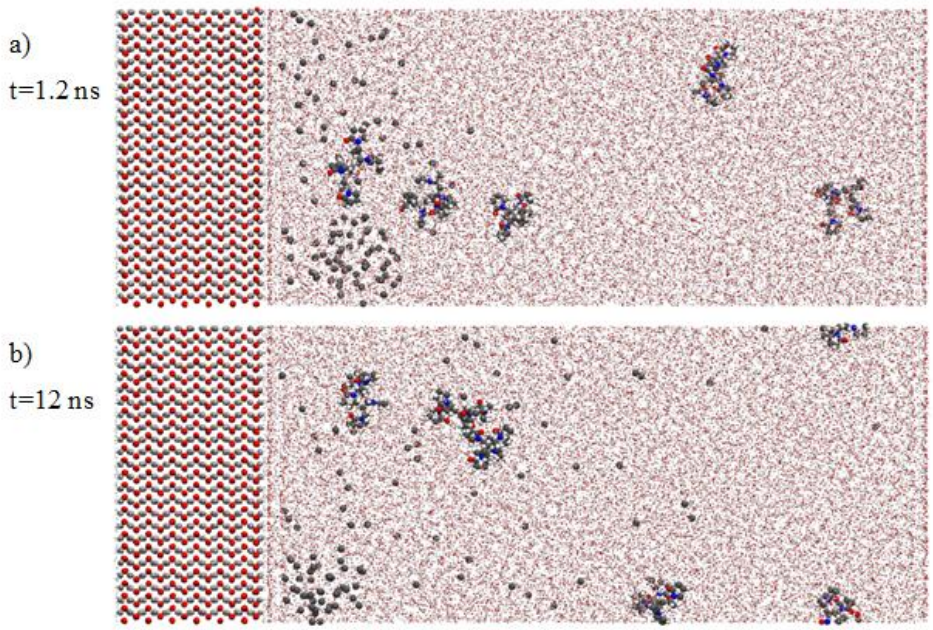

Figure 9.4: a) 1.2 ns after simulation start. Water has moved through the methane molecules and covers the surface. b) System 2 – NPT after 12 ns.

9.1.5 System 3 – NVT

System 3 – NVT is composed by the hematite crystal, a section of methane and a section containing water and PVP. In this system another water model is used, the TIP4P/2005 model. This is used because the water density in the previous simulations gets too high, and this model is supposed to better reproduce the correct density for water. Figure 9.5 (a) shows

a picture of the system before simulation start. After start water moves towards the surface straight through the methane molecules and methane gets dissolved into the water phase. This is shown in Figure 9.5 (b). Methane keeps getting more and more dissolved through the simulation.

In this simulation with TIP4P/2005 water molecules the water gets even more structured near the hematite surface than in the previous simulation systems. At least four layers of water can be observed in Figure 9.5 (c). When density is measured in this system it is ~914 kg/m^3 which is quite unexpected because this model was supposed to provide a better density. By looking at the pictures of the system it can be observed that it seems like the water molecules get some sort of structuring and because ice has a density of 916.7 kg/m^3 at 0° and atmospheric pressure [40, 41] which is lower than water and has more structure, it could indicate that some form of ice-structure is starting to form.

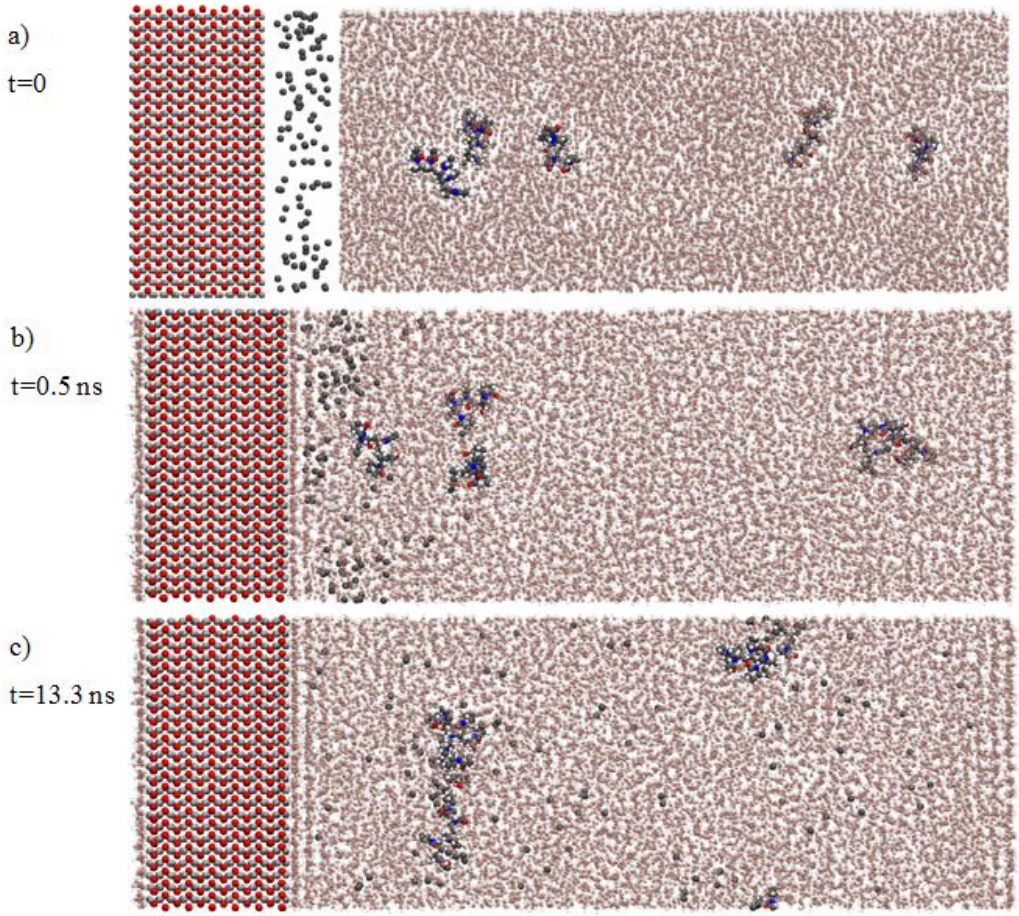

Figure 9.5: a) System 3 – NVT before simulation start. b) After 0.5 ns water has covered the hematite surface and methane starts to dissolve into the water. c) Methane is dissolved in the water phase together with the PVP molecules. Structured water can be observed near the surfaces.

9.1.6 System 3 – NPT

System 3 – NPT has the same components as the corresponding NVT system and the system before start is therefore equal to the NVT system before start and is shown in Figure 9.5 (a). In the start water moves towards the surface through the methane layer and the system vibrates in the z-direction to obtain the desired pressure. After some time the system has stabilized on a length of 164.2 Å and a picture of the system after 1.5 ns is shown in Figure 9.6 (a). After this the water molecules stops moving and it could look like ice-like structures have formed. The PVP molecules keep their position through the whole simulation and the methane molecules stays near the surface and only a few molecules are dissolved into the water phase where they are locked up. A vibration in every direction is the only movement observed in the simulation after this. Figure 9.6 (b) shows a picture of the system after 15 ns and it looks quite similar to Figure 9.6 (a), the only difference is that the system has been compressed a bit more in the z-direction and one of the PVP molecules has changed its orientation. As for the corresponding NVT simulation water shows several density layers near the surface. The measured density in this system is 1073 kg/m^3 which in contrast to the NVT simulation are higher than expected and far from the desired density of 1003.8 kg/m^3.

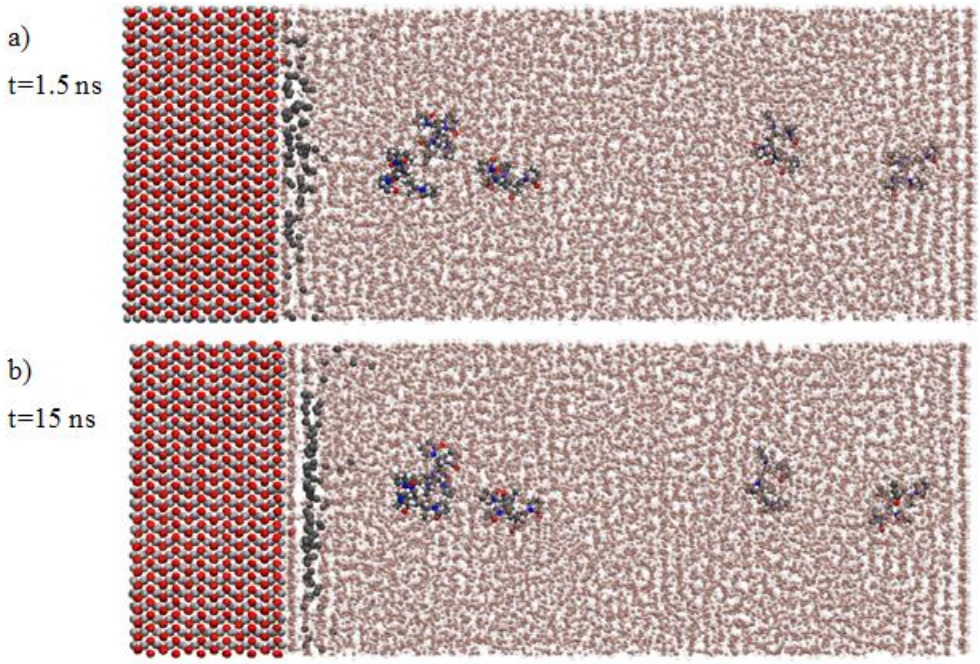

Figure 9.6: a) System 3 – NPT after 1.5 ns. b) Not much has happened through this simulation and after 15 ns it looks quite similar to the situation at 1.5 ns.

The oxygen in water position was tracked every 25 frame over 1000 frames for both the NPT and the NVT simulation and the result is shown in Figure 9.7. Here the NPT simulation can be compare to the NVT version and the water acts different in the two cases. In both simulation the density layers can be observed, where the NPT shows around five layers near the hematite surface without methane and up to six layers can be observed near the same surface in the NVT simulation. Water near the other side of the hematite gets disturbed by the presence of methane, so not that many layers can be observed there. Another thing worth noticing from the NPT simulation is that three of the oxygen atoms in the hematite crystal have moved out of the crystal and have been dissolved into the water phase. These three atoms are marked with a black circle in Figure 9.7 (a).

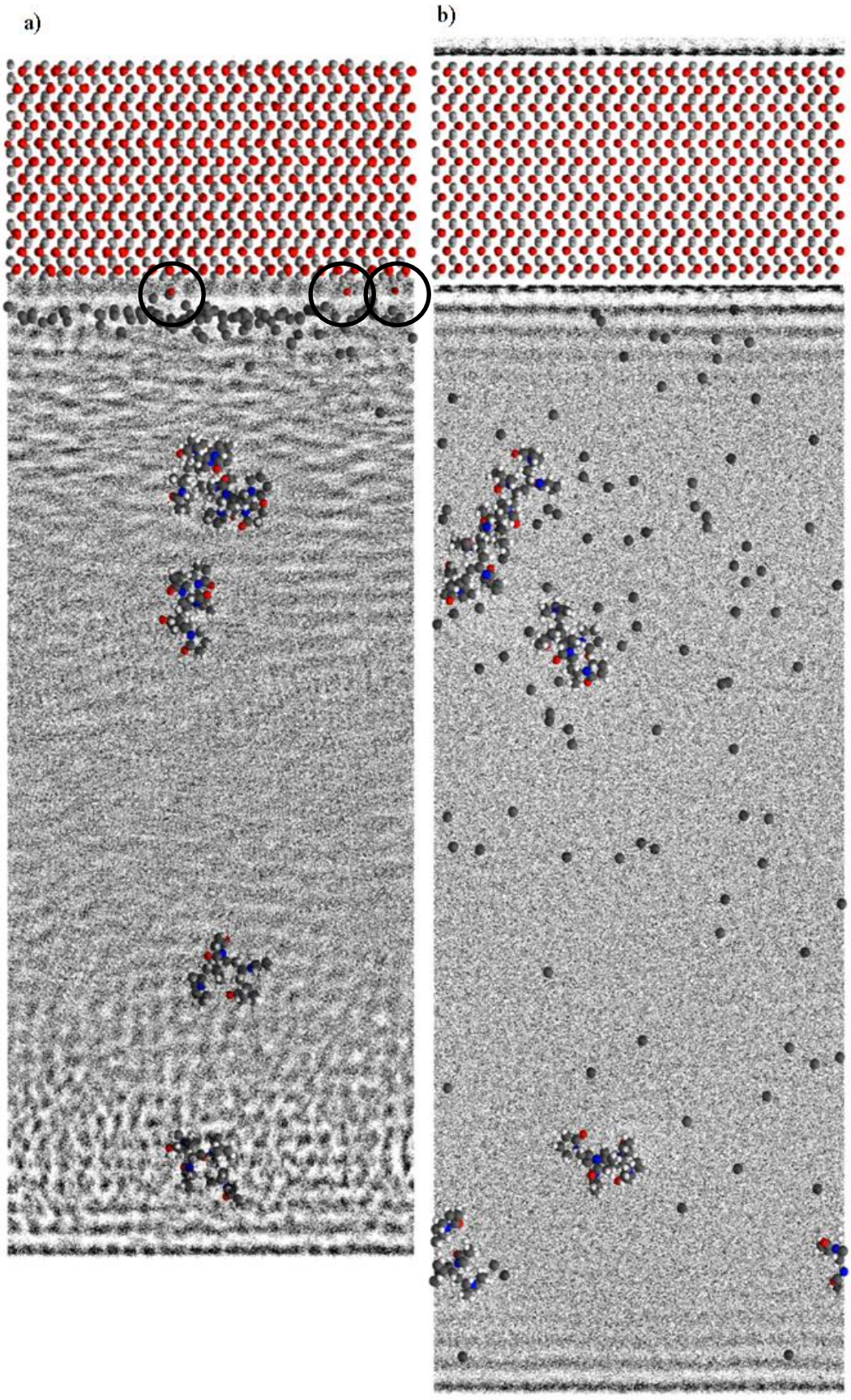

Figure 9.7: a) System 3 – NPT water density profile. b) System 3 – NVT water density profile.

9.2 Density Profiles

Because of the observation of structured water with different density regions towards the hematite surface, density profiles are made and further investigated. The number density of water and methane are measured and a plot for water and methane in each system is shown in Figure 9.8 - Figure 9.14. Water is shown in the upper plot and has a black line while methane is shown in the lower plot and has a grey line. The x-axis is the distance in the z-direction where point 0 is the middle of the system and the hematite is placed on the left side.

The number density plot for System 1 – NVT is shown in Figure 9.8. The water phase ranges from around -63 Å to around 92 Å in the z-direction and has a length of 155 Å. The hematite crystal surface is located on each side of the water phase. Water has a relatively high density near the surfaces compared to the density in bulk. This is due to the way hematite interacts with water and these density layers are made. The number density in water bulk is 0.0037 and the mass density is 1037 kg/m^3. Two peaks can be observed for water on the left side of the system and indicates the presence of two layers of structured water while three peaks can be observed on the right side which indicates that three layers of water are structured by the hematite. The length of the structured water face on the left side is around 8Å while the length on the right side is around 10 Å. A reason for the different amount of layers on the two sides is the presence of methane on the left side, which could disturb the water phase. The number density gets lower where methane is present in the system, but it does not necessarily indicate that the mass density of water is lower here. Most of the methane stays at the same place between -55 and -20 Å during the simulation which also is seen in the general observations where methane gathers together and forms a sphere.

Figure 9.9 shows a plot of the number density of water and methane in the system 2 – NVT simulation which looks quite similar to recently discussed plots for system 1 – NVT. The only difference between the two systems is that 5 molecules of PVP are present in system 2. Water has two peaks on the left side and three peaks on the right side in the system, an indication of two layers of structured water on the left side and three layers on the right side. Also here the number density in bulk water is 0.0037 and the length of the structured water layer on the left side is 8 Å and 10 Å on the right side. Methane is located in the same area around -55 and -20 Å. From the density profile it is impossible to discern any effect that PVP may have on the system.

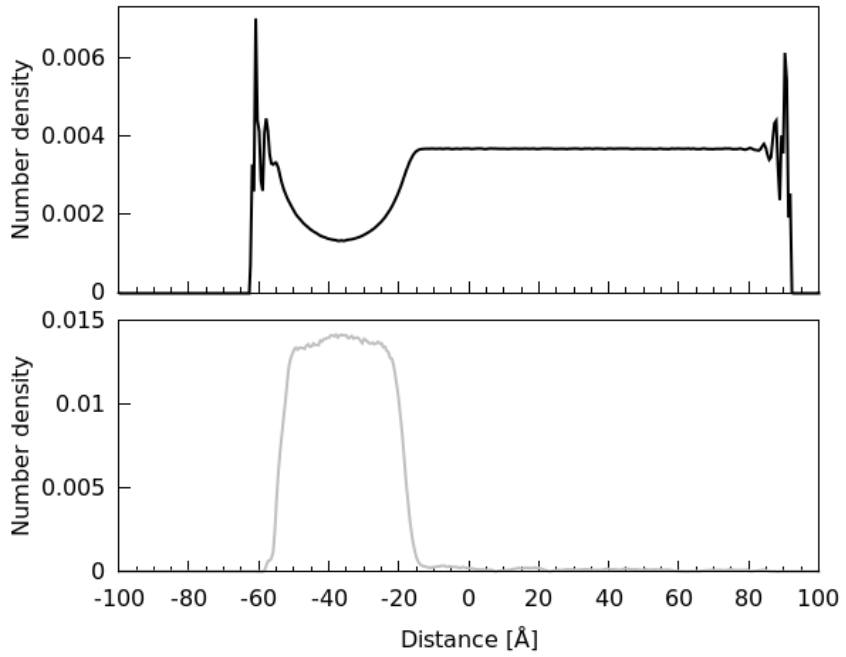

Figure 9.8: Density plot of system 1 NVT. The black line is for water and the grey line is for methane.

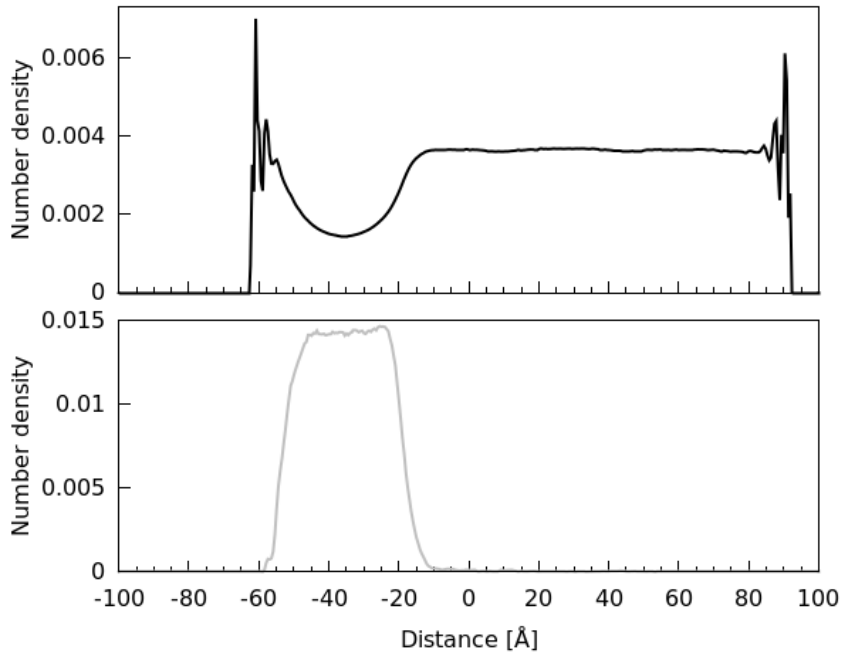

Figure 9.9: Density plot of system 2 NVT. The black line is water and the grey line is methane.

Number density for water and methane in the system 1 – NPT simulation is shown in Figure 9.10. The plots for system 2 – NPT are shown in Figure 9.11 and are almost identical so the following discussion applies to both of these systems. Here the black graph for water density has three peaks on both the left and the right side of the system, indicating three layers of structured water. The layer closest to the surface has a higher density than the second layer which again has a higher density than the third layer. For both systems the number density in bulk is 0.0037. Both sides have a similar length of the structured water of 10 Å. Methane is more distributed in the system 1 and 2 NPT simulations than in the system 1 and 2 NVT simulations, but most of the molecules are located on the right side of the system. The graph showing the methane number density has two peaks on the left side of the system. Where the water graph has a peak, the methane graph has a peak indicating that methane is located in the high-density area of the layers of structured water.

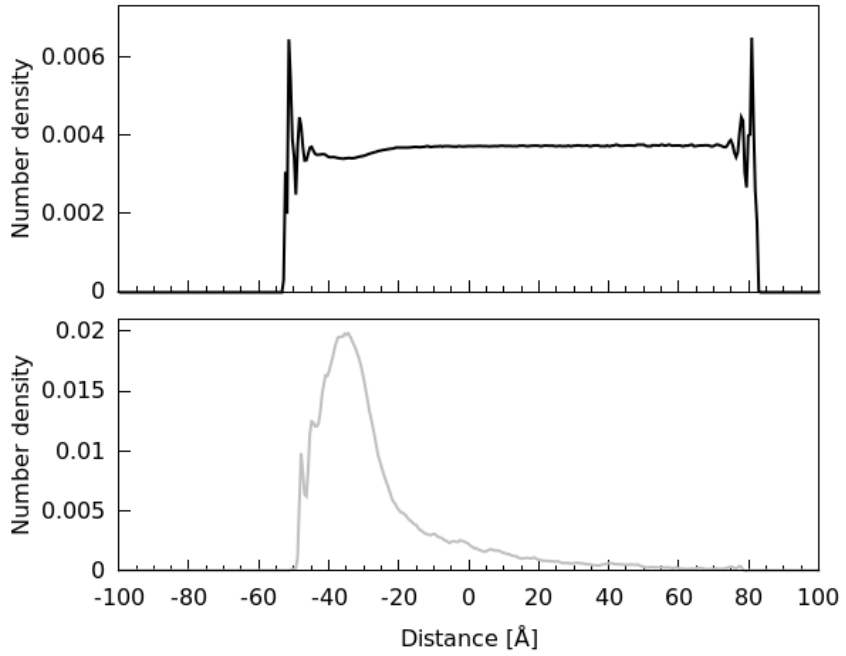

Figure 9.10: Density plot of system1 NPT. The black line is water and the grey line is methane.

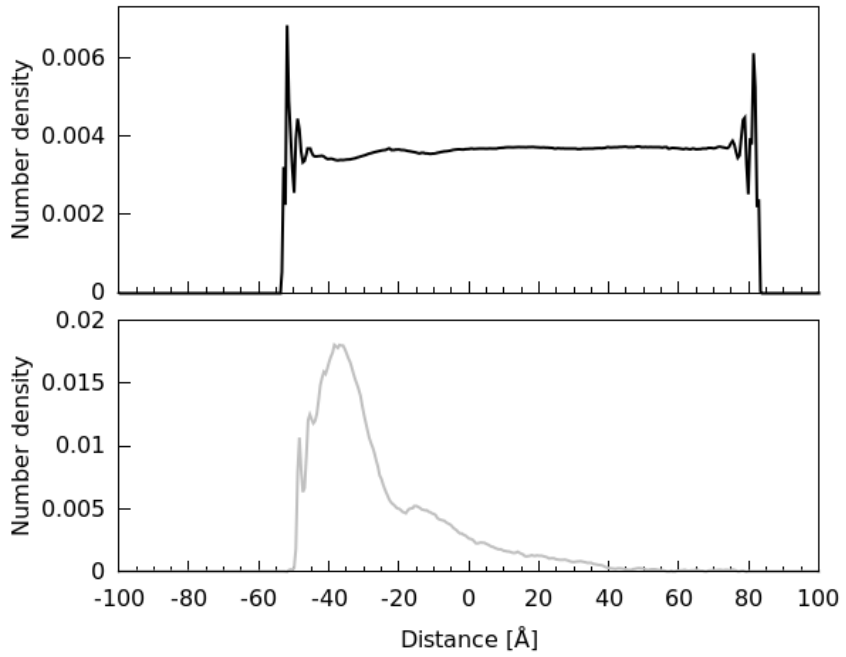

Figure 9.11: Density plot of system 2 NPT. The black line is water and the grey line is methane.

Figure 9.12 shows the number density of the System 3 – NVT simulation where TIP4P/2005 is used to model the water. This system gets a lot of peaks on the black graph showing the number density for water. A total of six peaks can be counted on each side of the system which indicates six layers of structured water. These six layers of structured water were also observed by visually looking at the simulation, discussed under general observations. The total length of structured water on each side is around 18 Å in contrast to the length of around 10 Å for the simulations using the modified TIP3P. Another difference from the systems with the modified TIP3P model is that the number density in water bulk is 0.0032, a lower number density. Because the modified TIP3P model provided a density that was too high the TIP4P/2005 model was used, but it provided an even lower density than the target density.

This system does also have the highest distribution of methane. Here the grey graph showing the methane density gets five peaks on the right side on the location where the water graph has its peaks, and this could indicate that the methane molecules are located in the high-density area of the layers of structured water, and not in the low-density area between the water layers. One reason for this could be that Lennard-Jones forces are responsible for the low-density area and when no water can be located there, there will be volume left for methane. This can also be observed on the left side of the system. Figure 9.13 shows a plot of both methane and water number densities where it can be observed that the top of the peaks

are located on the same spot. The peaks in the water graph has higher peaks on the right side than on the left side, and a reason for this may be that more methane is present on the left side and could have an effect on the structuring of water.

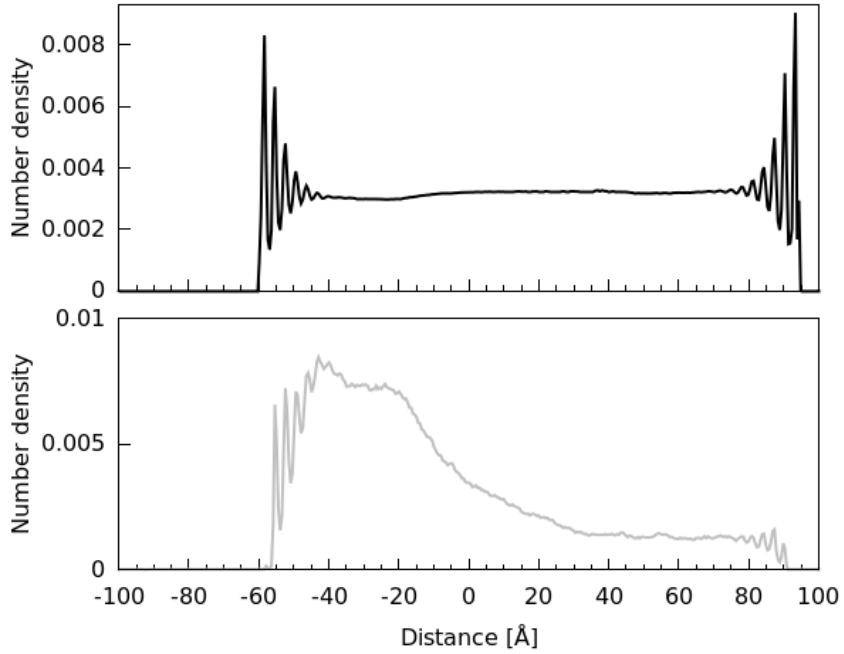

Figure 9.12: Density plot of system 3 NVT. The black line is water and the grey line is methane.

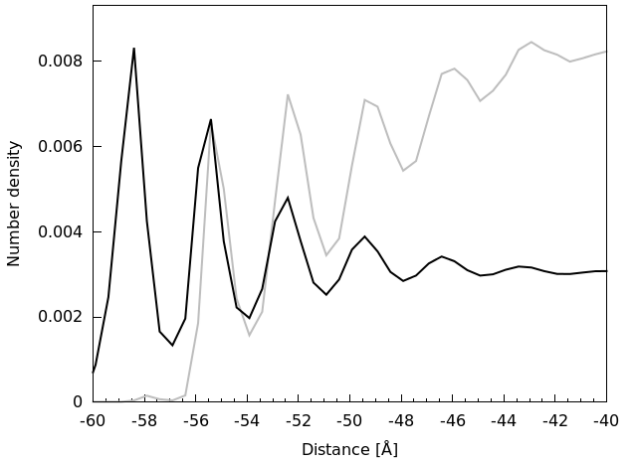

Figure 9.13: A close up of the plot from -60 to -40.

The plots for water and methane number density from the system 3 – NPT simulation are shown in Figure 9.12. This looks a bit different than the corresponding NVT simulation. Here there is only one peak on the left side of the black water graph while the right side has 6 peaks. The peak on the left side is in addition not as high as the highest peaks on the right

side. The length of the structured water layers on the right side is 18 Å, the same as the length on both sides in the system 3 – NVT simulation. On the left side there is a negative peak and on the same location on the grey methane graph there is a very high peak, implicating that all methane molecules are located there which also is confirmed in the visual observation. This is likely the explanation of the lack of structured water on this side. Another thing worth noticing is the number density in the water bulk. All the other simulations have a close to straight line for the number density in the water bulk area, implying a uniform density, but here it varies through the whole water phase. As no methane molecules are dissolved into the water bulk it is not reasonable to believe that methane has any influence on the water number density. Recalling from the visual observations in chapter 9.1 this system had a behavior that does not resemble any of the other systems. It looked like the system got an ice-like structure so this may be the reason for the variations in the number density in water bulk.

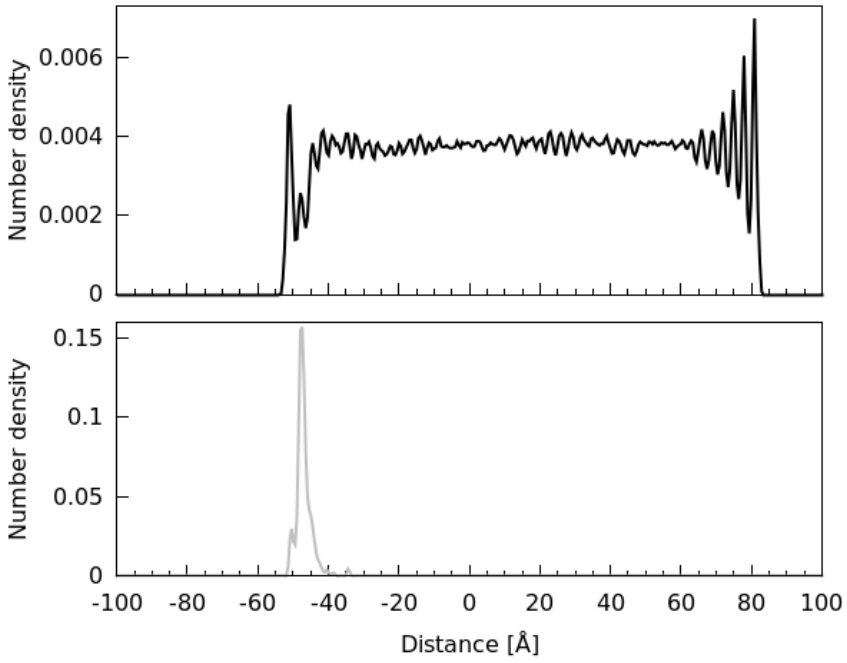

Figure 9.14: Density plot of system 3 NPT. The black line is water and the grey line is methane.

9.3 Orientation of Water Molecules

To find out how the water molecule is oriented towards the hematite surface the structure parameter is calculated. The structure factor S(z) and the cosine of the angle is plotted as a function of the distance in z-direction for each simulation system and they are shown in Figure 9.15 – Figure 9.21. Because the graph is stable in the water bulk this section is cut out of the plot and only the sides are shown. A small plot showing the complete graph is shown at the top of each plot on the left side.

Figure 9.15 shows the plots for the system 1 – NVT simulation. A structure factor close to 0.25 for water is measured on both sides of the water phase towards the hematite surface. This means that the average dipole vector in the water molecule is oriented close to either 45°, 135°, 225° or 315° on the surface. The corresponding negative peak in the cosine plot on the left side of the system with a value of around -8 corresponds to an orientation of either 135° or 225°. On the right side the corresponding cosine plot has a peak with a value of around 0.7 which corresponds to an orientation of either 45° or 315 ° and is pointing in the opposite directions from the left side. With these orientations one of the hydrogen atoms in water points towards the surface. The second peak on the cosine graph on the left side has a positive value of around 0.7 and indicates that the second layer of structured water has an opposite orientation from the first layer. This is also the case on the right side. In water bulk the structure factor is zero implying that there is no clear structuring of water here. Plots for system 2 – NVT are quite similar to the ones for system 1 – NVT so the recent discussion applies to this as well and the plots are shown in Figure 9.16.

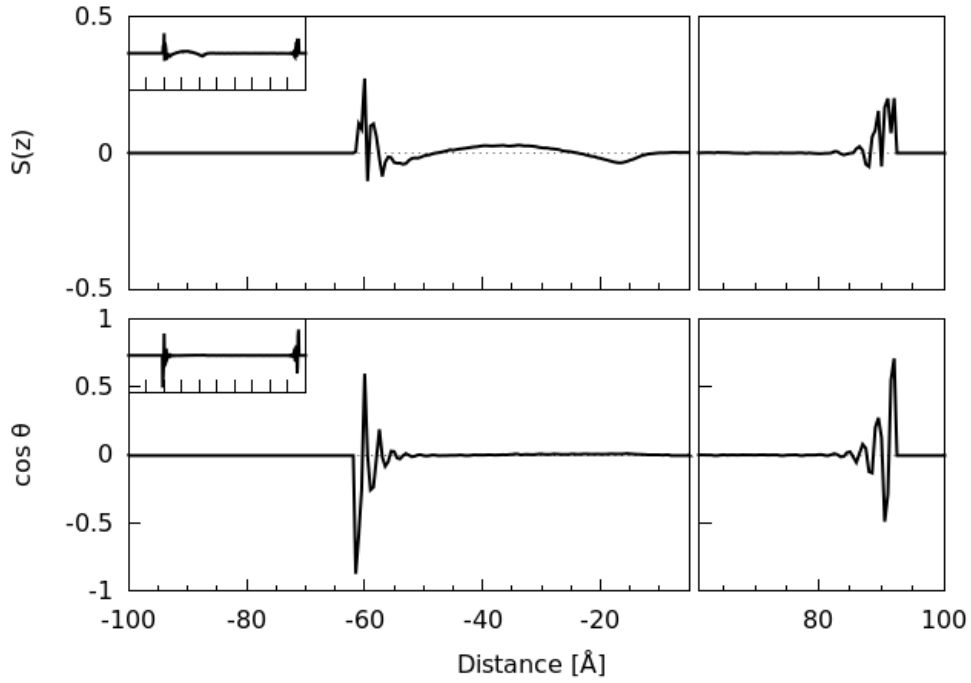

Figure 9.15: Structure parameter and cosθ for system 1 – NVT.

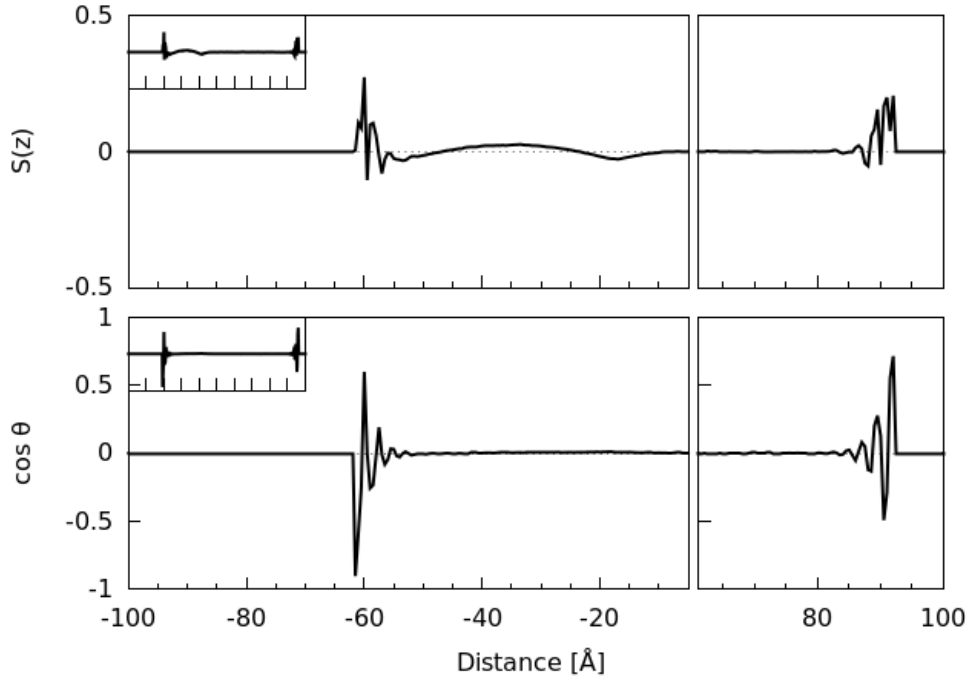

Figure 9.16: Structure parameter and cosθ for system 2 – NVT.

Figure 9.17 shows the plots for the system 2 – NPT simulation. These plots are not very different from the recently discussed simulation systems. The outermost peaks on both sides

on the structure parameter graph is close to 0.25 and the corresponding values for the cosine graph indicates that the first layer of structured water on the left side has an orientation of 135° or 225° on the hematite surface and the first layer on the right side has an orientation of 45° or 315° on the surface. Similar to the mentioned systems the second layer of structured water has the opposite orientation towards the surface. The structure factor in water bulk is zero here as well so it can be assumed that water does not get structured in bulk.

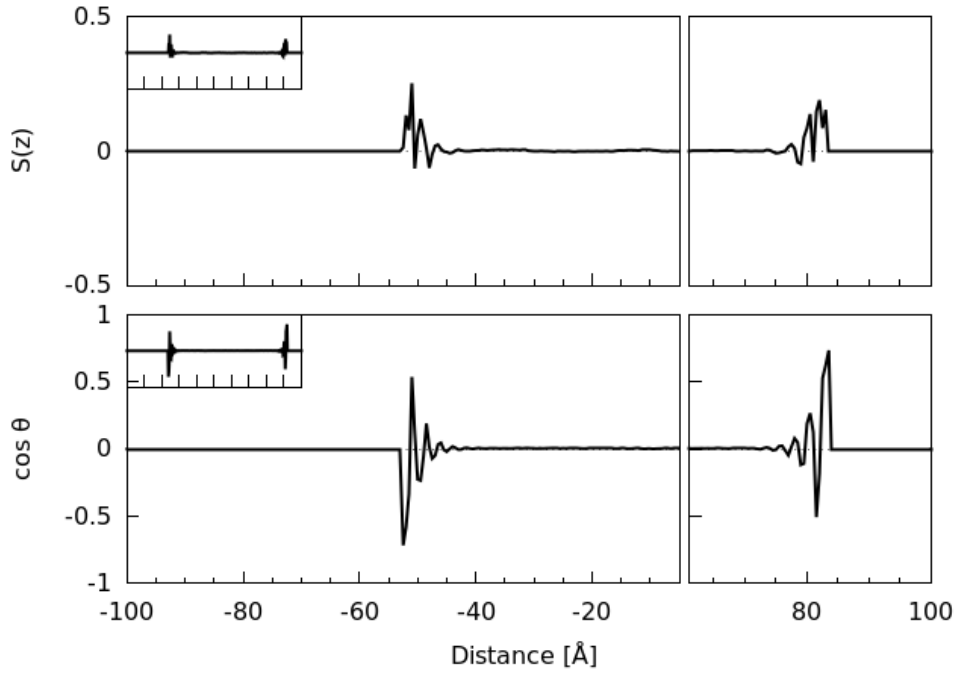

Figure 9.17: Structure parameter and cosθ for system 2 – NPT.

In Figure 9.18 the plots for the system 1 – NPT is shown. On the left side of the system the graph looks quite similar to the ones already discussed. The structure factor is close to 0.25 towards the hematite surface and the corresponding value from the cosine graph is approximately -0.7 implicating an orientation of water of around 135° or 225° on the hematite surface. The second peak on the cosine is close to 0.6 indicating that the second layer of structured water is oriented close to the opposite direction of the ones in the first layer.

On the right side of the system this plot has a value of 0.9 for the structure parameter which distinguishes this from the other graphs discussed. With a corresponding cosine value of 1 it indicates that the first layer of water is oriented close to perpendicular towards the hematite surface. By taking a closer look in the simulations it can be observed that ~7 molecules of

water has this orientation close to the surface and this is shown in Figure 9.19. It can also be seen that the water molecules have the expected orientation on the other side. The next peak on the structure factor is around 0.2 and the corresponding cosine is -0.6 indicating that the next layer looks more like the second layer on the left side and in the recently discussed simulations.

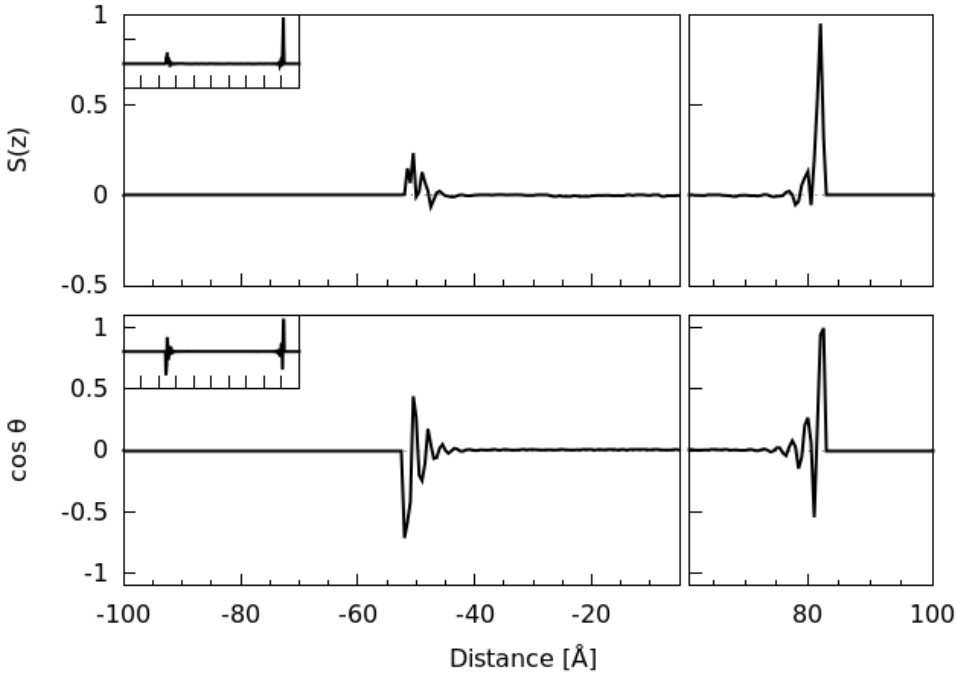

Figure 9.18: Structure parameter and cosθ for system 1 – NPT.

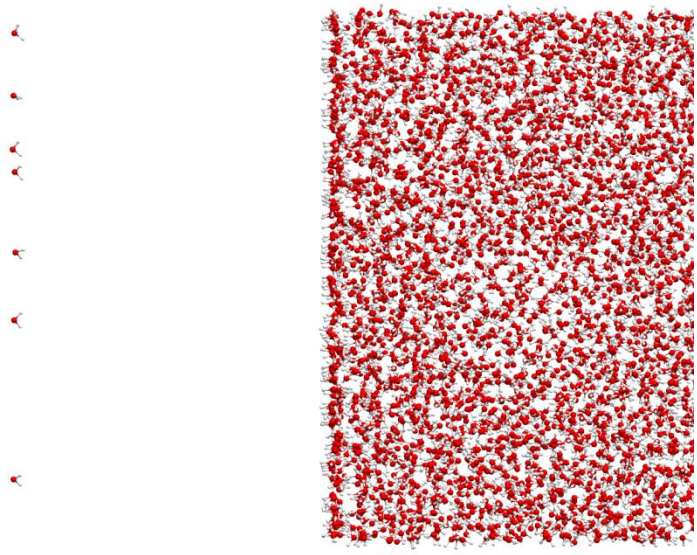

Figure 9.19: A picture showing the water molecules with a different orientation towards the surface.

The plot for the structure parameter for system 3 – NVT and the corresponding cosine plot are shown in Figure 9.20. The structure factor does not look like any of the previous graphs for structure factor. Here it has a structure factor of around -0.2 in water bulk which could imply a structuring of the water molecules in bulk. The corresponding cosine value is 0. On the sides close to the hematite crystal one peak on each side is slightly positive and the following peaks get a negative value. The cosine graph does not look that different from the other systems, it has a larger number of peaks but the density profile for this system showed that the systems with the TIP4P/2005 water model gets more layers of structured water and thereby more peaks. Recalling from the visual observation of this system it was noticed that it looked like water phase had some form of structuring and that maybe some type of ice is starting to form. This might be the reason for this value of -0.2 for the structure parameter.

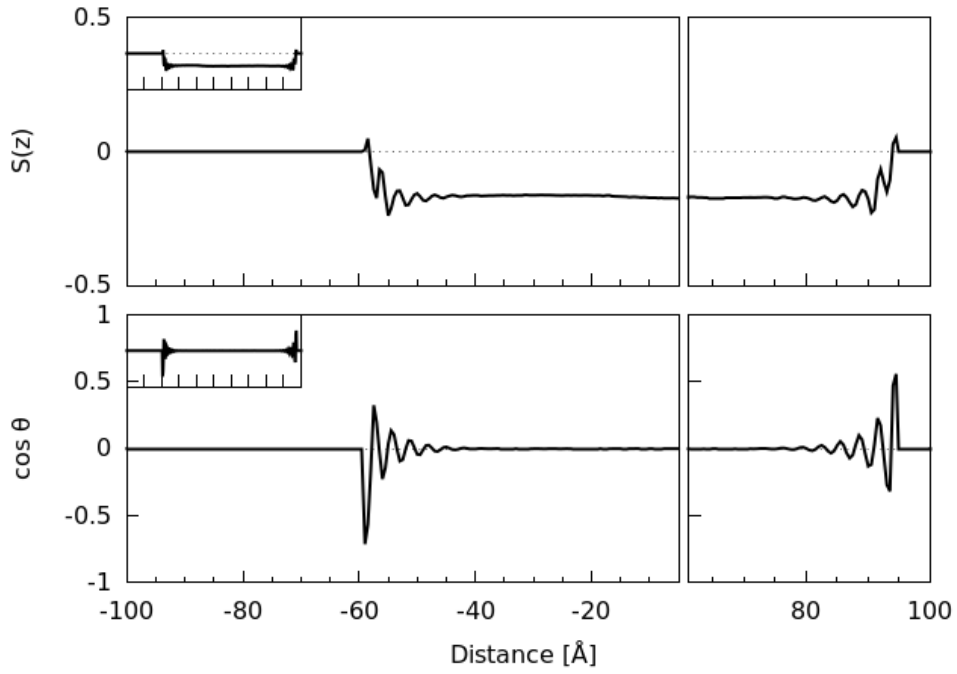

Figure 9.20: Structure parameter and cosθ for system 3 – NVT.

Figure 9.21 shows the structure parameter and cosine graph for the system 3 – NPT simulation. As for the system 3 – NVT simulation this simulation gets a negative structure factor for the water bulk area, but here it varies a lot between a value of -0.2 and -0.25. The corresponding cosine graph also varies a lot around a value of zero. Near the hematite surface

the structure factor has some peaks that are a bit clearer than the peaks in the water bulk. The cosine graph has two major peaks, one on the left side and one on the right side. These peaks are quite similar to the first peaks on the other systems cosine plots, but a second peak is not that easy to detect here. From the visual observations it was observed that after a short time the molecules stopped moving and it seemed like some sort of ice-structure was formed. This may be the reason that the structure factor comes out like this.

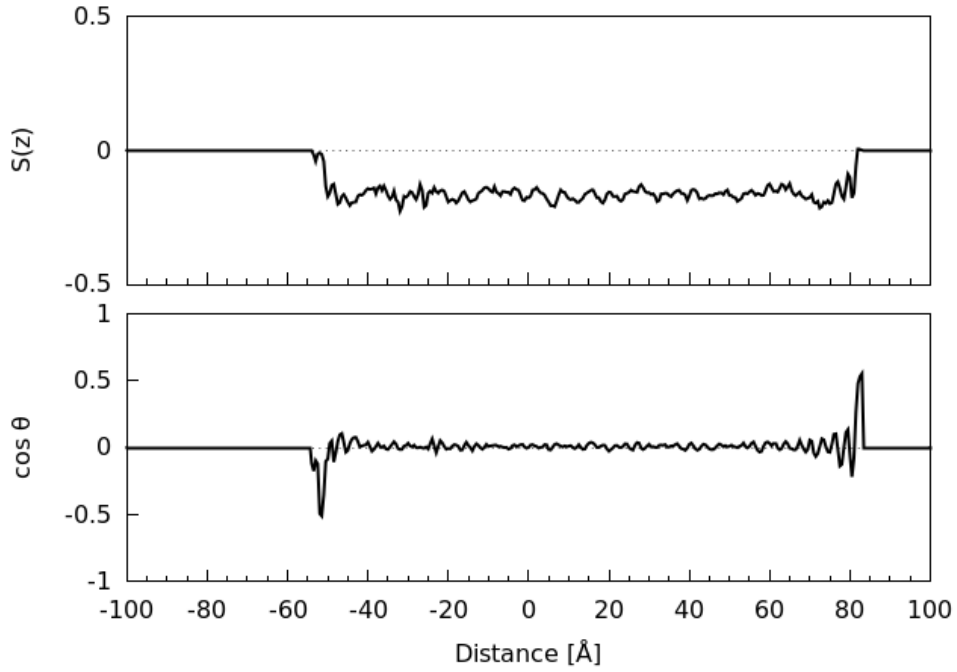

Figure 9.21: Structure parameter and cosθ for system 3 – NPT.

9.4 Radial Distribution Functions

The radial distribution functions (RDF) plots are presented and discussed in the following sections.

9.4.1 Water – Hematite

The RDF plots for water (TIP3P) and hematite are shown in Figure 9.22 and for water (TIP4P/2005) and hematite is shown in Figure 9.23. System 1 and 2 for both NVT and NPT simulations get comparable results for both sides of the hematite crystal so plots for only one of these systems are shown her, in this case for the system 1 – NVT simulation from the left side of the system. This indicates that depending on what type of water model being used (modified TIP3P or TIP4P/2005) water gets a slight change in the orientation towards the hematite surface even though this is unexpected. This is also verified on basis of the structure parameter, S(z) in chapter 9.3. A selection is made where only the outermost oxygen and iron atoms on the hematite crystal are regarded in these RDF plots, so the hematite bulk is not considered because water never interacts with these atoms. This affects the normalization of the plots because water only is present on one side of the selected atoms.

Figure 9.22 (a) shows a graph for hematite and oxygen in water (red), a graph for hematite and hydrogen in water (blue) and a graph for hematite and water (black). It can be observed that water can be found approximately 1.7 Å from the hematite surface due to the peak in the black graph. The corresponding peak in the blue graph indicates that it is the hydrogen atom in water which is the one that lies at this position and closest to the hematite surface. This can also be seen in the simulations. To find out which atom in the hematite that lie closest to water and the atoms in water, a similar plot is made for only oxygen in the hematite crystal shown in Figure 9.22 (b) and one is made for only iron in the hematite crystal shown in Figure 9.22 (c). From the black graph in (b) it can be concluded that water lies further away from the iron atoms than the oxygen atoms in the hematite. This is confirmed by looking at the black graph in (c) which shows that water lie closer to the oxygen atoms. From (b) it could also be observed from the red graph that the oxygen atoms in water lie closer to iron in hematite than the hydrogen atoms in water, seen from the blue graph. Around 2.2 Å separates iron in hematite and oxygen in water while the distance between iron and hydrogen in water is around 3 Å. Similarly from (c) it can be seen from the blue graph that the hydrogen atoms in water lie closer to the oxygen atoms in hematite than the oxygen atoms in water, observed from the red graph. The distance from oxygen in hematite to hydrogen in water is around 1.7

Å and to oxygen in water it is around 2.8 Å. The graphs in the three plots do all have several peaks for water which shows the different density layers of water near the surface discussed in chapter 9.2.

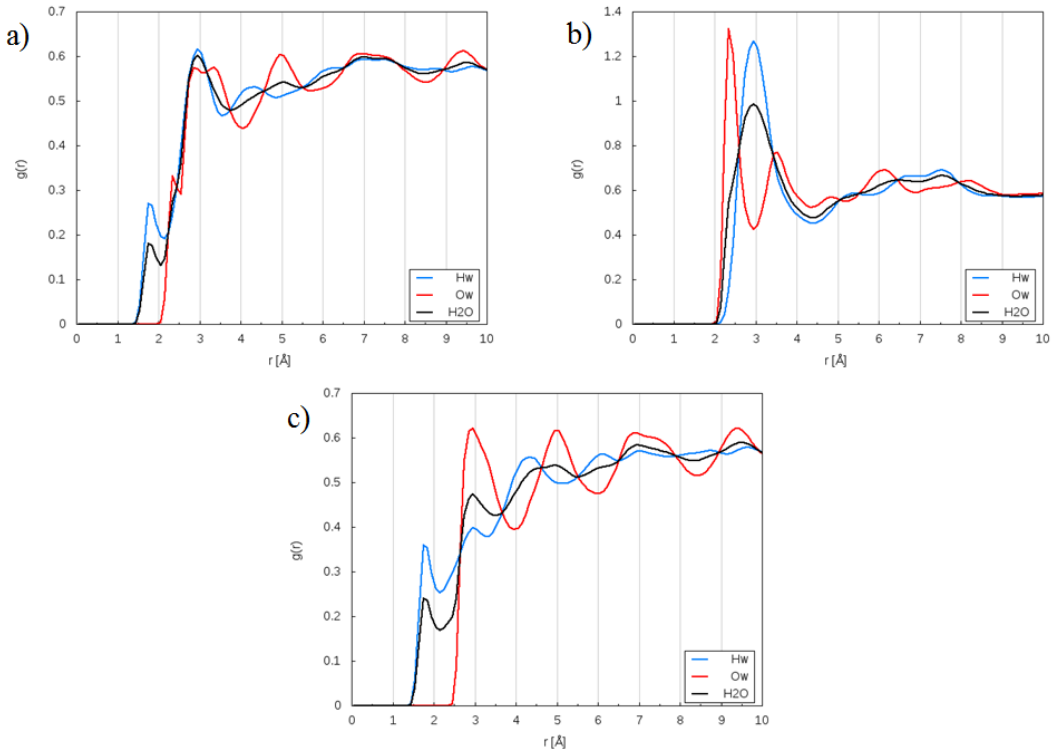

Figure 9.22: a) Hematite water RDF. b) Iron in hematite water RDF. c) Oxygen in hematite water RDF. This is for the modified TIP3P water model.

RDF plots for the different sides of the NVT simulation of system 3 are identical. The result for the left side of the NPT simulation are almost identical to the ones in the NVT simulation, but the right side of the system differs from the other sides so both sides of the system 3 – NPT simulation are shown here. The plots are shown in Figure 9.23 and Figure 9.24. In general the plots for the left side and the right side have the same peaks for water, hydrogen in water and oxygen in water towards the hematite surface (a), iron in hematite (b) and oxygen in hematite (c) as the previously discussed systems, but some peaks for hydrogen in water and oxygen in water have a shorter distance between them. This could indicate that water has a different orientation towards the hematite surface. The numbers of peaks on the water graphs in Figure 9.24 are greater than for the simulations recently discussed with the modified TIP3P water model, indicating that water from TIP4P/2005 gets more structured and gets more layers of water. Figure 9.23 (a) shows that the black graph only has three major peaks which

indicates that water only has three layers of structured water towards the surface on the left side, where the reason for this is that most of the methane molecules are located near the hematite surface on the left side of the system. This methane layer is also discussed in the general observations section. When analyzing the density profiles in chapter 9.2 the difference in amount of layers of structured water in a TIP3P system and a TIP4P/2005 system was observed.

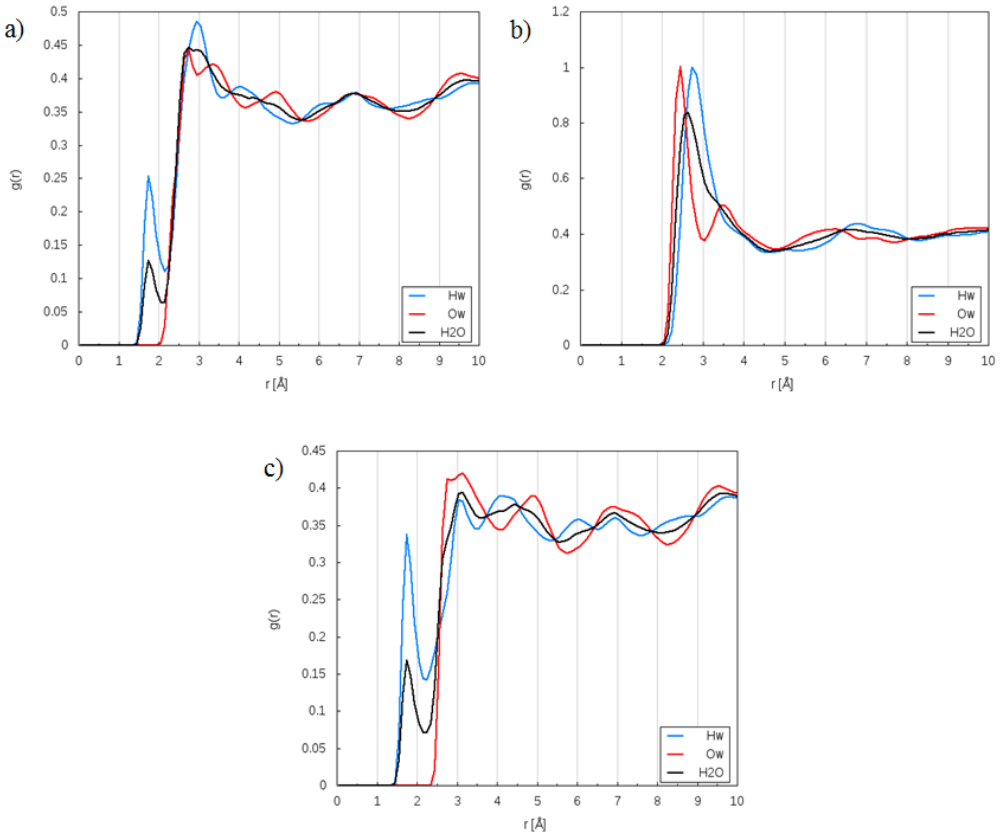

Figure 9.23: a) Hematite water RDF. b) Iron in hematite water RDF. c) Oxygen in hematite water RDF. These plots are for the left side of the system where methane is present and for the TIP4P/2005 water model.

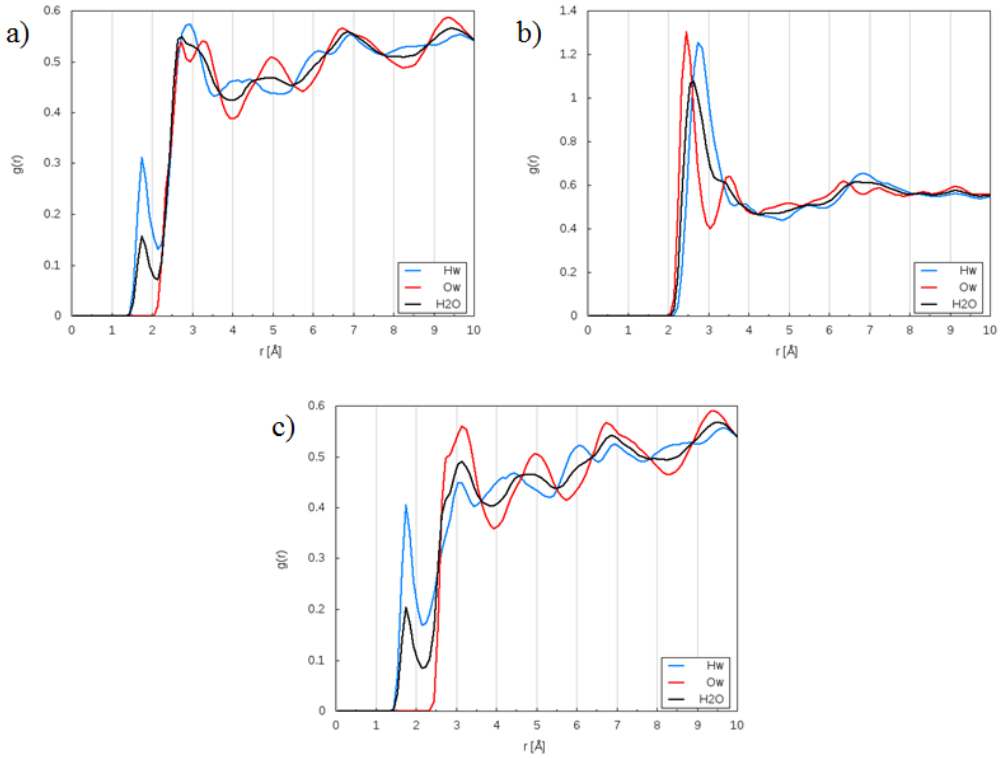

Figure 9.24: a) Hematite water RDF. b) Iron in hematite water RDF. c) Oxygen in hematite water RDF. These plots are for the right side of the system where no methane is present and for the TIP4P/2005 water model.

9.4.2 Water – PVP Interaction

Radial distribution function plots are also made for water and PVP. PVP is supposed to interact with water and restructure it and the most likely atoms to make sure of this are the oxygen atom and the nitrogen atom in the lactam ring. This can be assumed because both of them tend to make hydrogen bonds with hydrogen in water. System 2 and 3 both contain PVP molecules and the resulting radial distribution plots for both systems and for NVT and NPT simulations were nearly identical so they are only shown for one system, the system 2 – NVT simulation. The RDF plots are shown in Figure 9.25 where (a) is a RDF plot for PVP and water, (b) is a RDF plot for the oxygen atom in PVP and water and (c) is a RDF plot for the nitrogen atom in PVP and water. The black graph is for water, the blue graph if for hydrogen in water and the red graph is for oxygen in water.

In (a) the first peak on the black graph indicates that the distance between a PVP molecule and a water molecule is 0.8 Å, and because of a corresponding peak on the blue graph it can be assumed that it is the hydrogen atom in water that lie closest to the PVP molecule. The red graph has a peak on 2.8 Å Å which indicates that this is the distance between an oxygen atom in water and a PVP molecule. To find out if it is the oxygen atoms or the nitrogen atoms in

PVP that has the largest impact on the water structure plot (b) and (c) is studied. The black graph and the blue graph in (b) has a large peak around 1.8 Å and this could indicate that oxygen in PVP and hydrogen in water makes a hydrogen bond of this length. In the same plot the red graph has a large peak around 2.7 Å which is the indicated distance between oxygen in PVP and oxygen in water. For plot (c) the black graph has its first peak around 5.9 Å indicating that water in general are located this far away from the nitrogen atom in PVP. The blue graph shows a small peak around 3.7 Å so it is likely that hydrogen in water can be located at this distance from the nitrogen atom. This is not an indication of a strong hydrogen bond between nitrogen and water. Because of this it is most likely to believe that it is the oxygen atom in PVP that is responsible for restructuring the water molecules. Based on the molecular structure of PVP the nitrogen atoms may not be as exposed to water as the oxygen atom is, and it will not be as capable of making hydrogen bonds to water.

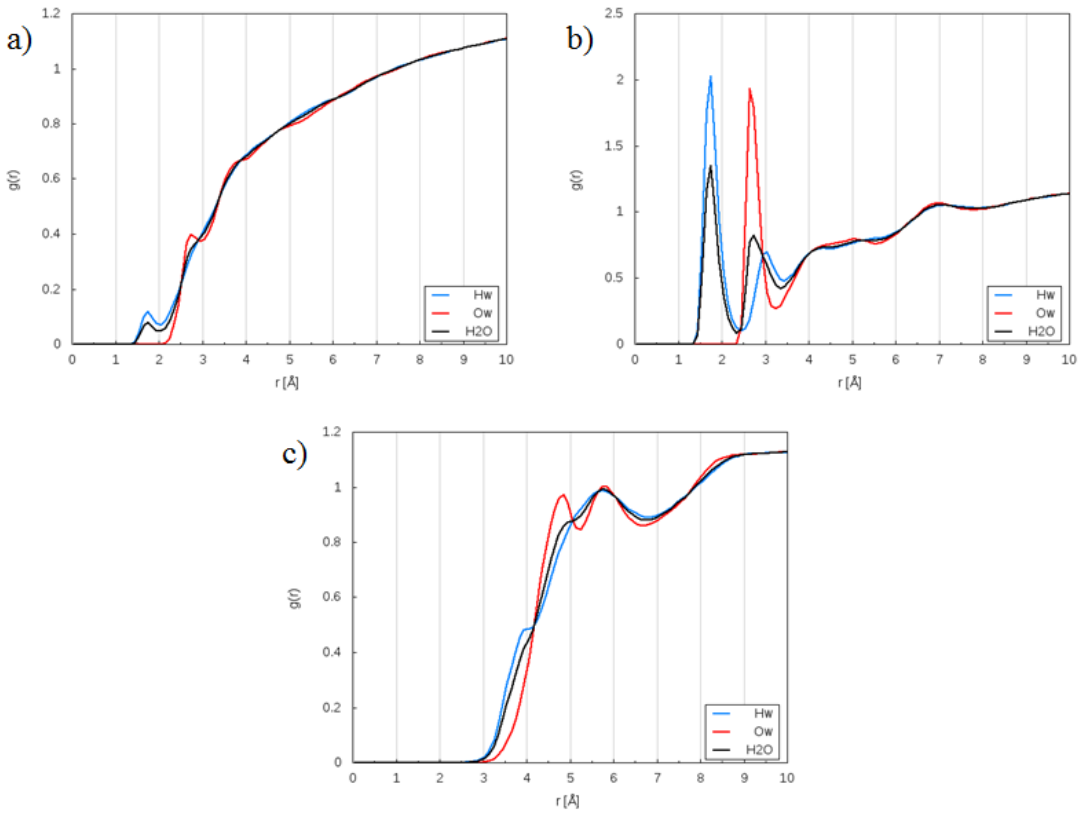

Figure 9.25: a) PVP – water RDF. b) Oxygen in PVP – water RDF. c) Nitrogen in PVP – water RDF.

9.5 Signs of Hydrate Structure

To check if there are signs of hydrate structure starting to form, an analysis of how many water molecules present around each methane molecule is done. A plot is made for each methane molecule, where the amount of water molecules within a distance of 5 Å surrounding it through the whole simulation is shown. The average number of water molecules is calculated by a rolling mean over 50 frames and this is used as data for the plots. In these systems the only guest molecule (hydrate former) is methane. Because only methane is present as a guest molecule (hydrate former) in these systems it is likely to believe that the type of hydrate which could form in these simulations is the structure I hydrate. Structure I hydrates consists of the small 5^{12} cavity which surrounds a guest molecule by 20 water molecules and has a mean cavity radius of 3.95 Å and the large $5^{12}6^2$ cavity which surrounds a guest molecule by 24 molecules of water and has a mean cavity radius of 4.33 Å [42].

In the simulations methane has three major types of locations, the first is in water bulk, the second is near the hematite surface inside the high-density layer of water and the last is inside the sphere which forms in the NVT simulation of system 1 and 2 with TIP3P as water model.

Figure 9.26 shows a plot of the number of water molecules surrounding one of the methane molecules in the system 1 – NVT simulation through the whole simulation. This methane molecule is dissolved into the water bulk for a long time through the simulation. From around frame 3000 to frame 7000 it has approximately 22-24 molecules of water surrounding it. Figure 9.26 also shows a picture of the methane molecule where the water molecules within a radius of 5 Å surrounds it. The blue bonds are hydrogen bonds. On the right side a hexagonal face is formed. As the large cavity contains two hexagonal faces this could be an indication of a hydrate cavity starting to form.

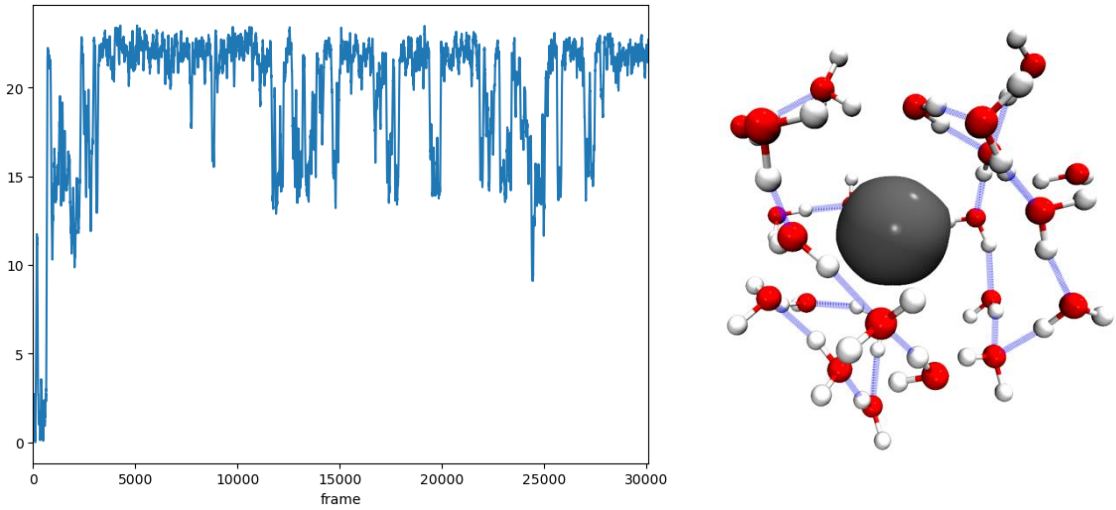

Figure 9.26: On the left side; the plot of number of water molecules surrounding a methane molecule in water bulk. On the right side; the corresponding methane molecule shown in the simulation with the surrounding water molecules shown.

A methane molecule placed in the methane sphere that forms in the NVT simulation for system 1 and system 2 is sometimes inside of the sphere and sometimes in the interface between methane and water. In Figure 9.27 a plot for such a methane molecule in the system 1 – NVT simulation and the same methane molecule with water molecules within a radius of 5 Å surrounding it. A methane molecule placed in the sphere has an average of one to eight molecules of water that surrounds it through the simulation. The methane molecule only has water on one half of its surface.

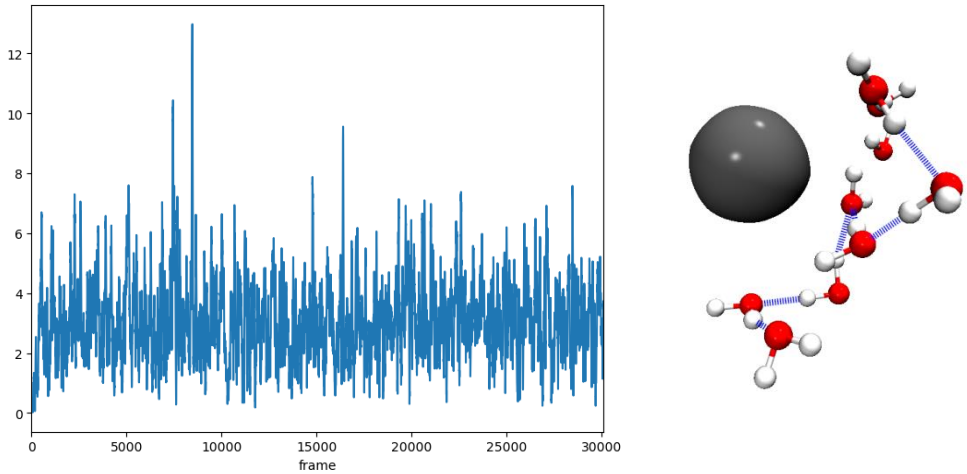

Figure 9.27: On the left side; the plot of number of water molecules surrounding a methane molecule lying in the sphere and which sometimes is located in the interface between methane and water. On the right side; the corresponding methane molecule shown in the simulation with the surrounding water molecules shown.

In Figure 9.28 the plot of a methane molecule that moves out of the sphere and gets adsorbed into the high-density layer of the structured water near the hematite crystal surface for a limited time is shown. It also shows a picture of this methane molecule when it is located in the high-density layer with water within a radius of 5Å surrounding it. From around frame 5500 to frame 9000 methane is located in this high-density layer. On the picture of the methane molecule no signs of faces making up cavities are formed, but that cannot confirm that no cavities could form here.

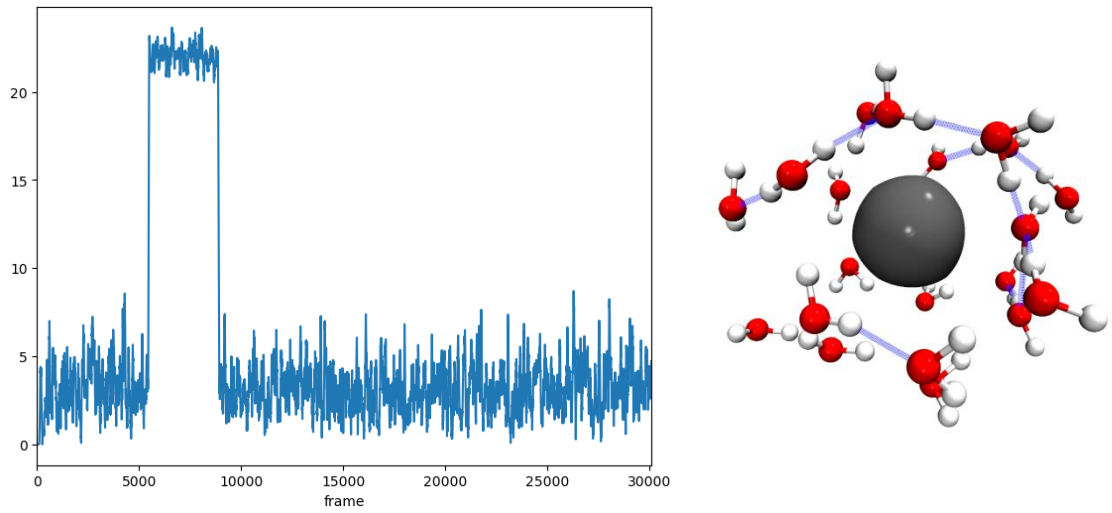

Figure 9.28: On the left side; the plot of number of water molecules surrounding a methane molecule first placed in the sphere and then for a limited time in the high-density layer near the surface. On the right side; the corresponding methane molecule shown in the simulation with the surrounding water molecules shown.

Based on these observations it is not possible to state that hydrate starts forming in these simulations. One reason for this is the total run time of the simulation; hydrate structures are not guaranteed to start to form after 15 ns because it is a stochastic process. Another argument is that to confirm that nucleation of hydrate take place several molecules of methane within a short radius need to show the tendency of cavities forming around them. The fact that one hexagonal face is formed may be a coincidence because hydrogen-bonds usually are present in water or it may be an indication of the early start of a hydrate nucleation.

10 Conclusions

The NVT simulation for system 1 without PVP and for system 2 containing PVP has nearly the same behavior when they are viewed in VMD[14] and gets similar results for density profiles and orientation order. The same applies for system 1 and 2 for the NPT simulations. From this it is assumed that the PVP molecules do not have a large effect on the simulation systems, where a reason for this may be that the PVP concentration or the amount of lactam rings is too low. Some of the PVP molecules are located in the interface between water and the methane sphere. The carbon backbone is nonpolar and hydrophobic and oriented towards the methane phase and the lactam rings is placed in the water phase. Water tends to make hydrogen bonds to nitrogen or oxygen in the lactam rings and in this system only oxygen is capable of making hydrogen bonds to water. This may be a result of the molecular structure of PVP where it can be difficult for the nitrogen atom to be exposed to water.

The modified TIP3P water model provided a higher density than the target density of 1003.8 kg/m^3 so a second water model was used, the TIP4P/2005. The resulting densities got an even larger error than the ones for the modified TIP3P model. The NVT simulations for system 3 got a density of 914 kg/m^3, which resembles the density of ice and could indicate that some sort of ice-structure is starting to form. Water is predominantly oriented with one of the hydrogen atoms pointing towards the hematite surface, especially towards the oxygen atoms in hematite probably because of the large attraction between these atoms. In one of the simulations the first layer of water gets a different orientation towards the surface with each of the hydrogen atoms in water pointing towards an oxygen atom in hematite.

The methane molecule placed in water bulk got more structured water surrounding it than the methane molecule located in the high-density layer close to the surface. This may be a coincidence or it may indicate that the water in the high-density layer is too structured to form cavities. Methane seems to prefer to be located in high density layer of water near surface rather than the low-density area in between the high-density layers. One reason for this could be that Lennard-Jones forces are responsible for the low-density area and when no water can be located there, there will be volume left for methane.

11 Suggestions to Further work

Based on the results, discussions and conclusion the following suggestions to further work are listed below.

11.1 Water Model

As both of the models for water (modified TIP3P and TIP4P/2005) reproduces a higher or lower pressure than the target pressure, these simulations could be run with another water model to see if a better density can be provided.

11.2 PVP Model

In this study the systems containing PVP molecules has five molecules present and each molecule has five sequences of the lactam ring. The PVP molecules do not significantly influence these systems so a system with a larger amount of PVP molecules could be studied. Another possibility is to increase the number of lactam rings in the PVP molecule.

11.3 Investigate Ice-structure

For the systems with the TIP4P/2005 water model the orientation order indicates that water in bulk gets a distinct structure, and there are indications of some sort of ice-structure is forming. A system consisting of ice could be investigated and the corresponding orientation order could be compared to the one obtained in this thesis to see if they resembles the one for ice.

11.4 Investigate the Hematite Crystal

Another interesting phenomenon to further investigate is the three oxygen atoms in the hematite crystal that get dissolved into the first layer of water in the NPT simulation of system 3.

References

1. Carroll, J.J., *Natural gas hydrates : a guide for engineers*. 2nd ed. 2009, Amsterdam ; Boston: Gulf Professional Pub. xvii, 276 p.
2. Sloan, E.D., *Fundamental principles and applications of natural gas hydrates.* Nature, 2003. **426**(6964): p. 353-359.
3. Kvamme, B., Austrheim, M., Knarvik, A., Zarifi, M., *Hydrate Formation During Transport of Natural Gas Containing Water and Impurities.* International Journal of Engineering Research and Development, 2017. **13**(5): p. 16.
4. Makogon, Y.F., S.A. Holditch, and T.Y. Makogon, *Natural gas-hydrates - A potential energy source for the 21st Century.* Journal of Petroleum Science and Engineering, 2007. **56**(1-3): p. 14-31.
5. Kvamme, B., et al., *Storage of CO2 in natural gas hydrate reservoirs and the effect of hydrate as an extra sealing in cold aquifers.* International Journal of Greenhouse Gas Control, 2007. **1**(2): p. 236-246.
6. Frenkel, D. and B. Smit, *Understanding molecular simulation : from algorithms to applications*. 2nd ed. Computational science series. 2002, San Diego: Academic Press. xxii, 638 p.
7. Hinchliffe, A., *Molecular Modeling for Beginners*. 2nd ed. . 2008, Chinchester: Wiley. 411.
8. Chandler, D., *Introduction to modern statistical mechanics*. 1987, New York: Oxford University Press. xiii, 274 p.
9. Andersen, H.C., *Molecular-Dynamics Simulations at Constant Pressure and-or Temperature.* Journal of Chemical Physics, 1980. **72**(4): p. 2384-2393.
10. Hoover, W.G., *Canonical Dynamics - Equilibrium Phase-Space Distributions.* Physical Review A, 1985. **31**(3): p. 1695-1697.
11. Nose, S., *A Unified Formulation of the Constant Temperature Molecular-Dynamics Methods.* Journal of Chemical Physics, 1984. **81**(1): p. 511-519.
12. Boda, D. and D. Henderson, *The effects of deviations from Lorentz-Berthelot rules on the properties of a simple mixture.* Molecular Physics, 2008. **106**(20): p. 2367-2370.
13. Cramer, C.J., *Essentials of computational chemistry : theories and models*. 2nd ed. 2004, Chichester, West Sussex, England ; Hoboken, NJ: Wiley. xx, 596 p.
14. Humphrey, W., A. Dalke, and K. Schulten, *VMD: Visual molecular dynamics.* Journal of Molecular Graphics & Modelling, 1996. **14**(1): p. 33-38.
15. Stockelmann, E. and R. Hentschke, *A molecular-dynamics simulation study of water on NaCl(100) using a polarizable water model.* Journal of Chemical Physics, 1999. **110**(24): p. 12097-12107.
16. Maslen, E.N., et al., *Synchrotron X-Ray Study of the Electron-Density in Alpha-Fe2o3.* Acta Crystallographica Section B-Structural Science, 1994. **50**: p. 435-441.
17. Barron, V. and J. Torrent, *Surface hydroxyl configuration of various crystal faces of hematite and goethite.* Journal of Colloid and Interface Science, 1996. **177**(2): p. 407-410.
18. Kerisit, S., *Water structure at hematite-water interfaces.* Geochimica Et Cosmochimica Acta, 2011. **75**(8): p. 2043-2061.
19. Olsen, R., Sjöblom, S., Kvamme, B., Kuznetsova, T., *Molecular Dynamics Simulation of Triethylene Glycol - Chemical Potentials on Surface Relevant to Gas Transportand Processing.* 2014.

20. Jorgensen, W.L., J.D. Madura, and C.J. Swenson, *Optimized Intermolecular Potential Functions for Liquid Hydrocarbons.* Journal of the American Chemical Society, 1984. **106**(22): p. 6638-6646.
21. Pedersen, B. *Vann*. Store Norske leksikon 2017 29.06.17; Available from: https://snl.no/vann.
22. Price, D.J. and C.L.B. III, *A modified TIP3P water potential for simulation with Ewald summation.* The Journal of Chemical Physics, 2004. **121**(20): p. 10096-10103.
23. Abascal, J.L.F. and C. Vega, *A general purpose model for the condensed phases of water: TIP4P/2005.* Journal of Chemical Physics, 2005. **123**(23).
24. Field, M.J., P.A. Bash, and M. Karplus, *A Combined Quantum-Mechanical and Molecular Mechanical Potential for Molecular-Dynamics Simulations.* Journal of Computational Chemistry, 1990. **11**(6): p. 700-733.
25. Lederhos, J.P., et al., *Effective kinetic inhibitors for natural gas hydrates.* Chemical Engineering Science, 1996. **51**(8): p. 1221-1229.
26. *Avogadro: an open-source molecular builder and visualization tool.*; Version 1.1.1:[Available from: http://avogadro.cc/.
27. Hanwell, M.D., et al., *Avogadro: an advanced semantic chemical editor, visualization, and analysis platform.* Journal of Cheminformatics, 2012. **4**.
28. Jorgensen, W.L., D.S. Maxwell, and J. TiradoRives, *Development and testing of the OPLS all-atom force field on conformational energetics and properties of organic liquids.* Journal of the American Chemical Society, 1996. **118**(45): p. 11225-11236.
29. Damm, W., et al., *OPLS all-atom force field for carbohydrates.* Journal of Computational Chemistry, 1997. **18**(16): p. 1955-1970.
30. Jorgensen, W.L. and N.A. McDonald, *Development of an all-atom force field for heterocycles. Properties of liquid pyridine and diazenes.* Theochem-Journal of Molecular Structure, 1998. **424**(1-2): p. 145-155.
31. McDonald, N.A. and W.L. Jorgensen, *Development of an all-atom force field for heterocycles. Properties of liquid pyrrole, furan, diazoles, and oxazoles.* Journal of Physical Chemistry B, 1998. **102**(41): p. 8049-8059.
32. Rizzo, R.C. and W.L. Jorgensen, *OPLS all-atom model for amines: Resolution of the amine hydration problem.* Journal of the American Chemical Society, 1999. **121**(20): p. 4827-4836.
33. Watkins, E.K. and W.L. Jorgensen, *Perfluoroalkanes: Conformational analysis and liquid-state properties from ab initio and Monte Carlo calculations.* Journal of Physical Chemistry A, 2001. **105**(16): p. 4118-4125.
34. Price, M.L.P., D. Ostrovsky, and W.L. Jorgensen, *Gas-phase and liquid-state properties of esters, nitriles, and nitro compounds with the OPLS-AA force field.* Journal of Computational Chemistry, 2001. **22**(13): p. 1340-1352.
35. Jorgensen, W.L., J.P. Ulmschneider, and J. Tirado-Rives, *Free energies of hydration from a generalized Born model and an ALL-atom force field.* Journal of Physical Chemistry B, 2004. **108**(41): p. 16264-16270.
36. Jensen, K.P. and W.L. Jorgensen, *Halide, ammonium, and alkali metal ion parameters for modeling aqueous solutions.* Journal of Chemical Theory and Computation, 2006. **2**(6): p. 1499-1509.
37. Argo, C.B., et al., *Commercial deployment of low-dosage hydrate inhibitors in a southern North Sea 69 km wet-gas subsea pipeline.* Spe Production & Facilities, 2000. **15**(2): p. 130-134.
38. National Institute of Standards and Technology (U.S.), *NIST chemistry webbook*, in *NIST standard reference database 69*. National Institute of Standards and Technology: Washington, D.C.

39. Martinez, L., et al., *PACKMOL: A Package for Building Initial Configurations for Molecular Dynamics Simulations.* Journal of Computational Chemistry, 2009. **30**(13): p. 2157-2164.
40. Feistel, R. and W. Wagner, *A new equation of state for H2O ice Ih.* Journal of Physical and Chemical Reference Data, 2006. **35**(2): p. 1021-1047.
41. (IAPWS), I.A.f.t.P.o.W.a.S. *Revised Release on the Equation of State 2006 for H2O Ice Ih*. 2009; Available from: www.iapws.org.
42. Chaplin, M. *Clathrate hydrates*. 2003 04.08.17; Available from: http://www1.lsbu.ac.uk/water/clathrate_hydrates.html.

12 Appendix 1

Appendix 1 contains the scripts used for making the analyses of the systems.

12.1 Script for Density Profiles

```
#Density profile

set resolution 0.5
set totalframes 0
set offset 3010
set N 30100
set chunksize [expr {($N-$offset)/10}]
set WAT [atomselect top "resname WAT"]
set MET [atomselect top "resname MET"]
set PVP [atomselect top "resname PVP"]
set zlength 600
set WATbins [list]
set METbins [list]
set PVPbins [list]

set numbins 0
for {set i 0} {$i <= [expr {($zlength / $resolution) + 1}]} {incr i} {
    lappend WATbins 0
    lappend METbins 0
    lappend PVPbins 0
    incr numbins
}

for {set chunk 0} {$chunk < ($N-$offset) / $chunksize} {incr chunk} {
    animate delete all
    set first [expr {$chunk*$chunksize + $offset}]
    set last [expr { ($chunk*$chunksize + $chunksize-1) + $offset}]
    mol addfile dump_hematite_system3.dcd first $first last $last step
1 waitfor all top
    set totalframes [expr {$totalframes + [molinfo top get numframes]}]
    puts "Total frames $totalframes"
    for {set frame 0} {$frame < [molinfo top get numframes]} {incr
frame} {
        animate goto $frame
        set Fe [atomselect top "name Fe"]
        set zplane [lindex [measure center $Fe] 2]
        $Fe delete
        unset Fe

        #Water molecules on the left side of the hematite crystal are
moved to the other side
        set movedist [lindex [pbc get] 0 2]
        set moveWAT [atomselect top "resname WAT and z<$zplane"]
        set movedist [list 0.0 0.0 $movedist]
        $moveWAT moveby $movedist
        $moveWAT delete
```

```
        unset moveWAT

        $WAT update
        set WATz [$WAT get z]
        set METz [$MET get z]
        set PVPz [$PVP get z]

        foreach z $WATz {
            set binIndex [expr {($z + $zlength / 2.0) / $resolution}]
            set binIndex [expr {round($binIndex)}]
            set value [lindex $WATbins $binIndex]
            incr value
            lset WATbins $binIndex $value
            unset binIndex
            unset value
        }
        foreach z $METz {
            set binIndex [expr {($z + $zlength / 2.0) / $resolution}]
            set binIndex [expr {round($binIndex)}]
            set value [lindex $METbins $binIndex]
            incr value
            lset METbins $binIndex $value
            unset binIndex
            unset value
        }
        foreach z $PVPz {
            set binIndex [expr {($z+$zlength/2.0)/$resolution}]
            set binIndex [expr {round($binIndex)}]
            set value [lindex $PVPbins $binIndex]
            incr value
            lset PVPbins $binIndex $value
            unset binIndex
            unset value
        }
        if {$frame % 100 == 0} {
            puts "Frame $frame"
        }
        unset WATz METz PVPz
    }
}


puts "DONE!"
set log [open "tetthetslog.log" w]
set normWAT [expr {[$WAT num] * 1.0 * $totalframes}]
set normMET [expr {[$MET num] * 1.0 * $totalframes}]
set normPVP [expr {[$PVP num] * 1.0 * $totalframes}]
for {set bin 0} {$bin < $numbins} {incr bin} {
    set z [expr {(-$zlength / 2.0) + (($zlength / ($numbins*1.0)) *
($bin*1.0))}]
    set value1 [lindex $WATbins $bin]
    set value1 [expr {$value1/$normWAT}]
    set value2 [lindex $METbins $bin]
    set value2 [expr {$value2/$normMET}]
    set value3 [lindex $PVPbins $bin]
    set value3 [expr {$value3/$normPVP}]
    puts $log "$bin $z $value1 $value2 $value3"
    unset z
```

```
}
close $log
$WAT delete
$MET delete
$PVP delete
unset WAT MET PVP WATbins METbins PVPbins
```

12.2 Script for Orientation Order

```
#Orientation Order

set resolution 0.5
set totalframes 0
set offset 3010
set N 30100
set chunksize [expr {($N-$offset)/10}]
set WAT [atomselect top "resname WAT and name Ow"]
#set zlength [lindex [pbc get] 0 2]
set zlength 600
set WATorderbins [list]
set cosThettabins [list]
set cosThettacounts [list]

set numbins 0
for {set i 0} {$i <= [expr {($zlength / $resolution) + 1}]} {incr i} {
    lappend WATorderbins 0
    lappend cosThettabins 0
    lappend cosThettacount 0
    incr numbins
}

for {set chunk 0} {$chunk < ($N-$offset) / $chunksize} {incr chunk} {
    animate delete all
    set first [expr {$chunk*$chunksize + $offset}]
    set last [expr { ($chunk*$chunksize + $chunksize-1) + $offset}]
    mol addfile dump_hematite_system2.dcd first $first last $last step
1 waitfor all
    set totalframes [expr {$totalframes + [molinfo top get numframes]}]
    puts "Total frames $totalframes"
    for {set frame 0} {$frame < [molinfo top get numframes]} {incr
frame} {
        set WATframeorderbins [list]
        set WATframecountbins [list]
        for {set i 0} {$i <= [expr {($zlength / $resolution) + 1}]}
{incr i} {
            lappend WATframeorderbins 0
            lappend WATframecountbins 0
        }

        animate goto $frame
        set Fe [atomselect top "name Fe"]
        set zplane [lindex [measure center $Fe] 2]
        $Fe delete
        unset Fe

        #Water molecules are moved to the other side
        set movedist [lindex [pbc get] 0 2]
        set moveWAT [atomselect top "resname WAT and z<$zplane"]
        set movedist [list 0.0 0.0 $movedist]
        $moveWAT moveby $movedist
        $moveWAT delete
        unset moveWAT
```

```
        $WAT update
        set residlist [$WAT get resid]

        foreach resid $residlist {
            # Velger vannmolekyl med resid og henter possisjon for alle
atomer
            set currentWAT [atomselect top "resid $resid"]
            set pos [$currentWAT get {x y z}]
            $currentWAT delete
            #Bruker z-koordinaten til oksygenet for å regne ut en index
            set z [lindex $pos 0 2]
            set binIndex [expr {($z + $zlength / 2.0) / $resolution}]
            set binIndex [expr {round($binIndex)}]

            #Øk tallet i bin med 1
            set count [lindex $WATframecountbins $binIndex]
            incr count
            lset WATframecountbins $binIndex $count

            #Lager possisjoner for atomene
            set O [lindex $pos 0]
            set H1 [lindex $pos 1]
            set H2 [lindex $pos 2]

            #regner ut vektorene
            set OH1 [vecsub $H1 $O]
            set OH2 [vecsub $H2 $O]
            set dipole [vecadd $OH1 $OH2]

            #finner cos til thetta
            set cosThetta [expr {[lindex $dipole 2] / [veclength
$dipole] }]

            #finner orderparameter
            set orderparam [expr {(($cosThetta * $cosThetta * 3.0) -
1.0) * 0.5)}]
            #finner gammel verdi i listen og plusser på ny verdi
            set order [lindex $WATframeorderbins $binIndex]
            set order [expr {$order + $orderparam}]
            lset WATframeorderbins $binIndex $order

            #finner gammel verdi i listen og plusser på ny verdi
            set old [lindex $cosThettabins $binIndex]
            set new [expr {$old + $cosThetta}]
            lset cosThettabins $binIndex $new

            #Øk tallet i bin med 1
            set coscount [lindex $cosThettacount $binIndex]
            incr coscount
            lset cosThettacount $binIndex $coscount

            unset currentWAT pos z binIndex O H1 H2 OH1 OH2 dipole
count cosThetta orderparam order old new coscount

        }
        for {set bin 0} {$bin < $numbins} {incr bin} {
           set count [expr {([lindex $WATframecountbins $bin] * 1.0)}]
           if {$count > 0.5} {
```

```
                set old [lindex $WATorderbins $bin]
                set new [expr {$old +[lindex $WATframeorderbins $bin] /
([lindex $WATframecountbins $bin] * 1.0)}]
                lset WATorderbins $bin $new

                unset old new
            }

            unset count
        }


        if {$frame % 100 == 0} {
            puts "Frame $frame"
        }

        unset WATframeorderbins WATframecountbins residlist movedist
zplane
    }

    unset first last
}


puts "DONE!"
set log [open "vannstruktur.log" w]


puts $log "# bin    z    s(z)    cos(theta)"

for {set bin 0} {$bin < $numbins} {incr bin} {
  set z [expr {(-$zlength / 2.0) + $zlength / $numbins * $bin}]
  set s [lindex $WATorderbins $bin]
  set s [expr {$s/($totalframes * 1.0)}]
  set c [lindex $cosThettabins $bin]
  set count [expr {[lindex $cosThettacount $bin] * 1.0}]
  if {$count < 0.5} {
      set count 1.0
  }
  set c [expr {$c / $count}]
  puts $log "$bin $z $s $c"

  unset z s c

}

close $log
$WAT delete
unset resolution totalframes offset N chunksize WAT zlength
WATorderbins cosThettabins cosThettacounts
```

12.3 Script for Radial Distribution Functions (RDF)

```
#Radial Distribution Functions

proc calc {selText1 selText2 filename} {
    #set up the atom selections
    set sel1 [atomselect top $selText1]
    set sel2 [atomselect top $selText2]

    #calculate g(r)
    set gr [measure gofr $sel1 $sel2 delta 0.1 rmax 10 usepbc 1
selupdate 1 first 0 last -1 step 1]

    #set up the outfile and write out the data
    set outfile [open $filename w]

    set r [lindex $gr 0]
    set gr2 [lindex $gr 1]
    set igr [lindex $gr 2]

    set i 0
    foreach j $r k $gr2 l $igr {
        puts $outfile "$j $k $l"
    }

    $sel1 delete
    $sel2 delete

    close $outfile

cd path to psf file and dcd file
mol new NameOfPsfFile.psf
mol addfile NameOfDcdFile.dcd waitfor all

calc “name of type one "name of type 2" "NameOfFile.dat"
```

12.4 Script for Number of Water Molecules Surrounding a Methane Molecule

```
cd path to psf and dcd file
mol new NameOfPsfFile.psf

set resolution 0.5
set totalframes 0
set MET [atomselect top "resname MET"]
set residMETlist [$MET get resid]

set N 30100
set offset 0
set chunksize [expr {($N-$offset)/10}]

set zlength 600
set Log [open "NameOfDataFile.dat" w]
puts -nonewline $Log "#frame    "
foreach resid $residMETlist {
    puts -nonewline $Log "$resid    "
}
puts $Log ""

#Kan ikke laste alt inn i minnet på en gang. Deler dcd i mindre biter
(chunks)
for {set chunk 0} {$chunk <($N-$offset)/$chunksize} {incr chunk} {
      animate delete all
      set first [expr {$chunk*$chunksize + $offset}]
      set last [expr {$chunk*$chunksize + ($chunksize-1) + $offset}]

      mol addfile NameOfDcdFile.dcd first $first last $last step 1
waitfor all top
      set totalframes [expr {$totalframes + [molinfo top get
numframes]}]
        puts "Total frames $totalframes"


        #går gjennom frame for frame
        for {set frame 0} {$frame < [molinfo top get numframes]} {incr
frame} {
            animate goto $frame
            set frameindex [expr {$chunk*$chunksize + $frame}]
            puts -nonewline $Log "$frameindex    "
            set data [list]

            foreach resid $residMETlist {
                #velger metanmolekyl med resid og velger vannmolekyl
nærmere enn 5.0Å
                set WATwithin [atomselect top "name Ow and same resid
as (resname WAT and within 5.0 of resid $resid)"]

                set numWATwithin [$WATwithin num]

           #puts -nonewline $Log "$numWATwithin    "
                lappend data $numWATwithin
```

```
                $WATwithin delete
                unset WATwithin numWATwithin
            }

          puts $Log [join $data "   "]

            if {$frame%50==0} {
                puts "Frame $frame"
            }
        }

}

close $Log
mol delete top
```

13 Appendix 2

This appendix contains the article done in conjunction with this Master thesis.

Hydrate Formation During Transport of Natural Gas Containing Water And Impurities

B. Kvamme, M. Austrheim, A. Knarvik, M. Zarifi.

International Journal of Engineering Research and Development, 2017. **13**(5): p. 16.

International Journal of Engineering Research and Development
e-ISSN: 2278-067X, p-ISSN: 2278-800X, www.ijerd.com
Volume 13, Issue 5 (May 2017), PP.01-16

Hydrate Formation During Transport of Natural Gas Containing Water And Impurities

Bjørn Kvamme*,Marthe Austrheim,Anette Knarvik,Mojdeh Zarifi
University Of Bergen, Department Of Physics And Technology, 5007 Bergen, Norway

ABSTRACT: The upper limit of water content permitted in a natural gas stream during its pipeline transport without a risk of hydrate formation is a complex issue. We propose a novel thermodynamic scheme for investigation of different routes to hydrate formation, with ideal gas used as reference state for all components in all phases including hydrate phase. This makes comparison between different hydrate formation routes transparent and consistent in free energy changes and associated enthalpy change. From a thermodynamic point of view natural gas hydrate can form directly from water dissolved in natural gas but quite unlikely due to limitations in mass and. The typical industrial way to evaluate risk of hydrate formation involves calculation of water condensation from gas and subsequent evaluation of hydrate from condensed water and hydrate formers in the natural gas. Transport pipes are rusty even before they are mounted together to transport pipelines. This opens up for even other routes to hydrate formation which starts with water adsorbing to rust and then leads to hydrate formation with surrounding gas. Rust consist on several iron oxide forms but Hematite is one of the most stable form and is used as a model in this study, in which we focus on maximum limits of water content in various natural gas mixtures that can be tolerated in order to avoid water dropping out as liquid or adsorbed and subsequently forming hydrate. Calculations for representative gas mixtures forming structure I and II hydrates are discussed for ranges of conditions typical for North Sea. The typical trend is that the estimated tolerance for water content is in the order of 20 times higher if these numbers are based on water dew-point rather than water dropping out as adsorbed on Hematite. For pure methane the maximum limits of water to be tolerated decrease with increasing pressures from 50 to 250 bars at temperatures above zero Celsius and up to six Celsius. Pure ethane and pure propane show the opposite trend due to the high density non-polar phase at the high pressures. Typical natural gas mixtures is, however, dominated by the methane so for systems of 80 per cent methane or more the trend is similar to that of pure methane with some expected shifts in absolute values of water drop-out mole-fractions.

Keywords: gas hydrates, natural gas transport, rust, alternative formation routes

NOMENCLATURE

C Number of components in the Gibbs phase rule
E_P Potential energy [kJ/mol]
F Number of degrees of freedom in the Gibbs phase rule
F Free energy [kJ/mol]
f Free energy density [kJ/(mol m^3)]
f_i Fugacity [Pa]
$g(r)$ Radial distribution function (RDF)
G Gibbs free energy [kJ/mol]
Δg_{kj}^{inc} Gibbs free energy of inclusion of component k in cavity type j [kJ/mol]
H Enthalpy [kJ/mol]
h_{kj} Cavity partition function of component k in cavity type j
k Cavity type index
K Ratio of gas mole-fraction versus liquid mole-fraction for the same component (gas/liquid K-values)
N_i Number of molecules
N Number of phases in the Gibbs phase rule
P Pressure [Pa]
P_0 Reference pressure [Pa]
r Distance [m]

* Corresponding author: Phone: +47 934 51 956 E-mail: bjørn.kvamme@uib.no

R Molar gas constant [kJ/(K mol)]
T Temperature [K]
T_c Critical temperature [K]
v_j No. of type j cavities per water molecule
v_mMolar volume [m^3/mol]
$\overline{V}_r$ Molar volume of *r*th component [m^3/mol]
$\overline{V}^{clath}$ Volume of clathrate [m^3]
x Mole fraction
y_w Mole fraction of water
Y Residual chemical potential per Kelvin
z Mole fraction
α Liquid (water) phase fraction
β Inverse of the gas constant times temperature
μ Chemical potential [kJ/mol]
$\mu_w^{0,H}$ Chemical potential for water in empty hydrate structure [kJ/mol]
θ_{kj} Fractional occupancy of cavity k by component j
γ Activity coefficient
ϕ Order parameter
ρ Molar density [kg/m^3]

I. INTRODUCTION

Pipeline transport of large volumes of natural gas at low temperatures and high pressures is a continuous operation. In the North Sea alone there is about 7800 km of pipeline transporting in the order of 96 billion standard cubic meter of gas per year. Most of the transport lines lie on the seafloor and are exposed to temperatures 2 – 6ºC. With pressures spanning the range from 200 atmto that at receiving terminals, large portion, if not all, of the pipeline transport will occur within hydrate formation conditions. Under these conditions, transported gas mixtures have shown a tendency to form ice like structures, known as clathrate hydrates (cf. [1] and references therein). Hydrate nucleation and growth within a dense stream of natural gas with significant admixtures of impurities (limited to water in this work) is a complex process involving competing phase transition mechanisms and pathways, where both kinetics and thermodynamics play an important role. Schemes currently employed by the industry toevaluatehydrate risks assume that hydrateformation will be determined by dropout of water within the gas bulk and thus calculate the dew-point temperature of the given mixture. This approach completely ignores the factthat the presence of rust on the pipeline walls will provide water adsorption sites and thus add additional pathways for hydrate formation.

The problem will be even further complicated by the general inability of hydrate formation within a pipeline to reach thermodynamic equilibrium due to restrictions imposed by either the Gibbs phase rule or transport limitations. Consider a simple case of methane hydrate forming from water present in methane; here *C*, the number of components is two (water and methane), and the number of phases, *N*, is two phases as well (solid hydrate and methanegas with impurities). According to the Gibbs phase rule ($F = C - N + 2$), this will leave two degrees of freedom, *i.e.*$F = 2$. Though this result would appear to indicate a chance for the system to achieve equilibrium by varying local temperature and pressure hydrate nucleus might never reach a critical size due to mass transport limitations and very low concentration of water in methane.Getting rid of crystallization heat will pose yet another issue that can severely limit the rate of hydrate formation, since methane is a much worse thermal conductor compared to hydrate and liquid water clusters prior to hydrate formation.

The presence of solid surfaces will also have an indirect effect on hydrate formation on the interface between the methane-rich gas and the aqueous phase adsorbed on rusty walls. Thispotential impact of water-wetting surfaces on the phase transitions should not be discounted just because of the gas phase will dominate as far as the mass is concerned. Hydrate nucleation and growth may occur when either**both**water and hydrate guest molecules are adsorbed on the surface or only water is in the adsorbed phase and guest molecules species are imported from the methane-rich phase. Given the general lack of equilibrium, chemical potentials of hydrate-forming species will not be the same across the phases.In accordance with statistical thermodynamics hydrate

models of[1], this will lead toformation of several different co-existing hydrate phases even in the simple case of only water present in methane. Mixtures of ethane and methane will form structure I hydrates due to the very favorable stabilization of the large cavity by ethane. Additional content of propane is likely to lead to a mixed hydrate since structure will be favorable as long as propane is left in the gas mixture. Subsequent hydrate formation for remaining ethane and methane will be structure I.

Different Hydrate Formation Routes: Impact Of Multiple Phases

Table 1 lists the alternative routes to hydrate formation and re-dissociation relevant for pipeline transport of natural gas analyzed and ranked basing on their associated free energy changes:

$$\Delta G_i = \delta\left[x_w^{H,i}(\mu_w^{H,i} - \mu_w^{p}) + x_{gas}^{H,i}(\mu_{gas}^{H,i} - \mu_{gas}^{p}) \right] \quad (1)$$

Subscript"w" stands for "water" in either hydrate or other phase, "gas" for hydrate guest molecules;*H*is for hydrate phase, "*i*"indicates the scenario, "*p*"refers to either liquid, gas or adsorbed phase, x is composition,μ, chemical potential. Sign$\delta$is 1 for hydrate formation or reformation and -1 for dissociation. As pointed out earlier, the different pathways of Table 1 will lead to creation of hydrate varying in filling fraction and thus free energy, i.e. its own individual hydrate phase.

When there are only two components (methane and water) involved, and the number of possible phases exceeds two, as it will for pipeline transport with four phases (methane-rich fluid, aqueous phase, adsorbed phase, hydrates), the Gibbs phase rule will correspond to a system over-determined by two parameters . It might seem that adding more components, like ethane and/or propane, to the fluid phasewould increase the number of degrees of freedom and make equilibrium attainable. From the dynamic point of view, it is however unlikely that hydrate equilibrium can be reached during pipeline transport of natural gas with impurities.One should keep in mind that thermodynamics will guide the system towards the lowest free energy state currently possible via driving forces proportional to the free energy differences. These forces will be fairly large in our case and resulting in more stable hydrates forming first and hydrate composition changing in time. While a stable hydrate are prevented from reforming into a less stable form, a less stable hydrate is unable to reform into a more stable one without a supply of new hydrate formers. Under continuous flow, the latter option may become feasible due to continuous supply of "fresh" components from the stream. In addition, when in contact with phases under-saturated with respect to hydrate formers, hydrate may dissolve or reform with different compositions.

Scenarios covered by conventional industrial hydrate risk evaluation schemes largely assume that hydrate will nucleate and grow from gas and liquid water (route 6). We are not aware of any available commercial or academic codes that consider homogeneous hydrate formation from hydrate guest components dissolved in water. And no hydrate code available at present is able to treat heterogeneous hydrate formation in the presence of solid surfaces. Given the growing body of evidence that growth and propagation of thin hydrate films on the interfaces will be impacted by hydrate formation towards surfaces even in stationary situations, ignoring these processes can constitute a serious oversight. We believe that this work will also contribute to stimulating the discussion on how to incorporate these aspects [2,3] into a new generation of hydrate risk evaluation tools based on non-equilibrium thermodynamics. The outlined approach can also be extended to other hydrate-forming fluids containing water, including transport of liquid hydrocarbons containing structure I and II hydrate formers. In general, the proposed analysis scheme can also include guest components that form structure H hydrates, although kinetic studies seems to indicate that structure H forms slowly compared to structure I and II.

The various possible hydrate phase transitions listed in table 1 is not even complete but at least provides a flavor of the complexity of competing hydrate phase transitions in a general non-equilibrium situation. Given all of the possibilities listed in Table 1, a truly rigorous approach to hydrate risk evaluation would be the one that incorporates mass and heat transport as constraintsinside a free energy minimization scheme that also accounts for hydrodynamic effects. A simpler (but less rigorous) analysis scheme more compatible with conventional hydrate equilibrium codes can provide a viable alternative when consistent absolute thermodynamic properties are available for the different phase transitions. One may apply either the classical nucleation theory or the Multi-component Diffuse Interface Theory (MDIT) [2,4] to evaluate the phase transitions in Table 1. Routes 1 through 4 can be excluded from consideration immediately since their corresponding free energy changes will be either positive or not negative enough to overcome the penalty of the surroundings work. Simple kinetic theories can be used to eliminate very slow phase transitions and thus focus the evaluation on a handful of truly important ones.

One of the main goals in this work involved presenting routes to absolute thermodynamic properties (i.e. with ideal gas as reference state) for all the co-existing. A section focusing on equilibrium thermodynamics that follows outlines approaches and models we have used for this purpose. While the models employed there may be refined and extended, the approach presented provides a good starting point for an accurate analysis of

hydrate formation. We then briefly discuss the consequences of the non-equilibrium nature of hydrate phase transitions. The subsequent sections describe our numeric simulations; theyare centered on assessing the possible hydrate formation routes with the aid of equation (1) and absolute thermodynamics.It should be pointed out that absolute thermodynamic properties obtained fromatomistic simulations have been quite successful at predicting hydrate equilibrium curves [1,2].

Table 1. Some of the various possible routes to formation and dissociation of natural gas hydrate. δ is the sign of free energy change involved in hydrate phase transition, in which value 1 indicates favorable formation and -1 dissociation. i is just a phase transition index.

i	δ	Initial phase(s)	Driving force	Final phase(s)
1	-1	Hydrate	Outside stability in terms of local P and/or T	Gas, Liquid water
2	-1	Hydrate	Sublimation (gas under saturated with water)	Gas
3	-1	Hydrate	Outside liquid water under saturated with respect to methane and/or other enclathrated impurities originating from the methane phase	Liquid water, (Gas)
4	-1	Hydrate	Hydrate gets in contact with solid walls at which adsorbed water have lower chemical potential than hydrate water	Liquid water, Gas
5	+1	Gas/fluid	Hydrate more stable than water and hydrate formers in the fluid phase	Hydrate
6	+1	Gas + Liquid water	Hydrate more stable than condensed water and hydrate formers from gas/fluid	Hydrate
7	+1	Surface reformation	Non-uniform hydrate rearranges due to mass limitations (lower free energy hydrate particles consumes mass from hydrates of higher free energy)	Hydrate
8	+1	Aqueous phase	Liquid water super saturated with methane and/or other hydrate formers, with reference to hydrate free energy	Hydrate
9	+1	Adsorbed	Adsorbed water on rust forms hydrate with adsorbed hydrate formers	Hydrate
10	+1	Adsorbed + fluid	Water and hydrate formers from gas/fluid forms hydrate	Hydrate

Equilibrium Thermodynamics Of Fluid

A thermodynamic equilibrium is achieved when temperatures, pressures and chemical potentials of all components are equal in all co-existing phases. To insure the same reference values for free energy, all the chemical potential estimates, no matter what the phase, should employ ideal gas as the reference state:

$$\mu_i(T,P,\vec{y}) - \mu_i^{ideal\,gas}(T,P,\vec{y}) = RT\ln\ _i(T,P,\vec{y}) \quad (2)$$

where ϕ_i is the fugacity coefficient of component *i* in a given phase.

Another reference state for the chemical potential of a liquid state component *i*may also be used as an intermediate:

$$\mu_i(T,P,\vec{x}) - \mu_i^{ideal liquid}(T,P,\vec{x}) = RT\ln\ _i(T,P,\vec{x}) \quad (3)$$

$$\lim(\gamma_i) = 1.0 \quad \text{when} x_i \to 1.0$$

whereγ_i is the activity coefficient for component i in the liquid mixture. Note that when chemical potential of pure water has been estimated using molecular simulations, the application of equation (3) in case of water will be also based on absolute thermodynamics. The data from Kvamme& Tanaka [1] will be used in this work.

Infinite dilution is yet another reference state that has proven useful in case of gases with low solubility in water (route 8):

$$\mu_i(T,P,\vec{x}) - \mu_i^{\infty}(T,P,\vec{x}) = RT\ln\left[x_i\ _i^{\infty}(T,P,\vec{x})\right] \quad (4)$$

$$\lim(\gamma_i^{\infty}) = 1.0 \quad \text{when } x_i \to 0$$

withsuperscript "∞" standing for infinite dilution. This particular convention is known as the non-symmetric convention since the limit of the activity coefficient for the component *i* will approach unity as its

mole fraction vanishes. As shown in [4,5], molecular dynamics combined with the Gibbs-Duhem relation provides a convenient method to estimate absolute values for the required chemical potential at infinite dilution.

Provided that thermodynamic properties of all phases can be defined and evaluated both in equilibrium and outside of it, the combined first and second laws of thermodynamics would enforce a certain partitioning of all available components (and the total mass) over all phases able to coexist under local pressure and temperature conditions. Theestimation of out-of-equilibriumvalues will be fairly straightforward for most of the relevant fluid phases, with only the hydrate phase requiring a special consideration (see extensive discussion in Kvamme*et al*[2]). Combining thermodynamic formulations for fluids in equations (2) to (4) with hydrate non-equilibrium formulations from Kvamme*et al*[2]will make it fairly straightforward to minimize the free energy and obtain estimates for the local phase concentrations that satisfy the first and the second law of thermodynamics. Several algorithms capable of implementing this approach are available in the open literature.

Except in the case of hydrates,relevant pressures and temperatureswill largely correspond to a liquid state. Cases and scenarios considered here entail very limited mutual solubilities and/or limited concentrations, especially that ofwater in methane.The following approximation should therefore prove sufficiently accurate for most industrial applications in which hydrate formation is a risk factor:

$$\mu_{i,j}(T,P,\vec{x}) \approx \mu^{\infty}_{i,j}(T,P) + RT\ln\left[x_{i,j}\gamma^{\infty}_{i,j}(T,P,\vec{x})\right] \quad (5)$$

where subscript *j* refers to components; subscript *i* denotes different phases. In the context of this work, *j* is "methane" in case of the methane-rich phase and "H_2O" for the aqueous phase, "∞" refers to infinite dilution.

Equilibrium Thermodynamics Of Hydrate

Chemical potential of water when in the hydrate phase can be found by applying the statistical mechanical model for water in hydrate [1]:

$$\mu_{w,H} = \mu^{O}_{w,H} \sum_{k=1,2} RT v_k \ln\left(1 + \sum_i h_{ik}\right) \quad (6)$$

where subscript H denotes the hydrate phase, superscript 0 stands for the empty hydrate structure;v_k is the fraction of cavity of type k per water molecule. In case of structure I hydrates;v_k = 1/23 for small cavities (20 water molecules) and 3/23 for large cavities (24 water molecules). h_{ik} is the canonical partition function for a cavity of type *k* containing a "guest" molecule of type *i*, given by the following equation:

$$h_{ik} = e^{\beta\left(\mu_i^H - \Delta g_{ik}^{inc}\right)} \quad (7)$$

where β is the inverse of the gas constant times temperature, while Δg_{jk}^{inc} reflects the impact on hydrate water from the inclusion of the "guest" molecule *i* in the cavity [1]. At equilibrium, chemical potential of hydrate guest molecule *i*, μ_i^H , must to be identical to its chemical potential in the phase it has been extracted from. The hydrate content of all guest gas components can be estimated by applying equation (4) to calculate their chemical potential when dissolved in the methane phase. It must be noted that chemical potential of liquid water will be influenced by the presence of hydrogen sulfide and carbon dioxide while the solubility of hydrocarbons in liquid water is so low that they might be approximated to not affect activity of liquid water.Since water will totally dominate the dew point location, a simple approximation for hydrate formation in case of liquid water dropout (*i.e.* route 6) can be achieved by applying equation (8) below. Solving equation (8) for the given local temperature will yield the corresponding hydrate formation pressure. If this formation pressure is lower than the local pressure defined by flow's fluid dynamics, one can then estimate the mole fractions of condensed water by simultaneously satisfying the mass balance and equilibrium criteria. This approach is quite similar to flash calculations commonly employed in chemical engineering, though in terms of fugacity formulation rather than a chemical potential one.

$$\mu^{O,H}_w - \sum_{k=1,2} RT v_k \ln\left(1 + \sum_i h_{ik}\right) = \mu^{purewater}_{i,H2O}(T,P) + RT\ln\left[x_{i,H2O}\gamma_{i,H2O}(T,P,\vec{x})\right] \quad (8)$$

We should emphasize here that chemical potential of empty hydrate structure estimated from Kvamme& Tanaka [1] has been verified to have predictive capabilities, which makes any empirical formulations

redundant and even possibly non-physical, given the fundamental nature of chemical potential. If the estimated hydrate formation pressure is lower than the local one, hydrate will form via this particular route.

Asubsequent flash calculation using local pressure and temperature will provide the upper limit of liquid water mole fraction that can be supported by the methane-rich phase. If water dew-point pressure is lower than the local pressure, water will drop out as a liquid phase. In this case, one may assume that free water will be available for the process of hydrate formation, with hydrate oflowest free energy appearing first. Given that ethane and propaneisamore vigorous hydrate former than methane, the initially formed hydrates will be much richer in ethane and propane compared to any later ones. In contrast to the "standard" calculations, this approach does not consider the usual hydrate formation from the "bulk"but rather searches for hydrate with the lowest absolute free energy able to nucleate from the available natural gas mixtureunder the kinetic restrictions of mass- and heat transport. In other words, one would aim to minimize the following equation in terms of hydrate formation pressure while taking into account the fact our system will be unable to reach equilibrium:

$$G^H = \sum_i x_i^H \mu_i^H \qquad (9)$$

One can apply the non-equilibrium description of hydrate due to Kvamme*et al*[2] to follow the free energy gradients until the methane phase has been mostly depleted of the best hydrate former, ethane/propane.The analysis of equation (9) will also require the knowledge of hydrate composition, which can be found by applying statistical thermodynamic theory to the adsorption hydrate model (left hand side of equation (8)); the composition will be given by:

$$\theta_{ik} = \frac{x_{ik}^H}{v_k\left(1-x_T\right)} \quad \frac{h_{ik}}{1+\sum_i h_{ik}} \qquad (10)$$

where θ_{ik} is the filling fraction of component*i* in cavity type k, x_{ik}^H is the mole fraction of component i in cavity type k, x_T is the total mole fraction of all guests in the hydrate, and v_k is, as defined above, the fraction of cavities per water of type k.

We have fitted computed free energies of guest inclusion in the large cavity of structure I to a series in inverse reduced temperature.

$$\Delta g^{inclusion} = \sum_{i=0}^{5} k_0 \left[\frac{T_c}{T}\right]^i \quad (11)\,,$$

where T_c is the critical temperature of the guest molecule in question (see figures 1 and 2).

The free energy of inclusion in equation (11) can be estimated followingKvamme& Tanaka [1] and Kvamme*et al*[5] for the components included in this study(methane, Ethane and Propane). Thermodynamic consistency has been a high priority throughout this work, and it was not our intention to adjust any parameters to fit experimental data. Molecular dynamics simulations reported in this work were meant to extending the approach of [1] to larger hydrate systems and temperatures ranging between 273.15 K and 280 K. This was done in order to get a better resolution in the range of interest for this study. The main focus of our efforts was to study hydrate risks during transport of natural gasbetween Norway and the continent (Germany) via the North Sea pipelines.

The seafloor temperatures there rarely rise above 6ºC. Figures 1 and 2 shows plots of the parameters applied as function of temperature. Parameters corresponding to empty hydrates and ice will not be significantly affected,allowing the parameters of Kvamme& Tanaka [1]to beused. Similarly, chemical potential estimates for liquid water were extended from 0ºC by means of thermodynamic relationships and experimental data on enthalpy of dissociation and liquid water heat capacities. See Kvamme &Tanaka[1] for moredetails.

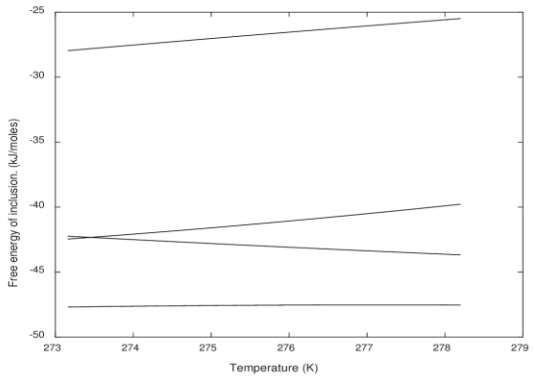

Figure 1.Free energy of inclusion of guest into hydrate structure II cavities (as positioned at 278 K). Lower curve is for propane in large cavity followed by ethane in large cavity and then methane in large cavity and then on top methane in small cavity.

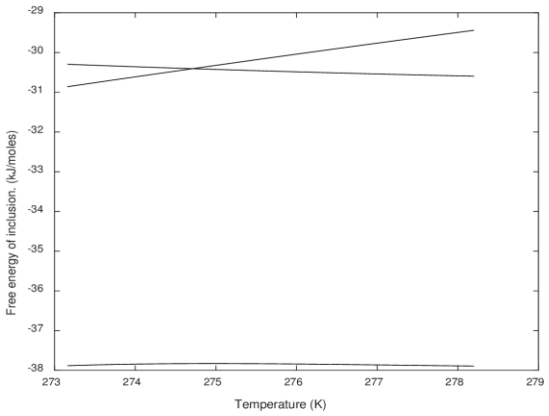

Figure 2. Free energy of inclusion of guest into hydrate structure I cavities (as positioned at 278 K). Lower curve is for ethane in large cavity followed by methane in small cavity and then methane in large cavity on top.

Verification Of Models And Other Assumptions

Since the free energies of guest molecule inclusions in equation (7) are based on molecular simulations of model systems we do not expect the resulting pressure, temperature equilibrium curves to match experimental data. But rather than making empirical fitting functions it is better in the context of this paper to stick to the values obtained and as plotted in figures 1 and 2 above.

Comparison for structure I hydrate of methane (figure 3) and ethane (figure 4) with experimental values show a fair agreement while structure II estimates for propane (figure 5) is underestimated in terms of stabilization. But they are nevertheless demonstrating that the model systems are suitable for qualitative evaluation of water drop out curves. It is also important to keep in mind that, as consequence of the first and second laws of thermodynamics, mixed hydrates will frequently occur. Like for instance in the system of 90% methane and rest ethane. Since this system will form structure I, and large cavities suitable for ethane are in a ratio of 3:1 versus small cavities, then it is clear that the first hydrates that forms will be very rich in ethane and the final hydrates will be methane. So within the scope of this work also estimates for that system is deemed sufficient. Possible users of the findings in this work can easily incorporate our models into their own hydrate codes. Very limited eexperimental data for the gas mixture hydrate consisting of methane, ethane and propane were found in open literature. For a system of 10% ethane in methane the estimated equilibrium curve is plotted

along with experimental data in figure 6. Given the limited amount of ethane in the system and a 3:1 ratio of large to small cavities in structure I it is expected that hydrate from this system in reality is a mixture of various hydrates ranging from an initial ethane rich hydrate to a final methane hydrate.

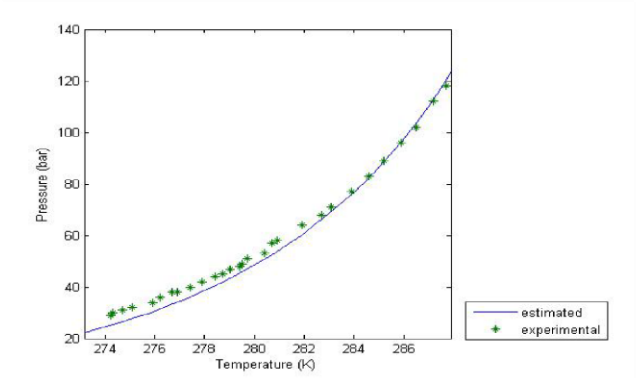

Figure 3. Estimated and experimental hydrate equilibrium curve for pure methane. Solid line – our estimates; asterisks – experimental data from Maekava[6].

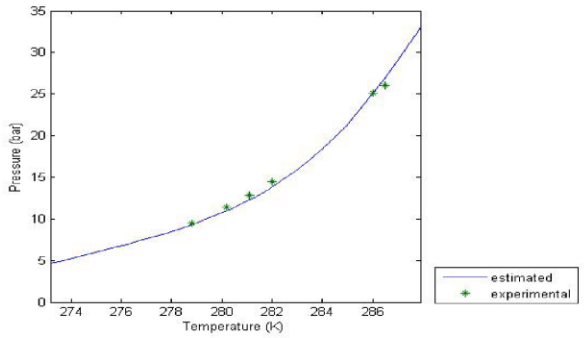

Figure 4. Estimated and experimental hydrate equilibrium curve for pure ethane. Solid line – our estimates; asterisks – experimental data from Holder and Hand[7].

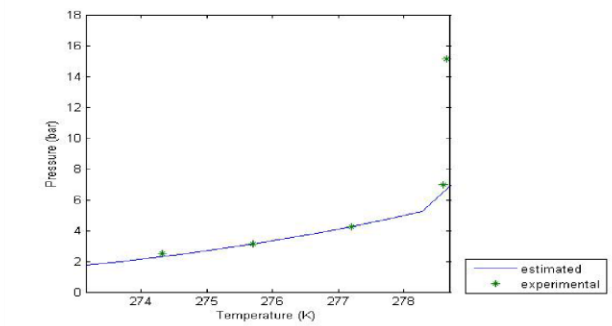

Figure 5. Estimated and experimental hydrate equilibrium curve for pure propane. Solid line – our estimates; asterisks – experimental data from Reamer *et al*[8].

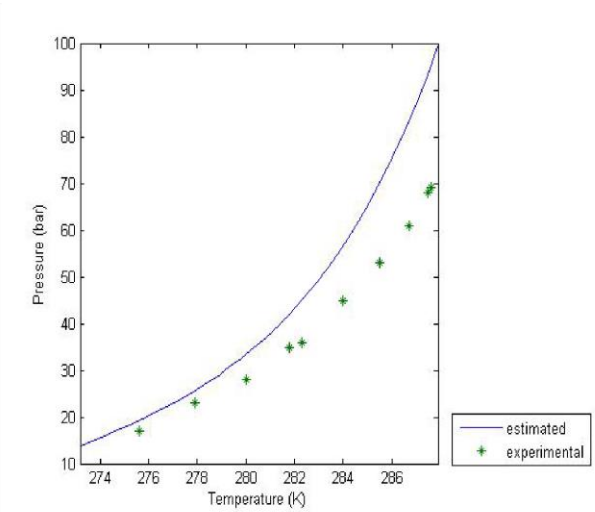

Figure 6. Estimated and experimental hydrate equilibrium curve fora mixture of 90% methane and 10% ethane. . Solid line – our estimates; asterisks – experimental data fromMaekava[6].

Analysis Of Routes To Hydrate Formation

The primary goal of this study was to gain insights into possible routes to hydrate formation and their relative importance during pipeline transport of natural gas, and also investigate how ethane and propane will influence the hydrate formation. In terms of the possible hydrate phase transitions listed in table 1, a conservative approach to hydrate risk evaluation would disregard all routes resulting in re-dissociation of hydrate (*i.e.* routes 1 – 4). The focus of this study was to investigate routes 6 and 10 and they are discussed below.

Hydrate formation involving condensed water and hydrate formers from the natural gas stream (routes 6)

Combining equation (3) for water in the condensed liquid phase with pure water in the ideal liquid water term from Kvamme& Tanaka [1] with residual thermodynamics (equation (2)) for water dissolved in natural gas will yield an approximate of water dew-point concentration for water in natural gas at given T and P. The above-described scheme might suffice for risk analysis related to route 6. Alternatively, combined mass balances and equilibrium can be solved iteratively for liquid water drop-out and water phase composition. If hydrate formation conditions are met, hydrate will form. Equation (2) with SRK [9] has been used as the equation of state forall components and natural gas mixtures. SRK is deemed accurate enough for the purposes of illustration. The SRK equation [9] was used to evaluate the deviations from ideal gas behavior via the fugacity coefficient.

While 50 bars may be a typical pressure during gas processing 250 bars is typical during pipeline transport. Seafloor temperatures in the North Sea are typically between -1 degrees Celsius and 6 degrees Celsius.Figures 7 to 9 shows plots of limits for water content before drop out as liquid. This is actually water dew-point curves under the simplification that the initial theoretical droplet is pure water. Due to the low density of methane (figure 7) at all conditions as compared to ethane and propane (figures 8 and 9 respectively) densities at same conditions there is a qualitative change.

For methane the water solubility decrease with increasing pressure while the opposite is the case for ethane and propane, which have substantially higher density for the high pressure and would make it make it more difficult for water to enter.

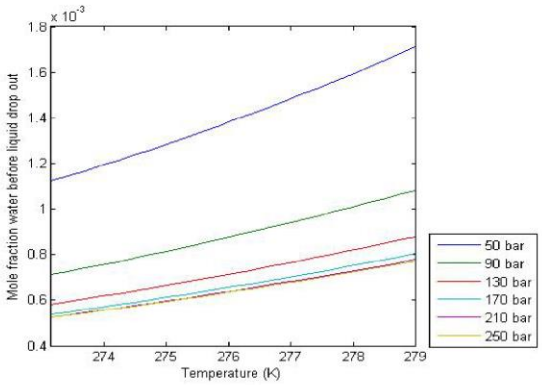

Figure 7. Maximum water content before liquid water drop out, for pure methane. Curves from top to bottom correspond to pressure 50 bar, 90 bar, 130 bar, 170 bar, 210 bar, 250 bar.

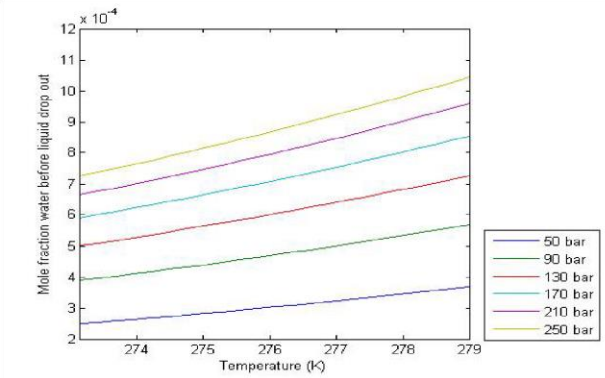

Figure 8. Maximum water content before liquid water drop out, for pure ethane. Curves from top to bottom correspond to pressure 250 bar, 210 bar, 170 bar, 130 bar, 90 bar, 50 bar.

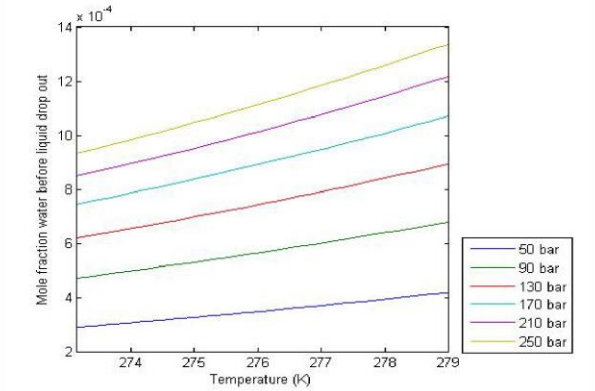

Figure 9. Maximum water content before liquid water drop out, for pure propane. Curves from top to bottom correspond to pressure 250 bar, 210 bar, 170 bar, 130 bar, 90 bar, 50 bar.

Natural gas mixtures are dominated by methane and some realistic mixtures are examined in figures 10 – 13. Although there are some differences in the behavior in terms of maximum water content before drop-out as liquid the trend is similar to that for pure methane in figure 7 although shifted slightly towards lower values for pressures up to 130 bars.

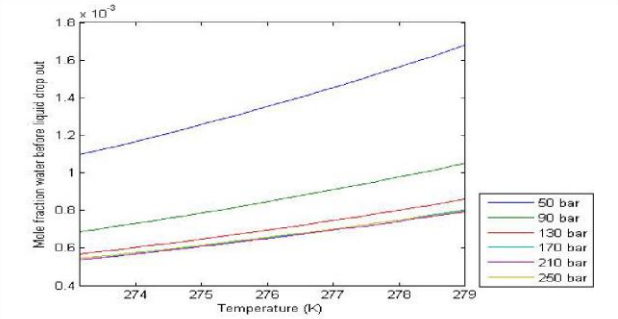

Figure 10. Maximum water content before liquid water drop out, for a mixture of 90% methane and 10% ethane. Curves from top to bottom correspond to pressure 50 bar, 90 bar, 130 bar, 170 bar, 210 bar, 250 bar.

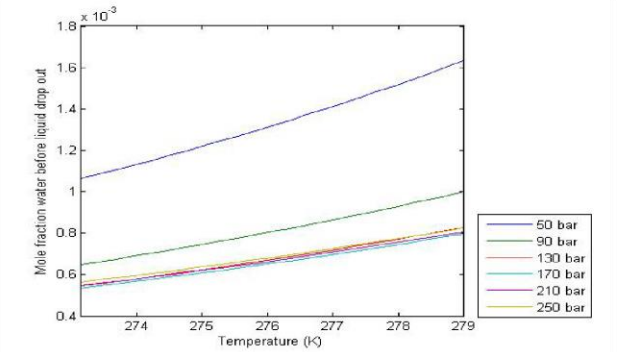

Figure 11. Maximum water content before liquid water drop out, for a mixture of 80% methane and 20% ethane. Curves from top to bottom correspond to pressure 50 bar, 90 bar, 130 bar, 170 bar, 210 bar, 250 bar.

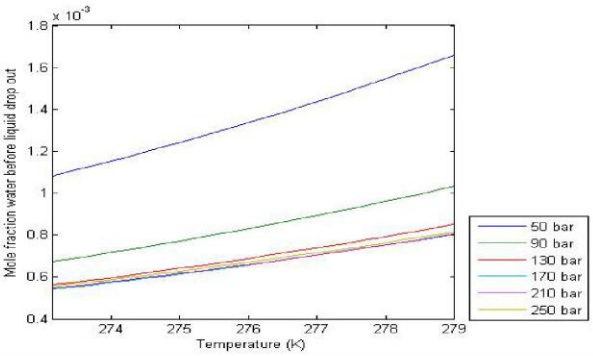

Figure 12. Maximum water content before liquid water drop out, for a mixture of 90% methane and 10% propane. Curves from top to bottom correspond to pressure 50 bar, 90 bar, 130 bar, 170 bar, 210 bar, 250 bar.

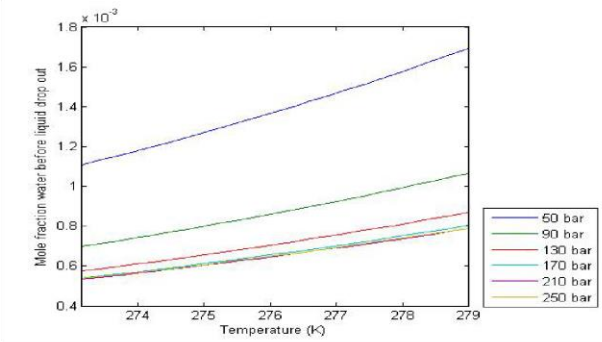

Figure 13. Maximum water content before liquid water drop out, for a mixture of 95% methane, 4% ethane and 1% propane. Curves from top to bottom correspond to pressure 50 bar, 90 bar, 130 bar, 170 bar, 210 bar, 250 bar.

Hydrate formation involving adsorbed water and hydrate formers from the fluid stream(route 10)

The maximum water content before drop-out as adsorbed on Hematite is plotted for methane, ethane and propane in figures 14, 15 and 16 respectively. The general trend is the same as for the water dew-point mole-fraction in the previous section but the actual limits are far smaller – in the order of 1/20 as compared to the water dew-point criteria.

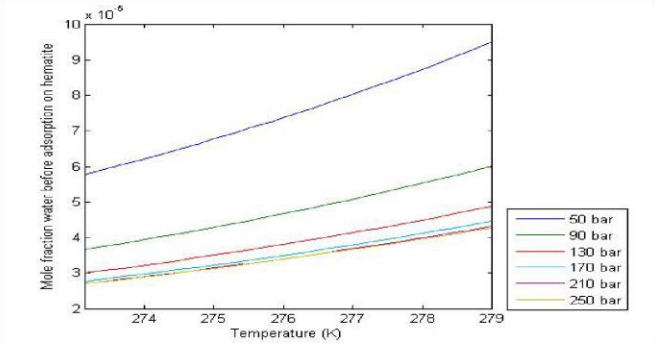

Figure 14. Maximum water content before adsorption on hematite, for pure methane as carrier gas. Curves from top to bottom correspond to pressure 50 bar, 90 bar, 130 bar, 170 bar, 210 bar, 250 bar.

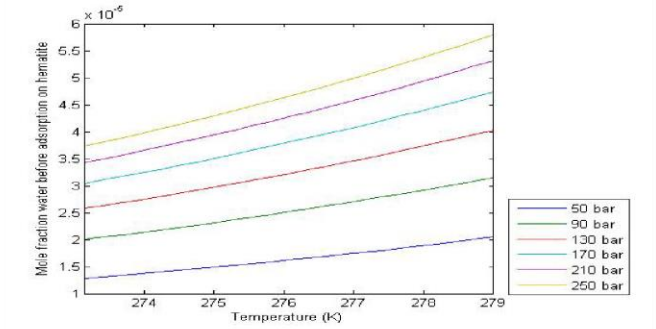

Figure 15. Maximum water content before adsorption on hematite, for pure ethane as carrier gas. Curves from top to bottom correspond to pressure 250 bar, 210 bar, 170 bar, 130 bar, 90 bar, 50 bar.

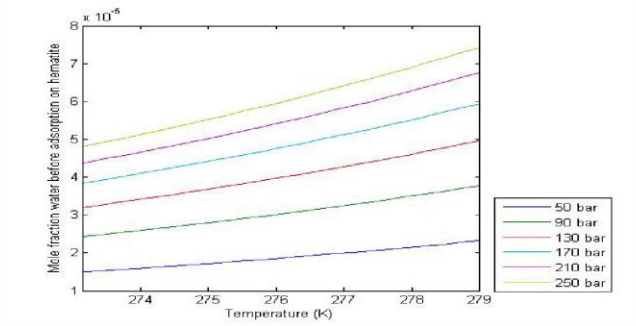

Figure 16. Maximum water content before adsorption on hematite, for pure propane. Curves from top to bottom correspond to pressure 250 bar, 210 bar, 170 bar, 130 bar, 90 bar, 50 bar.

Examining the same natural gas mixtures as in the previous section the trend is as expected still dominated by methane but the tolerance limits for water mole-fractions are shifted dramatically as compared to the water dew-point criteria, as can be seen from the plots in figures 17 – 20.

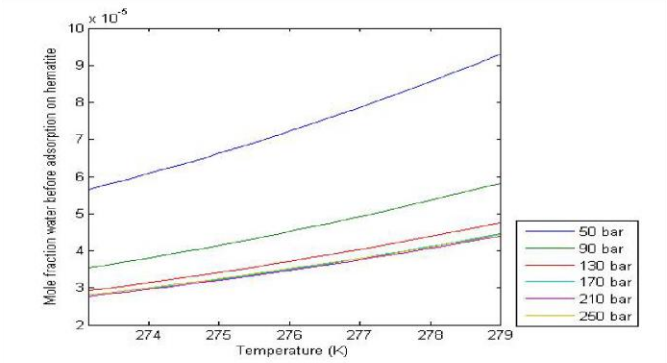

Figure 17.Maximum water content before adsorption on hematite, for a mixture of 90% methane and 10% ethane. Curves from top to bottom correspond to pressure 50 bar, 90 bar, 130 bar, 170 bar, 210 bar, 250 bar.

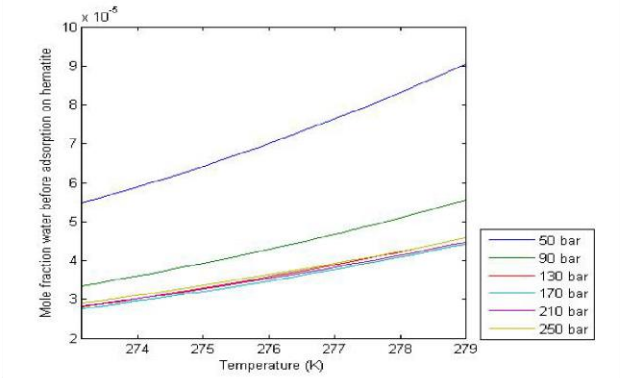

Figure 18. Maximum water content before adsorption on hematite, for a mixture of 80% methane and 20% ethane. Curves from top to bottom correspond to pressure 50 bar, 90 bar, 130 bar, 170 bar, 210 bar, 250 bar.

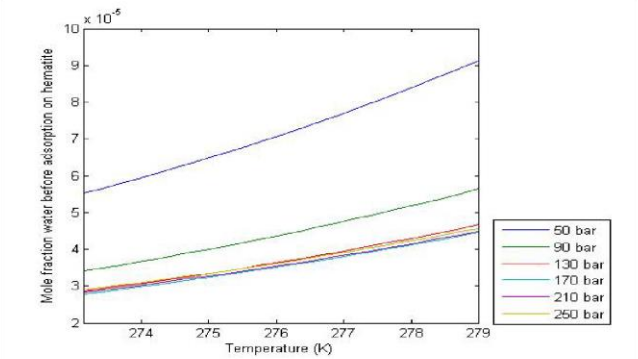

Figure 19.Maximum water content before adsorption on hematite, for a mixture of 90% methane and 10% propane. Curves from top to bottom correspond to pressure 50 bar, 90 bar, 130 bar, 170 bar, 210 bar, 250 bar.

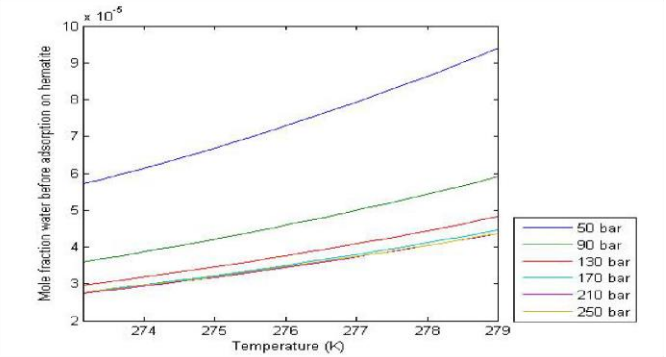

Figure 20.Maximum water content before adsorption on hematite, for a mixture of 95% methane, 4% ethane and 1% propane. Curves from top to bottom correspond to pressure 50 bar, 90 bar, 130 bar, 170 bar, 210 bar, 250 bar.

The main difference between route 10 and route 6 is the concentration at which water drops out from the gas. Hydrate formation according to route 10 is only possible at some distance from the rust surface since water chemical potential in the adsorbed layer will be too low to form hydrates. Our earlier Molecular Dynamics simulations [10] have shown that adsorbed water structure will strongly affect the liquid water until about 3 – 4 molecular diameters from hematite surface. A structured water film roughly 1.2 nm in thickness will form on the hematite surface and bridge it with the hydrate hematite surface. This formation of interface hydrate from bulk liquid water and hydrate formers from the gas phase will be the common feature for routes 6 and 10. Adsorbed water chemical potential as low as 3.4 kJ/mole less than liquid water chemical potential make a big difference in limits for water drop-out mole-fractions.

Figures 14 through 20showthe estimated upper water content supported by the natural gas mixtures before it starts dropping out via adsorption on hematite forpure methane, ethane and propane, and also a variety of mixtures of these. This includes a mixture of 95% methane, 4% ethane and 1% propane, which is comparable to the Troll composition[11].The trend for maximum water tolerance remains the same as in the case of water dew-point but shifted 1 to 2 orders of magnitude downwards.

The Consequences Of Non-Equilibrium Thermodynamics

The non-equilibrium aspects of hydrate phase transitions discussed above will impose substantial challenges for laboratory experiments conducted at temperatures and pressures falling with the hydrate stability regions. While methane solubility in water is so small that one can safely ignore any hydrate implications, the situation will be very different in case of impurities likeethane and propane. This will be due to ethaneand propanesolubility being largely controlled by the presence of hydrate phases. Within the hydrate stability region

where water exists as hydrate,chemical potential of water encaging hydrate guest molecules will be lower than that of liquid water at the same temperature and pressure. Hence, the solubility of ethane and propanewill be significantly smaller for a similar system that does not contain hydrate. This fact can be verified by a limited-range extrapolation of the rigorous version of Henry's law into the hydrate region. The difference between the hydrate-controlled maximum concentration of ethane and propanein water and the ethane and propane dissolved in water will correspond to the amount of hydrate that can be produced from ethane and propane dissolved in water [2,4]

The impact of solid surfaces will introduce additional challenges when it comes to interpretation of experimental results. We are not aware of any experiments that attempted to quantify the impact of solid water-wetting surfaces on carbon dioxide solubility in hydrate-controlled regions. Given the arguments presented above, even the most recent experiments on carbon dioxide solubility in hydrate-forming regions may still be subject to misinterpretation,leaving many of estimates presented in this work without experimental data to comparison to. Hydrate nucleation and growth under non-equilibrium conditions will be facilitated by heterogeneous nucleation (solid surfaces and hydrate former/water surface), and since chemical potentials of hydrate formers and water may differ from the bulk phase properties, the composition and free energy of formed hydrates will be different as well. Different experimental facilities with varying materials and set-ups that give rise to variations in the progresses of hydrate formation will impose additional uncertainties.

The challenge of non-equilibrium thermodynamics and competing hydrate phase transitions can be handled on several levels, a number of strategies discussed elsewhere (see [2,3] and references therein).These discussions can be supplemented by corresponding equations for hydrate sub- and super- saturation presented in this paper. The simplified discrete evaluation scheme outlined here can easily be implemented to extend the existing industrial hydrate risk evaluation codes by enumerating possible routes this will yield corresponding levels of acceptable carbon dioxide content. The rigorous schemes of [2,3] do require consistent reference values for thermodynamics of all phases interacting with the hydrate.Estimates based on routes 6 or 10 are conservative since no routes of hydrate dissociation have been accounted for. This can be accomplished through advanced modeling on nano to millimeter scale using Phase Field Theory (PFT)[12, 13]. Due to the low concentrations of water and possible resolutions in Computational Fluid Dynamics (CFD) simulations it is more unclear if a similar analysis is as feasible within CFD. But a conservative approach as demonstrated here is certainly feasible to implement in CFD tools.

II. CONCLUSIONS

Our rigorous analysis of the Gibbs phase rule applied together with the first and the second laws of thermodynamicshas proven that hydrate nucleation and growth during transport of methane-rich gas with water and other impurities is extremely unlikely to attain equilibrium. Instead, the time evolution of phase transitions will be governed by the free energy minimum. The correspondingthermodynamic analysis of phase transitions will require knowledge of consistent thermodynamic properties for all components in all the phases. In this work, we have shown the way to calculate the chemical potential for water in all phases, including empty hydrate, adsorbed phase, and aqueous solution by plugging properties yielded by molecular dynamics simulations into classical thermodynamic relationships. The most likely hydrate formation scenario will involve water dropping out via adsorption onto rusty pipeline walls. The hydrate formation will start from the accumulated water film. In a possible revision of current best practices for hydrate prevention, it is therefore recommended to reduce water level in the methane-rich phase to below the concentration triggering adsorption-dominated drop-out. Calculating this level will require a procedure similar to that of water dew-point estimation but using chemical potential values characteristic for adsorptionon the surface of interest (either hematite as in this work, or other iron oxide/hydroxide and iron carbonates).It is, however, important to point out that possible hydrate nucleating towards rusty surfaces are unable to attach directly to these iron oxide surfaces due to incompatibility of partial charges between hydrate water partial charges and partial charges on atoms in the mineral. These hydrate nuclei will be linked by structured water to the iron oxides but might be released by frictional forces induced by flow. As such continued hydrate growth can happen towards the iron oxide walls or in the hydrocarbon flowstream by attracting more water and hydrate formers from the hydrocarbon stream, or dissolving again if the local hydrocarbon composition is under saturated with water.

ACKNOWLEDGEMENTS

We acknowledge the grant and support from Research Council of Norway through the project "FME-SUCCESS". Support from TOTAL, Gassco and Research Council of Norway through the project "CO2/H2O+" is also greatly acknowledged.

REFERENCES

[1]. B. Kvamme,H. Tanaka,."Thermodynamic Stability of Hydrates for Ethane, Ethylene, and Carbon Dioxide,".J. Phys. Chem.,Vol.99, PP.7114-71191995

[2]. B.Kvamme,;T . Kuznetsova,,;P.-H.Kivelæ,.;J. Bauman,. "Can hydrate form in carbon dioxide from dissolved water,"PCCP., Vol.15,PP.2063-2074, 2013.

[3]. T. Buanes,."Mean-field approaches applied to hydrate phase transition kinetics,"PhD thesis, University of Bergen, Norway, 2008.

[4]. B. Kvamme, T.Kuznetsova, S.Stensholt, ;S. Sjøblom," Investigating chemical potential of water and H2S in CO_2streams using molecular dynamics simulations and the Gibbs-Duhemrelation,"J. Chem. Eng. DataVol. 60, PP. 2906-2914, 2015.

[5]. B. Kvamme, T. Kuznetsova,B. Jensen,S.Stensholt,J. Bauman,S.Sjøblom, K.N. Lervik," Consequences of CO2 solubility for hydrate formation from carbon dioxide containing water and other impurities,"*PCCP*Vol.16, PP. 8623 – 8638, 2014.

[6]. T. Maekava, "Equilibrium conditions for gas hydrates of methane and ethane mixtures in pure water and sodium chloride solution,"GJ, , Vol. 35, PP. 59-66, 2001.

[7]. G. D.Holder,J. H.Hand, "Multi-phase equilibria in hydrates from methane, ethane, propane and water,"AIChE J.,Vol. 28, PP. 440-4471982.

[8]. H.H. Reamer, F.T. Selleck, B. H. Sage, " Some Properties of Mixed Paraffinic & Other Olefinic Hydrate," Trans. Am. Inst. Min., Metall. Pet. Eng., Vol195, PP.197-202, 1952.

[9]. G. Soave"Equilibrium constants from a modified Redlich-Kwong equation of state,"Chem. Eng. Sci., Vol. 27, PP.1197-1203, 1971.

[10]. B. Kvamme, T.Kuznetsova,P.-H. Kivelæ."Adsorption of water and carbon dioxide on hematite and consequences for possible hydrate formation,".PCCPVol.14, PP.4410-4424.2012.

[11]. H.K. Ebbrell"The composition of Statoil (Norway) gas well Troll 31/6-6 [Internet]. [cited 2017-01-18]. Available from:http://www.npd.no/engelsk/cwi/pbl/wellbore_documents/127_05_31_6_6_The_Composition_of_Statoil_Gas_Well.pdf

[12]. B.Kvamme, M.Qasim, K.Baig, P. H. Kivelä, J. Bauman, "Phase field theory modeling of methane fluxes from exposed natural gas hydrate reservoirs,", International Journal of Greenhouse Gas Control., Vol. 29, PP. 263–278, 2014

[13]. K.Baig, B.kvamme, T. Kuznetsova, J. Bauman, "The impact of water/hydrate film thickness on the kinetic rate of mixed hydrate formation during CO_2 injection into CH_4hydrate", AIChE journal., Vol. 61, Issue 11, PP. 3944–3957, November 2015.